Chemical Engineering Division
Chemical Engineering Division
Chemical Engineering Division
Chemical Engineering Division
Chemical Engineering Division
Chemical Engineering Division
Chemical Engineering Division
Chemical Engineering Division
Chemical Engineering Division
Chemical Engineering Division
Chemical Engineering Division
Chemical Engineering Division
Chemical Engineering Division
Chemical Engineering Division
Chemical Engineering Division
Chemical Engineering Division
Chemical Engineering Division
Chemical Engineering Division
Chemical Engineering Division
Chemical Engineering Division

ANL-03/8

Status of Ceramic Waste Form Degradation and Radionuclide Release Modeling

by T. H. Fanning, W. L. Ebert, S. M. Frank, M. C. Hash, E. E. Morris, L. R. Morss, T. P. O'Holleran, and R. A. Wigeland

Argonne National Laboratory, Argonne, Illinois 60439
operated by The University of Chicago
for the United States Department of Energy under Contract W-31-109-Eng-38

Chemical Engineering Division
Chemical Engineering Division
Chemical Engineering Division
Chemical Engineering Division

Available electronically at http://www.doe.gov/bridge

Available for a processing fee to U.S. Department of Energy and its contractors, in paper, from:

U.S. Department of Energy
Office of Scientific and Technical Information
P.O. Box 62
Oak Ridge, TN 37831-0062
phone: (865) 576-8401
fax: (865) 576-5728
email: reports@adonis.osti.gov

ANL-03/8

ARGONNE NATIONAL LABORATORY
9700 S. Cass Ave.
Argonne, IL 60439

STATUS OF CERAMIC WASTE FORM DEGRADATION AND RADIONUCLIDE RELEASE MODELING

by

T. H. Fanning,* W. L. Ebert, S. M. Frank,** M. C. Hash, E. E. Morris,* L. R. Morss, T. P. O'Holleran,** and R. A. Wigeland*

Chemical Engineering Division

February 2003

*Nuclear Engineering Division
**Engineering Technology Division

TABLE OF CONTENTS

TABLE OF CONTENTS
(Contd.)

Page

LIST OF FIGURES

Page

LIST OF FIGURES
(Contd.)

Page

LIST OF TABLES

STATUS OF CERAMIC WASTE FORM DEGRADATION AND RADIONUCLIDE RELEASE MODELING

by

T. H. Fanning, W. L. Ebert, S. M. Frank, M. C. Hash,
E. E. Morris, L. R. Morss, T. P. O'Holleran, and R. A. Wigeland

ABSTRACT

As part of the spent fuel treatment program at Argonne National Laboratory (ANL), a ceramic waste form is being developed for disposition of the salt waste stream generated during the treatment process. Ceramic waste form (CWF) degradation and radionuclide release modeling is being carried out for the purpose of estimating the impact of the CWF on the performance of the proposed repository at Yucca Mountain. The CWF is composed of approximately 75 wt% salt-loaded sodalite encapsulated in 25 wt% glass binder. Most radionuclides are present as small inclusion phases in the glass. Since the release of radionuclides can only occur as the glass and sodalite phases dissolve, the dissolution rates of the glass and sodalite phases are modeled to provide an upper bound to radionuclide release rates from the CWF. Transition-state theory for the dissolution of aluminosilicate minerals provides a mechanistic basis for the CWF degradation model, while model parameters are obtained by experimental measurements. Performance assessment calculations are carried out using the engineered barrier system model from the Total System Performance Assessment—Viability Assessment (TSPA-VA) for the proposed repository at Yucca Mountain. The analysis presented herein suggests that the CWF will perform in the repository environment in a manner that is similar to other waste forms destined for the repository.

I. INTRODUCTION

Ceramic waste form (CWF) degradation and radionuclide release modeling is being carried out at Argonne National Laboratory (ANL) for the purpose of evaluating the performance of the CWF to support its qualification for disposal in the proposed repository at Yucca Mountain. The analysis presented in the following sections suggest that the CWF will perform in the repository environment in a manner that is similar to other waste forms destined for the repository. (A companion report[1] describes the status of corrosion and release rate modeling for the metal waste form.)

The CWF is composed of approximately 75 wt% salt-loaded sodalite blended with 25 wt% glass binder. Since the release of radionuclides can only occur as the glass and sodalite phases dissolve, the dissolution rates of the glass and sodalite phases are modeled to provide an upper bound to the radionuclide release rates. Transition-state theory for the dissolution of aluminosilicate minerals provides a mechanistic basis and rate expression for the CWF dissolution model, while model parameters are obtained by experimental measurements on nonradioactive surrogates to the CWF. Performance assessment calculations are carried out using the engineered barrier system (EBS) model from the Total System Performance Assessment—Viability Assessment[2,3] (TSPA-VA) for the proposed repository at Yucca Mountain.*

Section II describes the composition and microstructure of the CWF and introduces the transition-state theory expression for the dissolution of aluminosilicate minerals. This expression is simplified to produce the dissolution model that was used for defense high-level waste (HLW) glass in the TSPA-VA. Environmental conditions that the CWF may be subjected to in the repository are also described, along with a discussion of radiation effects and why they are expected to have a negligible effect on CWF degradation.

---

* Hereafter, the acronym TSPA-VA refers to the Total System Performance Assessment—Viability Assessment for Yucca Mountain as described, in part, by Ref. 2, with waste form degradation and radionuclide release models described by Ref. 3.

Section III describes the CWF degradation and release model and how the transition-state theory expression is applied to a multiphase material. Tests conducted to measure the temperature and pH dependence of the CWF dissolution rate are discussed, along with tests used to estimate the solubilities of the two major phases present in the waste form. Finally, the status of additional testing for future model development is outlined.

Section IV presents the approach to performance assessment modeling, starting with a description of the EBS model from the TSPA-VA and the implementation of the CWF degradation model within the framework of the EBS model. Cumulative release is calculated for two important radionuclides: ^{129}I and ^{237}Np. Results for the CWF are compared to those of HLW glass, commercial spent nuclear fuel (SNF) and Department of Energy (DOE) spent nuclear fuel.

II. BACKGROUND

As part of the spent fuel treatment program at Argonne National Laboratory, a glass-bonded sodalite waste form is being developed for disposition of the molten salt waste stream generated during the treatment process. Molten LiCl-KCl salt is used in the electrorefining treatment of irradiated sodium-bonded metallic fuel. During treatment, the salt accumulates sodium, fission product, and transuranic chlorides. Periodically, the salt must be discarded or recycled to maintain concentrations of these materials below specified limits.

A. Ceramic Waste Form Composition and Microstructure

To immobilize the radioactive salt waste for disposal, it is first blended with granulated zeolite-A at a 9:1 zeolite-to-salt mass ratio and heated to about 500°C to incorporate the salt into the cage-like crystalline structure of the zeolite. During blending, rare earth and actinide elements react with residual water from the zeolite to form oxide crystallites on the surface of the zeolite granules. The salt-loaded zeolite is then mixed with glass frit at a 3:1 zeolite-to-glass mass ratio and processed by heating to a temperature of 850°C or higher. As the mixture is heated, the salt-loaded zeolite transforms to sodalite and the glass frit melts and encapsulates the sodalite, binding the granulated material into a monolithic form. Small amounts of nepheline and halite are also

generated during the processing step. These phases and the oxides that had formed during the salt-loading step form inclusions within the glass phase. The end product is a glass-bonded sodalite material that is referred to as the ceramic waste form (CWF). CWF have been made by heating under pressure, which is referred to as hot isostatic pressing (HIP), and by heating at ambient pressure, which is referred to as pressureless consolidation (PC). The PC process has been selected as the preferred option for preparing CWF with Experimental Breeder Reactor No. 2 (EBR-II) spent fuel. The baseline processing conditions (e.g., temperature and time at temperature) are currently being developed.

The gross microstructure of the CWF is dominated by relatively large domains of sodalite surrounded by glass binder. The sizes of the sodalite domains are similar to the sizes of the zeolite granules used in the blending step, although clusters of several granules result in larger sodalite domains. The starting zeolite material consists of granules averaging approximately 100 μm in size composed of individual grains of zeolite approximately 4 μm in size aggregated with a clay binder. Examination of the CWF with scanning electron microscopy and transmission electron microscopy indicates that each sodalite domain consists of aggregates of sodalite grains approximately 4 μm in size surrounded by glass binder. The glass flows into the sodalite aggregates and between the grains during processing. The conversion from zeolite to sodalite does not affect the overall microstructure within the aggregates.

Oxides that were present at the outer surface of the salt-loaded zeolite become fixed in the glass phase near the sodalite boundaries in the CWF. Small halite inclusions are also formed in the glass binder near the sodalite boundaries. The distribution of the inclusion phases depends on the processing conditions. At the processing temperatures used in the HIP process (e.g., 850°C), the inclusions remain near the sodalite domain boundaries. In CWF samples prepared using the PC process at higher temperatures (e.g., 915°C), the inclusions become more uniformly distributed in the glass phase. This is probably because the glass is more fluid at higher temperatures. The PC process results in a CWF with a slightly higher (closed) porosity and lower bulk density than the HIP process. The pores are distributed fairly uniformly throughout the PC CWF.

Analyses of the composition of the glass binder near the sodalite interface indicate that chemical interactions occur between the sodalite and glass binder during processing. For example, the potassium concentrations of glass near the sodalite is observed to be slightly higher than that in the bulk glass, suggesting an ion exchange reaction occurs, and increases in the aluminum content in the glass near the sodalite domain boundary suggests that sodalite dissolves into the glass to a small extent. The small changes in the glass composition due to interactions with sodalite are not expected to have a significant effect on the chemical durability of the glass phase. This is being confirmed (see Sect. III-D-3).

X-ray diffraction shows the CWF to contain sodalite and small amounts of nepheline ($Na_6Al_6Si_6O_{24}$), halite (NaCl), and mixed rare earth and actinide oxides. The chemical composition of natural sodalite is $Na_8Al_6Si_6O_{24}Cl_2$, with partial substitution of K for Na possible. The composition of the sodalite in the CWF as measured with X-ray emission spectroscopy in the scanning electron microscope (SEM) has less Na and Cl. This is probably because glass between the sodalite grains in the CWF was included in the analyzed volume. The measured composition of the glass has less Na than the starting glass frit and contains more K and Cl. These differences are probably due to the presence of halite inclusions in the glass phase of the CWF.

The most abundant inclusion phases in the CWF are halite (NaCl), AnO_2, and R_2O_3, where An and R represent actinide and rare earth elements or mixtures. The NaCl inclusions range in size from tens to thousands of nanometers. The rare earth and actinide oxides are typically tens of nanometers in size. Very small amounts of other phases have been identified in some samples, including clays and silicates.

The distribution of radionuclides in the CWF is of particular interest. Samples of CWF made with surrogate salts doped with radionuclides and samples made with actual waste salts have been examined to measure the distribution of radionuclides. Plutonium and uranium are observed in the $(U,Pu)O_2$ mixed oxides and rare earth elements in oxide inclusions. The concentrations of these elements in the glass and sodalite phases are below analytical detection limits. The distribution of some radionuclides has been inferred from their release behavior as the CWF dissolves. For example, dissolution test results show that iodine is released stoichiometrically

with chlorine, which suggests that iodine and chlorine are distributed in the same proportions in halide inclusions and the sodalite. While small amounts of most radionuclides are expected to dissolve in the glass binder, most radionuclides are sequestered in inclusion phases within the glass binder. The primary role of sodalite in the CWF is to contain the high levels of Na, K, and Cl in the salt waste stream and the primary role of the glass is to bind the crystalline phases in a robust monolithic waste form.

Phases that contain radionuclides are of primary importance from the perspective of the impact of the CWF on the performance of the disposal system. However, the release of the radionuclides from the CWF into the environment is controlled first by the chemical durability of the glass and sodalite phases and second by the durability of the phases containing the radionuclides. Radionuclides in soluble halite inclusions will be released immediately upon contact with groundwater, whereas mixed rare earth and actinide oxides are highly insoluble under anticipated groundwater conditions. Laboratory tests have shown the rare earth and actinide oxides to be released primarily as colloidal material as the glass binder corrodes.

B. Dissolution Modeling

The starting point for both glass and sodalite dissolution is the transition-state theory expression for the dissolution of aluminosilicate minerals. At constant pressure and temperature, the rate equation can be expressed as[4]

$$\frac{dm}{dt} = k(T)\left(\prod_i a_i^{-\eta_i}\right)\left[1 - \exp\left(-\frac{A}{\sigma RT}\right)\right], \qquad (1)$$

where m is the mass of material dissolved per unit area, $k(T)$ is the intrinsic rate constant as a function of temperature, a_i represents the activity of the i^{th} dissolved species that contributes to the activated complex of the rate-limiting microscopic dissolution reaction,[5] η_i is the order of the rate-limiting reaction with respect to i, A is the chemical affinity of the overall reaction, R is the gas constant, and T is the temperature. σ represents a stoichiometric factor that relates the rate-controlling microscopic reaction to the overall solid dissolution reaction and, in this model, is assumed to be 1.

Chemical affinity can be written as $A = -RT\ln(Q/K)$, where Q is the activity product and K is the equilibrium constant for the rate-determining reaction step. With this, the dissolution rate equation is written as

$$\text{rate} = k_0 10^{\eta \text{pH}} \exp\left(-\frac{E_a}{RT}\right)\left(1 - \frac{Q}{K}\right), \tag{2}$$

where the temperature dependence on the intrinsic rate is shown explicitly, E_a is the activation energy, and the activity product has been reduced to include only the dependence on hydrogen ion activity (i.e., pH). Because temperature, pH, and activity product will change with time in a repository, dissolution rates are implicitly a function of time. This is the basic equation from which the degradation model for the CWF is developed. It is also the equation from which the high-level waste (HLW) glass dissolution model is derived.

The most widely used HLW glass dissolution model, and the model used in the TSPA-VA for Yucca Mountain, is the Grambow model.[6] Based on a simplification of Eq. (2), the model includes only aqueous silica for the value of Q in the affinity term, and K corresponds to an aqueous silica (i.e., orthosilicic acid, H_4SiO_4) saturation value for amorphous silica. Also, because glass is not thermodynamically stable and never reaches true equilibrium, an additional term, k_{long}, was included to account for continued dissolution once "saturation" ($Q/K \rightarrow 1$) is achieved. The final form of the glass dissolution model is written as

$$\text{rate} = k_f(T, \text{pH})\left(1 - \frac{Q}{K}\right) + k_{\text{long}}, \tag{3}$$

where "rate" is the dissolution rate (g/m^2/y), k_f is the forward dissolution rate (g/m^2/y) defined by $k_f = k_0 10^{\eta \text{pH}} \exp(-E_a/RT)$, k_0 is the intrinsic dissolution rate, η is the pH dependence, E_a is the activation energy, Q is the orthosilicic acid activity in solution, K is the orthosilicic acid saturation activity, and k_{long} is the dissolution rate at saturation.

Parameters for Eq. (3) have been measured for typical HLW glasses. The TSPA-VA used a regression analysis for k_f that is based on experimental data taken at 25, 50, and 70°C for a

five-component analogue to the SRL-165 HLW glass.[3] This regression is shown in Fig. 1, where the dissolution rate of the simplified glass is shown as a function of pH for three different temperatures. Similar measurements have been made for the CWF and are described in Sect. III-B.

The orthosilicic acid saturation value, K, used for HLW glass is based on the solubility of amorphous silica.[3] This provides an upper bound on K_{HLW}. Observed solubilities for HLW glass vary with glass composition and experimental conditions.[3] Providing an upper bound results in conservative release rate calculations. Equilibrium solubilities for amorphous silica are presented in Table 1 in terms of aqueous silica (SiO_2). The determination of orthosilicic acid saturation values for sodalite, binder glass, and the CWF is described in Sect. III-C.

Because there is no mechanistic model to describe the continued dissolution of glass once saturation is achieved, the TSPA-VA used an averaged value of $k_{\mathrm{long}} = 0.002\ \mathrm{g/m^2/d}$. This value was obtained from glass corrosion tests at 90°C.[7] Because no temperature dependence was available, the temperature dependence for the forward rate was assumed for k_{long} in the TSPA-VA. No estimates of k_{long} have been made for the CWF, however it is expected to be relatively unimportant for the current calculations (see Sect. IV-C).

C. Environmental Conditions

In a repository setting, the most likely release pathway is through interaction between the groundwater and the CWF, followed by transport of the radionuclide-bearing groundwater to the accessible environment. The repository environment influences the interactions that take place between groundwater and the CWF. As described in the preceding section, aluminosilicate dissolution rates are commonly modeled as a function of temperature, pH, and aqueous silica.

Due to thermal loading from radioactive decay, the temperature in the repository will initially be higher than ambient conditions and then gradually decline. At higher temperatures, the waste package will remain dry, and aqueous corrosion cannot take place. Waste package temperatures were calculated in the TSPA-VA based on an assumed thermal loading. Average waste package temperature as a function of time as calculated by the EBS model for the TSPA-VA is shown

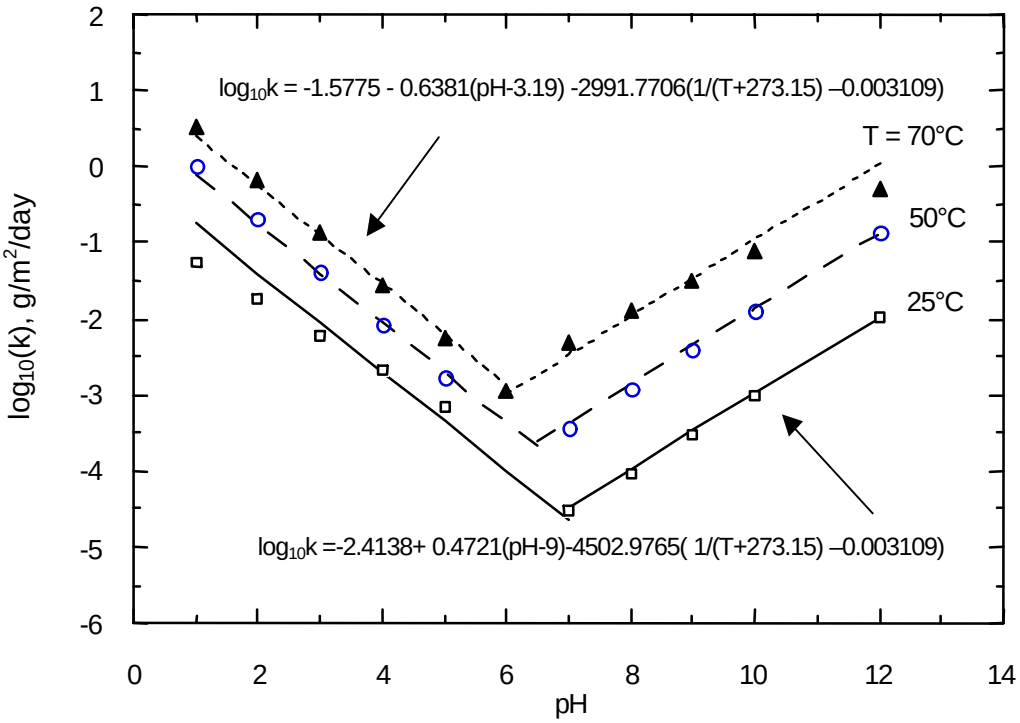

Fig. 1. Dissolution Rate versus Solution pH for High-Level Waste Glass. (Reprinted from Ref. 4, Fig. 6-31, p. F6-27.)

Table 1. Equilibrium Solubilities for Amorphous Silica and Cristobalite,[3] Log_{10} (molality)

Temperature, °C	0	25	60	90	100	150
Amorphous Silica ($K_{HLW} = K_{SiO_2(am)}$)	-2.99	-2.71	-2.43	-2.26	-2.20	-1.98
Cristobalite ($Q = K_{cristobalite}$)	-3.89	-3.45	-3.02	-2.75	-2.68	-2.36

in Fig. 2. Initially, temperatures exceed 115°C but decline below 80°C after only 1000 years. In the absence of juvenile failures, waste package failures are not predicted to occur until after 2500 years.[2] This suggests waste form degradation will occur at temperatures below 60°C. Although not shown in the figure, waste package temperatures reach a nearly steady-state value of less than 20°C after 100,000 years.

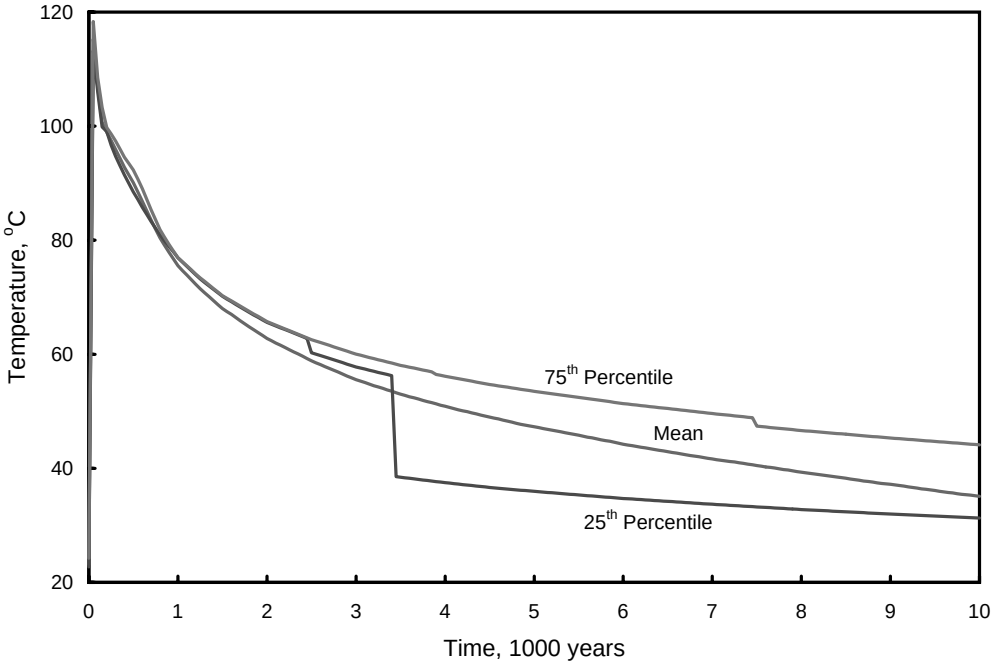

Fig. 2. Average Waste Package Temperature as a Function of Time. Waste package temperatures were calculated by the EBS model from the TSPA-VA for Yucca Mountain.

In addition to a strong temperature dependence, Fig. 1 shows a strong pH dependence on the forward dissolution rate for HLW glass. In the alkaline region, an increase in pH by one unit nearly triples the dissolution rate. (This corresponds to the 0.4721 coefficient in the regression.) Results from the buffered Materials Characterization Center (MCC-1) tests (Sect. III-B) indicate a similar behavior for the glass phase of the CWF, while sodalite has a weaker pH dependence in this region. The average pH values of incoming groundwater used in the EBS model for the TSPA-VA are shown in Fig. 3 as a function of time. Although pH peaks above 10 within the first 1000 years, it drops below 9 after 2000 years and just above 8 after 4000 years, suggesting waste form degradation will continue to occur under alkaline conditions. After 100,000 years (not shown in the figure) the pH drops to approximately 7.5.

Waste form degradation alters the pH of the groundwater.[8] Under the low flow conditions expected in a repository, the small amount of water that enters the waste package will undergo a change in pH due to waste form dissolution once it contacts the waste form. The TSPA-VA did not

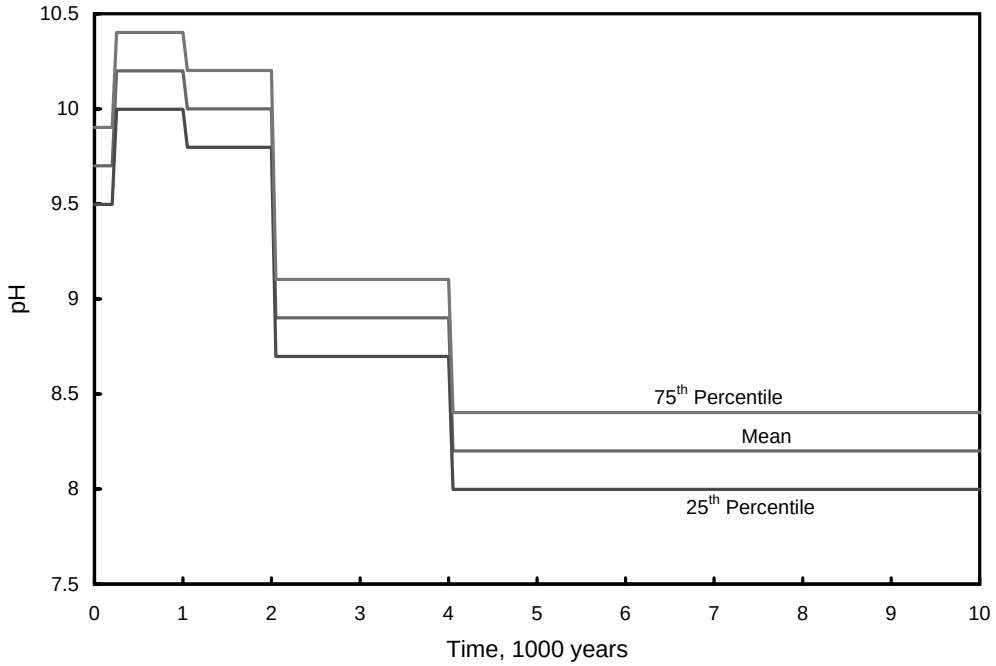

Fig. 3. Incoming Groundwater pH as a Function of Time. Groundwater pH values were calculated by the EBS model from the TSPA-VA for Yucca Mountain.

consider changes in groundwater pH or other in-package chemistry effects in the HLW glass model. The current performance assessment calculations for the CWF are based on the EBS model for the TSPA-VA, therefore, in-package chemistry effects for the CWF are not included in the analysis presented in Sect. IV.

The amount of aqueous silica present in solution affects waste form dissolution rates by altering the orthosilicic acid activity product, Q. The TSPA-VA assumes the incoming groundwater that comes into contact with the waste forms has been equilibrated with cristobalite, a common constituent of the host rocks at Yucca Mountain. Equilibrium solubilities for cristobalite are shown in Table 1. For HLW glass, it is assumed that the ratio Q/K_{HLW} is fixed (at a given temperature) by the solubilities of cristobalite and amorphous silica (i.e. $Q = K_{\mathrm{cristobalite}}$ and $K_{\mathrm{HLW}} = K_{\mathrm{SiO_2(am)}}$). Because waste form degradation introduces more aqueous silica into the groundwater, the ratio Q/K increases towards 1 over time. The TSPA-VA does not account for changes in aqueous silica concentration as waste glass dissolves. This provides a conservative

bound on glass dissolution rates, as aqueous silica is an important factor in limiting dissolution. These same assumptions are maintained in the analysis presented in Sect. IV.

An indirect effect of the environmental conditions in the repository is the formation of colloids. Colloid concentrations in the repository are modeled in the TSPA-VA as a function of groundwater ionic strength and pH. Because plutonium has low solubility and high sorption onto the host rock, it is one of the radionuclides most likely affected by colloid transport and the only radionuclide considered for colloid transport in the TSPA-VA. In the near-field environment, the TSPA-VA considers four types of colloids for reversible plutonium attachment: clay, iron oxides, spent fuel colloids, and glass waste colloids. For the purposes of the current analysis, the same models are applied to the mobilization of plutonium that is released from the CWF. (The results described in Sect. IV-D for iodine and neptunium release are not affected by the colloid model.) Dissolution experiments on plutonium-loaded CWF samples are underway to determine the extent to which plutonium release from the CWF is correlated to colloid generation (see Sect. III-D-4).

D. Radiation Effects

Radiation effects on waste form dissolution are quite complex[9] due to interactions with dissolved waste components, generation of radiolysis products, and the buffering capacity of bicarbonate or silicate groundwater. Additionally, structural changes in the waste form itself, such as bubble formation, phase separation, and microfracturing, can increase the reactive surface area. Self-annealing processes may limit cumulative radiation damage, which further complicates analysis of these effects. Table 2 shows the radiation source strength expected for the CWF after processing EBR-II driver assemblies.

Radiation effects can generally be categorized in one of two ways: those which cause chemical changes in the surrounding environment and those which cause physical or chemical changes in the waste form matrix. Alpha decay can cause physical damage through helium bubble formation, swelling, and microfracturing or through ballistic damage resulting in metamict transformation (amorphization) of crystalline phases. In order to determine the long-term effects on

Table 2. Ceramic Waste Form Radiation Source Strength from EBR-II Driver Assemblies,[10] (Ci/m^3)

Cooling Time (y)	Gamma	Beta	Alpha	Neutron
0 (present)	78400	253000	376	2.50×10^{-4}
1,000	32.7	51.9	292	1.84×10^{-4}
10,000	11.4	27.3	189	1.15×10^{-4}
100,000	1.26	4.27	13.2	7.92×10^{-6}
1,000,000	0.540	1.79	0.184	1.10×10^{-7}

CWF performance due to alpha decay, radiation damage studies are presently underway with ^{238}Pu-loaded CWF samples (see Sect. III-D-6).

Chemical changes to the near-field environment are caused by the generation of radiolysis products in air, steam, or water by ionizing radiation. Irradiation of moist air produces mostly nitrous oxide and ozone.[11] When dissolved in water, these products alter the pH. In the absence of air, pH tends to increase due to increased glass reaction with water radiolysis products, however, this effect diminishes as temperature increases.[9]

The groundwater at Yucca Mountain contains constituents that buffer the pH. In saturated conditions, significant changes in leachate pH and glass reaction rates were not observed when samples were irradiated in water equilibrated with tuff.[9] Several tests have been conducted with exposure rates ranging from 10^3–10^5 R/h with total exposures exceeding 10^8 R. Essentially no difference in glass reaction was found.[11] In some cases, glass reaction rates were actually reduced due to the stabilization of the pH to near neutral values by the buffering capacity of the groundwater.[9]

In unsaturated conditions, the buffering capacity of the thin film of water that condenses on the waste form may be insufficient to neutralize the radiolytic acids that are produced. Saturated air-steam experiments on HLW glass at 150°C were performed with an external 3500 rad/h gamma source and internal (due to radionuclide loading) 23 μCi/g alpha and beta source.[12]

Results showed that the quantity of alteration products was increased and the development of secondary phases was accelerated above that observed in nonirradiated tests.[13] Development and growth of an alteration layer was accelerated four-fold due to radiation exposure under these high surface area to water volume conditions. However, no transuranics were found in the clay or precipitated layer, suggesting these elements were retained within the alteration layers rather than dissolving and precipitating on the surface.[13] Although actinides tend to have higher solubilities under acidic conditions, it is unlikely that mobilization would be possible in the absence of a fluid phase.[11]

During the first several hundred to thousands of years of repository operation, the waste package (and waste forms) will remain dry due to thermal loading from radioactive decay. The first waste package failures are not predicted to occur until after 2500 years. After only 1000 years the exposure due to gamma radiation from the CWF will fall to a few R/h, far below the levels typically used in experiments. Gamma exposure from other waste forms will also become negligible.

The TSPA-VA for Yucca Mountain did not consider the possible effects of radiation on waste form degradation. Additionally, the implementation of the HLW glass degradation model makes no distinction between unsaturated and saturated flow conditions within the waste package. Changes to in-package chemistry were not considered in any of the degradation models in the TSPA-VA. This would be the place to consider potential radiolysis effects and its impact on in-package chemistry. In-package chemistry and in-package transport will be considered by the forthcoming site recommendation (SR).[14,15] The CWF model will be updated at that time to adapt to changes in the EBS model.

The above issues relating to HLW glass performance are all relevant to CWF performance. However, the studies described above suggest radiolysis effects do not significantly alter waste form performance and are relatively unimportant. Furthermore, since radiolysis affects primarily groundwater chemistry by altering the pH, it is implicitly a part of CWF degradation modeling. These effects are addressed by accounting for a pH dependence on waste form performance under

both saturated and unsaturated flow conditions. The aqueous degradation model for the CWF already includes terms to account for pH effects (see Sect. III-B).

III. CERAMIC WASTE FORM DEGRADATION AND RADIONUCLIDE RELEASE

A. Degradation and Release Modeling

Degradation of the CWF will occur by the dissolution of both sodalite and glass. As these phases dissolve, other phases containing radionuclides will be exposed to groundwater. Once exposed, radionuclides in these phases will be released and made available for transport to the environment. In the present model, the minor phases are assumed to have uniform distribution in the CWF and zero durability. That is, as these phases are exposed to groundwater through glass and sodalite dissolution, radionuclides in these phases will be immediately released and made available for transport. As a result, sodalite and glass degradation rates provide a conservative bound on radionuclide release from the CWF.

A simplified schematic of CWF degradation and radionuclide release is shown in Fig. 4. Sodalite and glass both dissolve when exposed to groundwater, but may do so at different rates. To provide an upper bound on release from the more durable phase, overall durability of the CWF is assumed to be equal to that of the less durable phase. To illustrate, if glass is less durable than sodalite in the repository environment, then faster glass dissolution will lead to additional sodalite exposure as shown in Fig. 4 by the broken lines. The additional surface area of sodalite that is exposed will lead to more sodalite dissolution. However, the extent of sodalite dissolution would still be limited by the extent of glass dissolution. In this example, therefore, glass dissolution rates provide a conservative bound on overall release from the CWF. The level of conservatism provided by this assumption has not been determined.

The rate equation developed for HLW glass dissolution is also applicable to the glass phase of the CWF. Because the rate equation for glass dissolution is derived from the transition-state theory expression for the dissolution of aluminosilicate minerals, it is also applicable to the sodalite phase of the CWF. Based on experimental evidence that shows similar dissolution

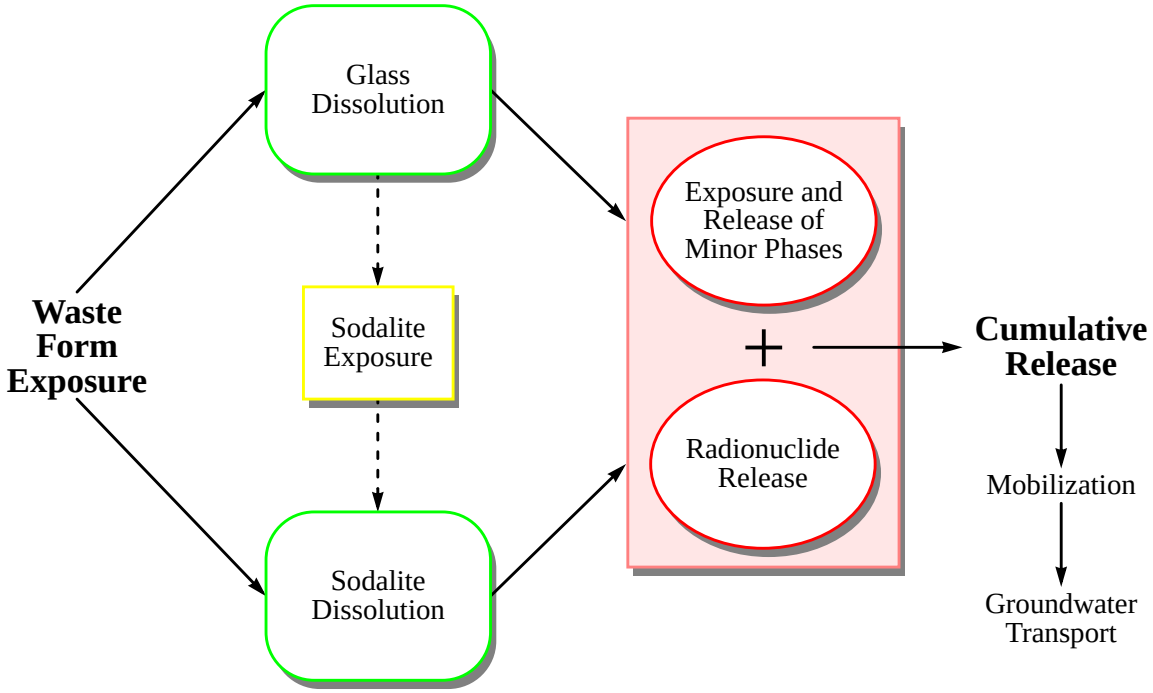

Fig. 4. Ceramic Waste Form Degradation and Radionuclide Release. This figure assumes glass is less durable than sodalite so that glass dissolution leads to additional sodalite exposure. Also, no credit is taken for the durability of the minor phases.

behavior between sodalite, binder glass, the CWF and HLW glass,[16] the rate equation being used for the CWF is the same as the one used for the HLW glass degradation model.

Dissolution tests using dilute, pH-buffered solutions have been conducted at 40, 70, and 90°C to determine the intrinsic dissolution rate (k_0) along with the temperature and pH dependence (E_a and η, respectively) on the forward dissolution rates of sodalite, binder glass, and the CWF. These tests are described in Sect. III-B. Tests for estimating the equilibrium constant K are described in Sect. III-C. A value for k_{long} has not been measured for the CWF. Section III-D outlines additional testing that is being carried out for future model development.

B. Temperature and pH Effects

The Materials Characterization Center 1 (MCC-1) test[17,18] is a standard test method used in the leach testing of glasses and ceramics. Here, short-term, pH-buffered MCC-1 tests are used to determine the temperature and pH dependence on the dissolution of sodalite, binder glass, and the composite CWF. By conducting short-term tests, the buildup of orthosilicic acid is minimized and the affinity term from Eq. (3) remains near 1. This allows the measurement of the forward rate without the influence of saturation effects. By controlling temperature and pH in the experiments, the temperature and pH dependence on dissolution rates can be determined.

1. pH-Buffered MCC-1 Testing Methodology

Samples of borosilicate binder glass, synthetic sodalite with a clay binder, and CWF were prepared by hot isostatic pressing.[16] Monoliths of each material were cored and cut into wafers nominally 10 mm in diameter and 1 mm thick. The wafers were polished with abrasives to a 600-grit finish. Preparation details and sample characterizations have been published.[16]

The polished pellets were tested according to the MCC-1 procedure in capped perfluoroalkoxy (PFA) Teflon containers with buffered solutions having the compositions and pH values shown in Table 3. The buffer solutions were selected to minimize chemical interactions with components of glass and sodalite. Concentrations were selected to maintain nearly constant ionic strength and adequate buffering capacities to maintain pH within 0.1 pH unit. The pH values of the buffer solutions were determined with an Orion Ross combination semi-micro electrode that was calibrated at the test temperature with commercial buffer solutions before each group of measurements.

To achieve a ratio of 10 m^{-1} for the specimen surface area to leachant volume (S/V), a typical wafer with geometric surface area of 2.00 cm^2 was placed in buffer solution of volume 20.0 mL. The sealed vessels were placed in a constant-temperature oven at either 40, 70, or 90°C for various test durations. The pH of the test solutions was measured before and after each test using an Orion Ross combination semi-micro electrode calibrated with commercial

Table 3. Buffer Compositions Used in pH Buffer Tests and Measured Buffer pH Values

Buffer Composition	pH, 25°C	pH, 40°C	pH, 70°C	pH, 90°C
0.0095m KHph[a] + 0.00270m LiOH	4.86	4.93	5.03	5.18
0.00380m KHph[a] + 00031m LiOH	5.87	5.99	6.20	6.25
0.0130m TRIS[b] + 0.0100m HNO_3	7.52	7.22	6.65	6.31
0.0263m TRIS[b] + 0.0100m HNO_3	8.47		7.25	6.15
0.0640m H_3BO_3 + 0.0100m LiOH	8.39	8.31	8.27	8.14
0.0120m H_3BO_3 + 0.0100m LiOH	9.84	9.68	9.56	9.37
0.00098m HNO_3 + 0.0117m LiOH	11.96		10.66	10.23

a. KHph: Potassium hydrogen phthalate.
b. TRIS: Tris(hydroxymethyl)aminomethane.

buffer solutions at the test temperatures of 40, 70, and 90°C. All pH measurements were carried out with the test and reference solutions in a controlled temperature bath that maintained temperature constant to ±0.5°C. For each pH measurement the combination electrode was agitated gently to stir the solution, then allowed to come to a constant reading (less than 0.01 pH unit drift within one minute) in the (unstirred) solution being measured.

MCC-1 tests were conducted at 40°C for 7, 14, 28, 56, and 91 days, at 70°C for 3, 5, 7, and 10 days, or at 90°C for 1, 2, 3, and 5 days. The test durations were selected to be short enough that the rate of corrosion would be as close as possible to the forward rate. The results of tests at shorter durations may be dominated by surface effects, while tests at longer durations show the effect of the affinity term, $1 - Q/K$. Blank tests were run with the buffer solutions to measure background concentrations.

To terminate the tests the test vessels were first allowed to cool for about one hour. Aliquots were taken for pH measurement at the testing temperature and at 25°C. Solutions were passed through 0.45-μm filters, acidified, and analyzed for concentrations of matrix and minor elements by inductively coupled plasma—atomic emission spectroscopy (ICP-AES) or

inductively coupled plasma—mass spectroscopy (ICP-MS). The vessels were then subjected to acid stripping with 1% HNO_3 solution.

2. Results

The concentration of silicon in solution provides the best measure of matrix dissolution of glass-bonded sodalite since silicon is a key structural element in both the glass and sodalite phases. The measured Si concentrations in solutions from buffered MCC-1 tests with each material (glass binder, sodalite, and CWF) were used to calculate the normalized mass loss of silicon, defined as

$$\mathrm{NL_{Si}} = \frac{m_{\mathrm{Si}} - m_b}{f_{\mathrm{Si}} S} \tag{4}$$

where m_{Si} is the mass of silicon in the test solution, m_b is the mass of silicon in the experimental blank, f_{Si} is the mass fraction of silicon in the material, and S is the sample surface area. Cation concentrations in the acid-strip solutions were negligible.

At each temperature and pH, the concentration of silicon increased rapidly during the shortest test duration, then increased at a slower but nearly linear rate for longer test durations. Silicon concentrations and normalized mass losses are listed in Tables A1 through A9 in Appendix A for each material, temperature and pH.

3. Regression Analysis

Normalized dissolution rates, $\mathrm{NR_{Si}} = d\mathrm{NL_{Si}}/dt$, were calculated by linear regression at each pH of the 7- to 91-day normalized release of Si for glass, sodalite, and CWF at 40°C; the 3- to 10-day normalized release at 70°C; and the 1- to 5-day releases at 90°C. Individual regression fits for each material, temperature, and pH are shown in Figs. A1 through A9 in Appendix A. The release rates were determined from the slope of each regression fit and are summarized in Table 4. Dissolution rates as a function of pH are plotted at 40, 70, and 90°C for each material in Fig. 5.

Table 4. Normalized Dissolution Rates in g/m^2-d for Sodalite, Binder Glass, and CWF as a Function of pH at (a) 40°C, (b) 70°C, and (c) 90°C

(a) 40°C

pH	Sodalite	Glass	CWF
4.9	0.14	0.0027	0.13
6.0	0.062	0.00096	0.041
6.8	–	0.00056	–
7.2	0.012	0.00060	0.0074
7.8	–	0.0021	–
8.3	0.029	0.024	0.022
9.6	0.030	0.031	0.023

(b) 70°C

pH	Sodalite	Glass	CWF
4.9	1.0	–	–
5.1	–	0.025	1.4
6.0	–	0.0093	0.48
6.4	0.48	–	–
7.2	0.11	0.016	0.19
8.3	0.23	0.22	0.40
9.4	0.36	–	–
9.6	–	0.50	0.50

(c) 90°C

pH	Sodalite	Glass	CWF
5.1	2.6	0.088	1.8
6.0	0.64	0.056	0.67
7.0	0.39	0.056	0.69
8.1	0.99	0.93	1.3
9.2	1.2	1.5	1.5
10.2	2.5	5.3	3.3

The intrinsic dissolution rate and the temperature and pH dependence on the forward dissolution rates for sodalite, glass binder, and composite CWF can be calculated from the normalized dissolution rates in Table 4. Because of the low surface to volume ratio and short test durations, the orthosilicic acid activity remained low and the value $(1 - Q/K)$ remained near one. Also, since saturation is not achieved, k_{long} can be dropped from Eq. (3). This leaves

$$\text{rate} \approx k_f = k_0 10^{\eta \text{pH}} \exp(-E_a/RT) \tag{5}$$

When the logarithm of Eq. (5) is taken, a linear expression is obtained:

$$\log(k_f) = \log k_0 + \eta \text{pH} - \frac{E_a}{R \ln 10} T^{-1} \tag{6}$$

It can be seen from Eq. (6) that k_0, η, and E_a can be obtained by performing a linear regression on the logarithm of the normalized dissolution rates as a function of pH and inverse temperature. Linear regression of the data in Table 4 was performed using separate regression fits for dissolution rates measured in acidic and alkaline buffers.

The pH and temperature dependence on the dissolution rates for each material was fit to the function

$$\log k_f = C_0 + C_1(\text{pH} - C_{\text{pH}}) + C_2(1/T - C_T), \tag{7}$$

where C_0, C_1, and C_2 represent regression coefficients. The constants C_{pH} and C_T represent the average pH and average inverse temperature, respectively, of the data used in the regression. Variance weighting of the data was not performed. The resulting coefficients and standard errors for each fit are shown in Table 5. Equation (7) is plotted in Fig. 5 for each material at 40, 70, and 90°C. The dissolution rate parameters k_0, η, and E_a can be determined by comparing Eq. (7) with Eq. (6) to show that $\log k_0 = C_0 - C_1 C_{\text{pH}} - C_2 C_T$, $\eta = C_1$, and $E_a = C_2 R \ln 10$. These parameters are shown in Table 6 along with calculated parameters from the regression for HLW glass from the TSPA-VA. A comparison of parameter values in the repository-relevant alkaline region shows that binder glass has the lowest intrinsic rate but the strongest pH dependence. The

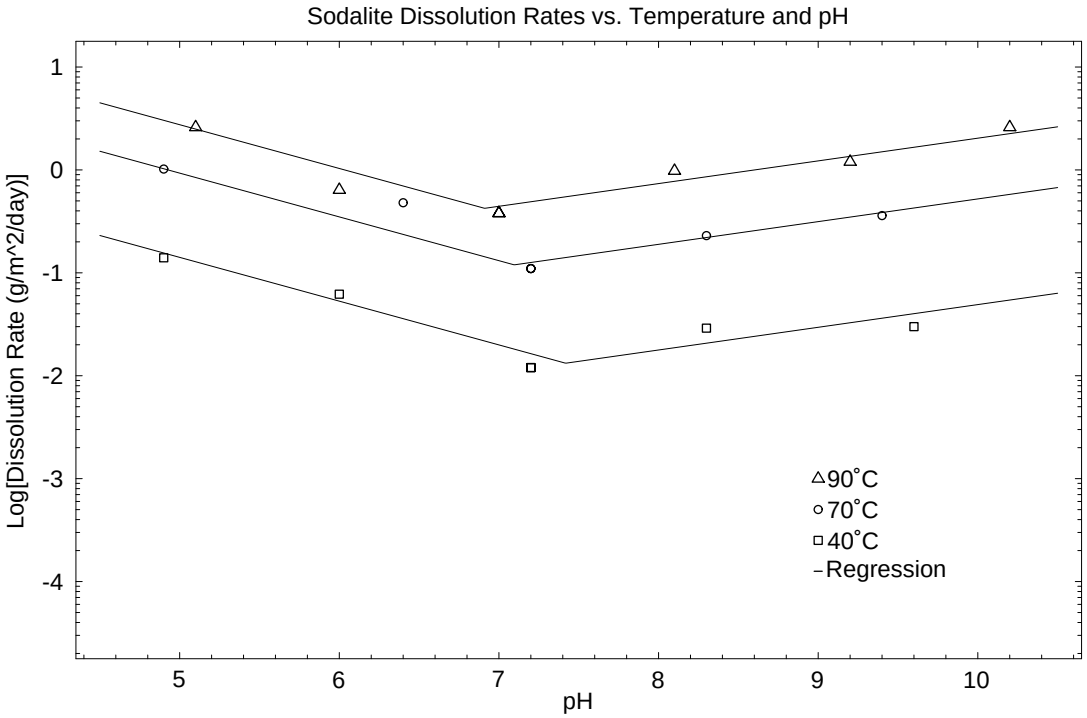

(a) Sodalite

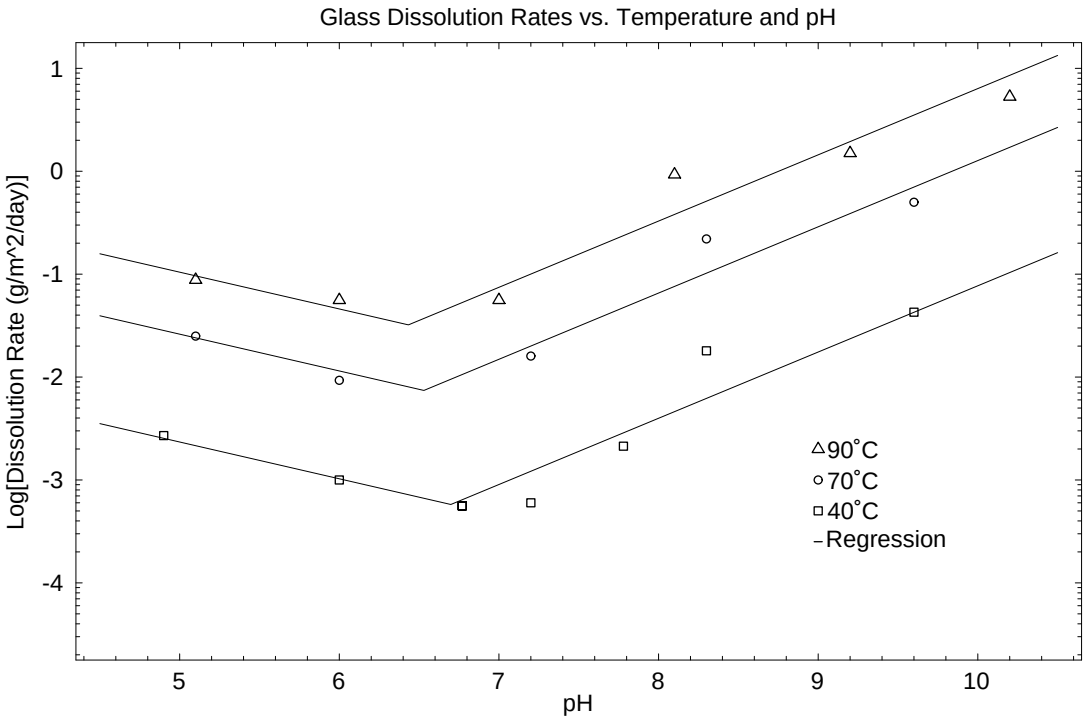

(b) Binder Glass

Fig. 5. Dissolution Rates as a Function of Temperature and pH for (a) Sodalite, (b) Binder Glass, and (c) CWF

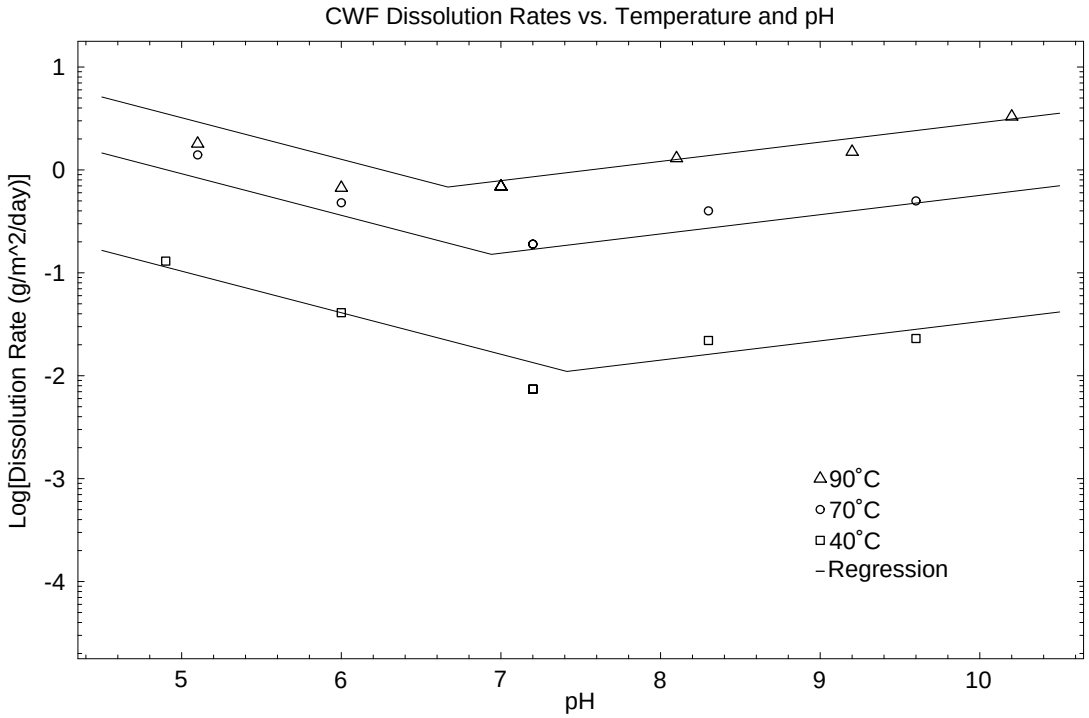

(c) CWF

Fig. 5. Dissolution Rates as a Function of Temperature and pH for (a) Sodalite, (b) Binder Glass, and (c) CWF (Continued)

temperature dependence on the dissolution rate of the binder glass is slightly lower than that of HLW glass. Although the intrinsic rate for binder glass is the lowest, the stronger pH dependence and weaker temperature dependence result in a higher forward dissolution rate as compared to HLW glass.

Dissolution rates measured for the CWF reflect dissolution of both the sodalite and binder glass phases. A comparison of Fig. 5(a) with Fig. 5(c) shows similar dissolution behavior between sodalite and the CWF. The regression parameters for the CWF and sodalite in Table 5 show a similar result. This is due in part to the higher forward dissolution rate of sodalite and also to the fact that sodalite comprises approximately 75 wt% of the waste form.

As described previously, overall durability of the CWF is assumed to be equal to that of the less durable phase. Sodalite dissolves faster than binder glass over much of the pH

Table 5. Regression Parameters for the Acid and Base "Leg," Corresponding to Eq. (7). For sodalite and the CWF, measured dissolution rates in near-neutral pH are used in both the acid and base leg regression fits. For binder glass, only the pH = 6.8 result is used in both the acid and base leg regression fits.

	"Leg"	C_0	C_1	C_2	C_{pH}	C_T
Sodalite	acid	–0.604 ±0.055[a]	–0.424 ±0.061	–2937 ±303	6.078	0.002955
	base	–0.695 ±0.030	0.219 ±0.028	–3682 ±164	8.450	0.002935
Binder Glass	acid	–2.109 ±0.026	–0.357 ±0.042	–3750 ±141	5.696	0.002989
	base	–1.283 ±0.080	0.644 ±0.076	–4355 ±432	8.271	0.002978
CWF	acid	–0.598 ±0.077	–0.404 ±0.089	–3388 ±422	6.056	0.002955
	base	–0.620 ±0.037	0.187 ±0.034	–4389 ±204	8.470	0.002935

a. Uncertainties represent standard errors in the regression fit.

Table 6. Dissolution Rate Parameters for Sodalite, Binder Glass, the CWF, and HLW Glass

	"Leg"	$\log k_0$ ($g/m^2/d$)	η	E_a (kJ/mole)
Sodalite	acid	10.7	-0.424	56.2
	base	8.26	0.219	70.5
Binder Glass	acid	11.1	-0.357	71.8
	base	6.36	0.644	83.4
CWF	acid	11.9	-0.404	64.9
	base	10.7	0.187	84.0
HLW Glass[a]	acid	9.76	-0.638	57.3
	base	7.34	0.472	86.2

a. HLW glass parameters were calculated from data in the TSPA-VA.

range tested. However, because of the weak pH dependence on sodalite dissolution, glass is predicted to dissolve faster than sodalite above pH 9. Although the dilute conditions of the buffered MCC-1 tests provide a convenient method to measure model parameter values, they do not reflect repository relevant conditions. In the TSPA-VA, the incoming groundwater is assumed to be in equilibrium with cristobalite (a major constituent of the host rock at Yucca Mountain), and the value of Q in Eq. (3) is fixed by the solubility of cristobalite. As shown in Sect. III-C, the solubility of sodalite is much lower than that of cristobalite, suggesting that the affinity term $(1 - Q/K)$ in Eq. (3) would tend toward zero for the sodalite phase of the CWF. Therefore, under repository conditions, the binder glass is predicted to dissolve faster than sodalite. Tests are in progress to differentiate between the dissolution rates of binder glass and sodalite under repository relevant conditions. For the performance modeling results described in Sect. IV, regression fits of the binder glass dissolution rates are used to represent a conservative upper bound on CWF dissolution and radionuclide release rates. The level of conservatism provided by using the binder glass dissolution rates to model the CWF is being determined experimentally.

C. Orthosilicic Acid Saturation Values

1. Testing Methodology

Saturation concentrations for the CWF and for the individual sodalite and glass binder phases were determined using long-term product consistency tests (PCT). The PCT method was selected because it is based on the MCC-3 test,[18] which was designed for this purpose. Tests were conducted at 90°C with crushed materials (-100+200 mesh fraction) in demineralized water with surface area to volume (S/V) ratios of approximately 2300 and 23,000 m^{-1}. (The sample surface area is calculated using a specific surface area of 2.3×10^{-2} m^2/g for the crushed material.) The crushed material was washed with absolute ethanol to removed fines prior to testing. Tests were conducted at two S/V ratios to verify that the measured saturation concentrations were independent of the test conditions and the solution pH. High S/V ratios were used to hasten the approach to saturation. At the end of the test duration, an aliquot was taken for pH measurement and the remaining solution was passed through a 0.45-μm pore size filter to remove any suspended particulates and then analyzed.

2. Results

Test results are shown in Table 7 and plotted in Fig. 6 as a function of the product of the S/V ratio and the test duration t in units of days per meter (d/m). This product is used as an index for the extent of reaction. Uncertainty bars are drawn at 15% of the measured value to represent analytical uncertainty. Because the measured solution pH values were less than 9.7 in all cases, it is assumed that orthosilicic acid (H_4SiO_4) is the only silicon-bearing species in solution. The concentrations of orthosilicic acid that were attained were lowest in the tests with sodalite and highest in the tests with the binder glass. The concentrations appear to reach nearly constant values after about 1×10^6 d/m in tests with sodalite and the CWF, but continue to increase slightly with $(S/V)\times t$ in the tests with glass binder.

To estimate the orthosilicic acid saturation concentration, K, for modeling, the highest concentrations measured in the tests were selected and an additional 15% was added to account for analytical uncertainty. Horizontal lines are drawn in Fig. 6 to indicate the estimated

Table 7. Orthosilicic Acid Concentrations from Long-Term PCT Tests with Sodalite, Binder Glass, and CWF

	Duration (d)	$(S/V)\times t$ (d/m)	$[H_4SiO_4]$, mg/L		
			Sodalite	Binder Glass	CWF
Tests at 2,300 m^{-1}	7	1.6×10^4	35.0	240	52.8
	28	6.5×10^4	35.0	237	78.9
	91	2.1×10^5	21.3	280	96.4
	182	4.2×10^5	36.3	229	59.3
	364	8.4×10^5	47.7	253	119
Tests at 23,000 m^{-1}	7	1.6×10^5	40.5	–	42.5
	28	6.6×10^5	9.94	–	65.8
	91	1.2×10^6	9.77	294	127
	182	3.9×10^6	19.2	321	97.7
	364	8.9×10^6	–	–	151

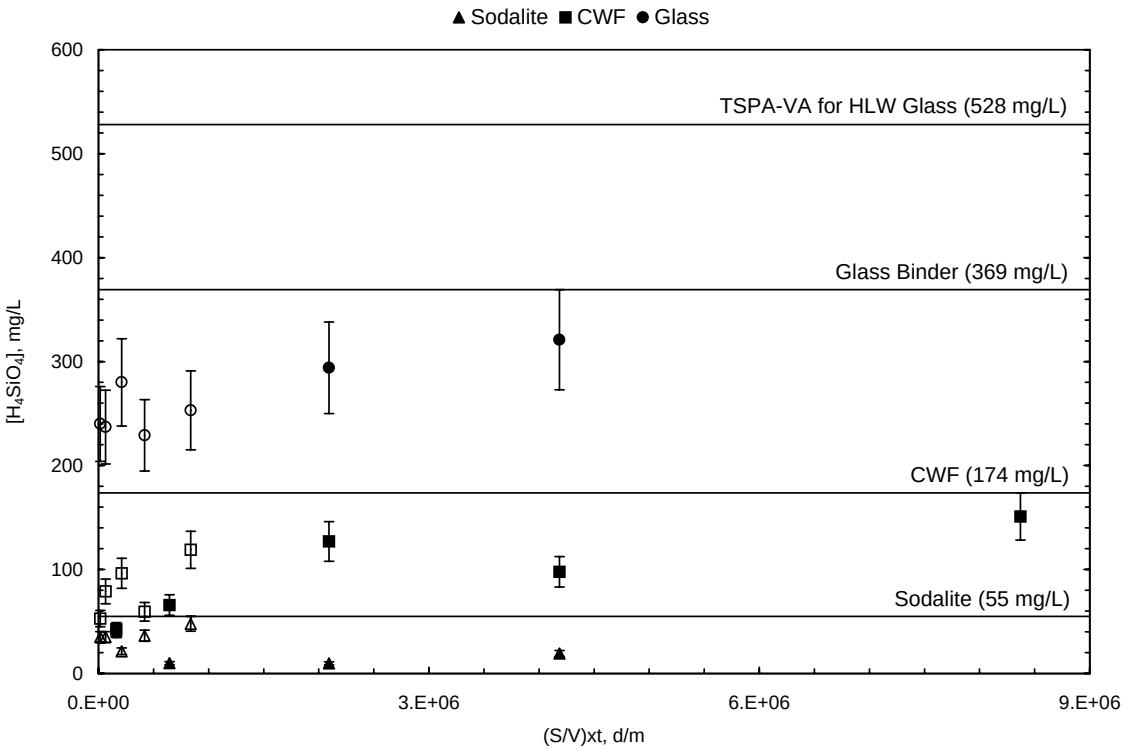

Fig. 6. Results of Long-Term PCT at 90°C with Sodalite, Glass Binder, and HIP CWF. Open symbols represent tests at 2,300 m^{-1}, filled symbols represent tests at 23,000 m^{-1}. Uncertainty bars are drawn at 15%. Horizontal lines represent estimates of orthosilicic acid saturation values for different materials (see Sect. III-C-2).

saturation concentrations for sodalite, binder glass, and the CWF. The saturation concentration of amorphous silica is also plotted. This value was used in the TSPA-VA for Yucca Mountain as a conservative bound on the saturation concentration, K, for HLW glasses. The saturation concentration of cristobalite at 90°C (not shown) is approximately 170 mg/L.[3] This is higher than the corresponding value for sodalite, suggesting sodalite would not dissolve in solutions equilibrated with cristobalite. For the performance assessment calculations presented in Sect. IV, the value from the binder glass (369 mg/L) was selected to represent a conservative bound for the CWF.

D. Status of Testing for Future Model Development

As additional results from CWF testing become available, updates to the CWF model will be made. The following subsections describe additional testing that is being pursued to refine and improve the CWF degradation and radionuclide release model. The heading for each subsection

identifies the Work Breakdown Structure (WBS) element[19] number under which the described work falls within the spent fuel treatment project. Results in these sections are typically preliminary and have not been incorporated into the CWF model and are not part of the performance assessment calculations presented in Sect. IV.

1. Effects of Process Changes (WBS No. 7.03.04)

Pressureless consolidation (PC) has been chosen to replace hot isostatic pressing (HIP) for consolidation of the CWF. PC is designed to employ existing, in-cell, powder processing equipment and technology to provide a "plug-in" alternative to HIP. PC technology enables both consolidation and forming without the need for high-pressure equipment. In addition, heat treatments used to complete consolidation of the CWF using PC methods can be achieved using basic, electric furnaces. The elimination of high pressure sources in-cell, simplification of forming operations, and the capital savings from using common heating equipment all factored into the decision to direct future scale-up efforts towards the PC process.

PC CWF specimens have a different processing history than the reference HIP CWF specimens. While the processing temperatures of 850–950°C are similar, the PC CWF is processed under atmospheric pressure while the HIP CWF is processed under 15,000–25,000 psi. The current CWF model parameters were measured in experiments using HIP CWF samples. Although no significant differences are expected, tests are needed that support the use of data obtained from tests using HIP CWF material to qualify the PC CWF. Tests are in progress to study the behaviors of PC CWF material prepared at different temperatures and for different hold times. The results of these tests will be used to select baseline processing conditions for the PC CWF.

An extensive set of specimens has been prepared using PC techniques. In addition to representing potential differences caused by processing pressure, the specimens were also held at different processing temperatures for various lengths of time ranging from 1 to 36 hours. The specimens are being tested to determine their corrosion behavior, bulk density, residual porosity, and phase assemblage and distribution.

2. Density, Porosity, and Cracking (WBS No. 7.03.04)

PC CWF specimens have higher levels of residual porosity than the reference HIP specimens. The primary impacts of the higher porosity of the PC CWF are a lower bulk density and a slightly higher specific surface area for the waste form. Lower bulk density leads to an increased waste form volume, however the containers for the PC CWF occupy space more efficiently than those used for the HIP CWF. This results in no net change to the radionuclide inventory per waste package in the repository. Although the radionuclide inventory per package is the same, a higher specific surface area leads to an increase in the waste form surface area that can be exposed to groundwater.

Residual porosity in the PC CWF is on the order of 15 vol% whereas the HIP CWF typically showed levels less than a few vol%. In a repository setting, the presence of residual porosity also increases the surface area exposed to groundwater through pores on the surface. An extensive set of PC CWF samples having a range of residual porosity levels has been prepared for corrosion testing. This set of specimens is also being characterized using electron microscopy and X-ray diffraction techniques.

Cracking has not been observed in small-scale PC CWF samples. However, scale-up, off-normal processing conditions, or transportation accidents could result in such an event. Cracking increases the exposed surface area that can be contacted by groundwater and is usually reported as a cracking factor, or multiplier, that is attached to the geometric surface area determined for a given waste form. Measured cracking factors[16] on small-scale HIP CWF samples were in the range of 4.2–4.8. In previous performance assessment calculations of the CWF,[20] a bounding value of five was used to represent cracking in the CWF degradation model. Since the extent of cracking, if any, has not yet been determined for the PC CWF, no cracking factors have been incorporated into the present model.

3. Intergranular Glass and Preferential Corrosion (WBS No. 8.01.06)

(1) Introduction

Results from microanalysis (electron microscopy with X-ray spectroscopy) of the intergranular glass phase in the CWF indicate a composition different from that of the starting glass frit used to fabricate the waste form. The glass composition changes as a result of reactions that occur during the consolidation process. Reactions such as ion exchange (primarily involving alkali ions) between the glass and crystalline aluminosilicate phases (zeolite and/or sodalite) and dissolution of aluminosilicate by the glass have been postulated to explain experimental observations.

The experimental observations and postulated reaction mechanisms may have important implications for the CWF degradation model, particularly in terms of predicting long-term radionuclide release behavior. The current CWF degradation model assumes glass dissolution rates bound overall degradation and radionuclide release rates. Glass dissolution rates have been measured in tests using the starting glass material used to fabricate the waste form. However, if the composition of the intergranular glass is sufficiently different from the starting glass to result in a significantly different dissolution rate, then the current CWF dissolution model will not correctly represent dissolution of the intergranular glass.

Experiments are underway to investigate the issues related to intergranular glass composition. The results of these experiments will feed back into degradation model development, and may also have implications for process development, such as adjustment of the starting glass composition to control ion exchange reactions and sodalite dissolution into the glass at high processing temperatures.

(2) Experimental

Initial experiments are focused on learning more about the composition of the intergranular glass. The X-ray spectroscopic methods used so far are not sensitive to light elements such as lithium and boron. Furthermore, elements such as cesium that are low in bulk

concentration and do not form small inclusions (as do the actinides) are below detection limits for X-ray spectroscopy.

Solid state nuclear magnetic resonance (NMR) methods are being investigated to provide additional characterization data. An initial set of standards has been synthesized, and experiments are underway to establish the instrumental conditions necessary to perform NMR measurements. Powder X-ray diffraction studies of the sodalite phase are also being conducted in an attempt to gain further insight into the postulated ion exchange reactions.

Once the intergranular glass composition is specified more precisely, bulk samples of glass representing a range of compositions near the observed composition will be prepared. Leach tests will be performed on samples of the synthetic intergranular glasses to assess the degradation behavior of the glass phase of the CWF and its sensitivity to glass composition.

(3) Results

Results from microanalysis of the intergranular glass, along with assumptions derived from basic glass and crystal chemistry, were used to derive an initial estimate of the intergranular glass composition. This composition is shown in Table 8, along with the composition of the starting glass for comparison. In determining the composition for the intergranular glass, it was assumed that boron did not substitute into the sodalite but remained in the glass phase. The lithium concentration (which cannot be measured by the X-ray spectroscopic methods used here) was calculated based on the requirement to maintain charge balance since the amount of experimentally measured potassium that ion exchanges from the sodalite into the glass is not sufficient to balance the sodium that ion exchanges from the glass into the sodalite.

The intergranular glass composition shown in Table 8 was used to synthesize a sample of glass for use as an initial NMR standard. So far, NMR has been able to distinguish between silicon in the glass phase and silicon in sodalite. Efforts are underway to detect a chemical shift in the lithium signal, and to detect cesium. Experimental salt mixtures high in cesium have been prepared to assist with this effort. Mixtures of glass and zeolite occluded with

Table 8. Initial Estimate of the Intergranular Glass Composition as Oxide Weight Percents. The measured composition of the starting glass frit (P57) is shown for comparison.

Oxide	Intergranular Glass (wt%)	P57 Glass
SiO_2	65.9	63.2
Al_2O_3	17.6	7.3
B_2O_3	9.4	17.8
K_2O	1.6	0.5
Li_2O	2.8	n. a.[a]
CaO	2.7	2.0
Na_2O	0	6.9

a. This oxide is not present.

this experimental salt have been heated to pressureless consolidation process temperatures. Microanalysis of this material has shown cesium in both the glass and sodalite phases, indicating that some partitioning of cesium does take place during consolidation.

4. Colloid Generation (WBS No. 08.01.02)

Examination of the reaction of zeolite 4A (dried to <0.2 mass percent H_2O) with uranium-doped eutectic salt (UCl_3 + LiCl-KCl) by temperature-resolved X-ray diffraction, evolved gas analysis, and differential scanning calorimetry showed that the uranium in this simulated electrorefiner salt reacted with residual water in the dried zeolite to form UO_2 as follows:[21]

$$2UCl_3(\text{in salt}) + 4H_2O(\text{in zeolite}) = 2UO_2(\text{solid}) + 6HCl(\text{gas}) + H_2(\text{gas})$$

X-ray diffraction and scanning electron microscopy studies of salt-loaded zeolite doped with uranium and plutonium showed that the uranium and plutonium in a simulated electrorefiner salt reacted with residual water in the dried zeolite to form the mixed oxide $(U,Pu)O_2$. Transmission electron microscopy (TEM) images of U/Pu-doped HIP CWF revealed inclusions of ~10-nm

$(U,Pu)O_2$ particles clustered mostly within the glass phase near sodalite interfaces (see Ref. 16, Sects. II-B and II-C). Since the $(U,Pu)O_2$ particles are of colloidal size, the corrosion testing program included three types of analyses to determine the size and concentration of colloidal particles released during PCT: sequential filtration of solutions after testing, dynamic light scattering of test solutions, and TEM examination of carbon grids through which test solutions were wicked.

Results from corrosion tests of U/Pu-doped HIP CWF to date, including chemical analyses of solutions that have been passed sequentially through filters of 450, 100, and 5 nm pore sizes, indicate that the normalized releases of U and Pu are much smaller than the normalized releases of matrix elements, that the concentration of Pu in the 450-nm and 100-nm filtrates is much higher than the known saturation concentration of Pu(IV) under laboratory conditions, and that most of the uranium and almost all of the plutonium are released as colloid-sized particles in the 5-100-nm size range or become adsorbed on test vessel walls. TEM examination of wicked test solutions show $(U,Pu)O_2$ particles 10-50 nm in diameter, sometimes associated with larger aluminosilicate colloids of about 100 nm in size. Dynamic light scattering results indicate the colloidal-sized particles have diameters of 90 ± 40 nm. The corrosion tests of U/Pu-doped HIP and PC CWF, as well as analyses for colloids by TEM and dynamic light scattering, are still in progress.

Three types of colloids are recognized to be important as components in the mobilization of radionuclides released from HLW glass: waste-form colloids from the glass, corrosion-product colloids formed during corrosion of iron-containing waste packages, and groundwater colloids.[22] The $(U,Pu)O_2$ particles released from the CWF are similar to the first of these three colloid types. Further research is necessary to establish that the linear isotherm sorption model used for smectite clay colloids released from HLW glass is appropriate for $(U,Pu)O_2$ particles released from the CWF.

5. Effects on Dissolution Due to Aqueous Species (WBS No. 08.01.01)

Only the effect of orthosilicic acid is considered in the rate expression for borosilicate waste glasses. The concentration of dissolved silica (as orthosilicic acid) and its saturation

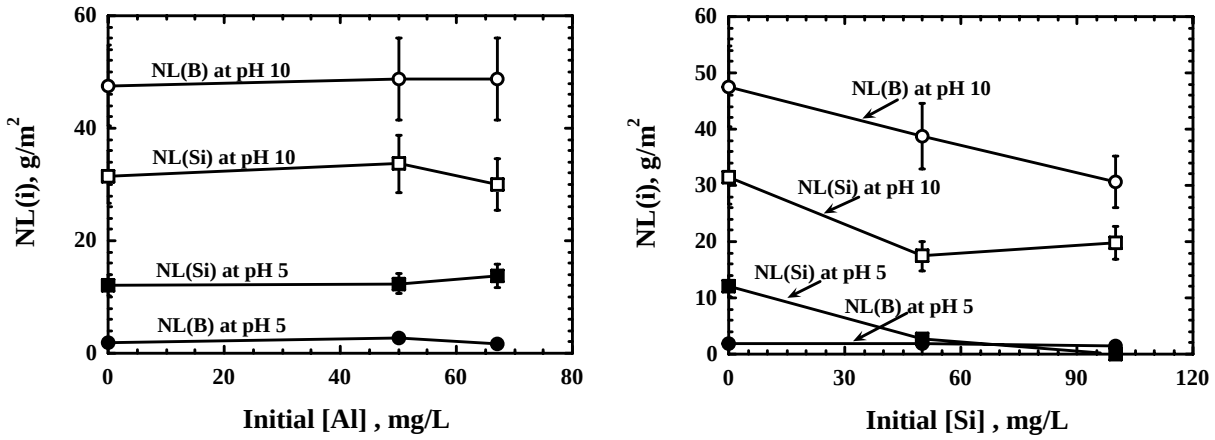

(a) Dissolved Al (b) Dissolved Si

Fig. 7. Normalized Mass Losses of Boron and Silicon from Corrosion Tests to Measure the Effects of (a) Dissolved Al and (b) Dissolved Si on Dissolution of HIP CWF

concentration are used for Q and K, respectively. Dissolved aluminum has been found[23] to affect the dissolution rate of some minerals. Therefore, tests were conducted with the HIP CWF to determine if both silicon and aluminum affected the dissolution rates of the glass binder and sodalite phases of the CWF.

Tests were conducted for seven days at 90°C with monolithic samples in dilute pH-buffered solutions. Solution pH was adjusted to 5 or 10 with dilute buffers as in Sect. III-B-1 above. Similar buffered solutions were spiked with dissolved aluminum or dissolved silicon. The results are shown as the normalized mass losses of boron and silicon in Fig. 7. Boron is used to track the dissolution of the glass and silicon is used to track the dissolution of the glass binder and the sodalite. (The values of NL_{Si} plotted in Fig. 7 have been corrected for silicon in the initial solutions.) The presence of silicon in the solution slows the dissolution of both the glass and sodalite phases. The presence of aluminum does not slow the dissolution of either phase. The presence of silicon in the test solution also slowed the dissolution of pure sodalite and pure glass binder phases, whereas the presence of aluminum did not have a measurable effect.

6. Radiation Damage Studies (WBS No. 8.01.03)

(1) Introduction

One aspect of waste form qualification for geological repository acceptance is to be able to predict the behavior and radionuclide release mechanisms of the waste form after prolonged radiation exposure. Of primary concern is waste form alteration due to alpha-decay damage, although beta and gamma decay of radionuclides in the CWF can also damage the waste form. For a recent review on studies of the effects of radiation damage to materials, see Ref. 24.

Alpha-decay damage results from dissipation of energy from both the alpha particle and the recoil nucleus that emitted the alpha particle. The alpha particle, with an approximate energy of 5 MeV and a typical range of 20 μm, imparts its energy to the surrounding matrix by both electronic excitation and direct elastic collision. The recoiled nucleus, with energies of 80–100 keV and ranges of only tens of nanometers, disrupts neighboring atoms primarily by elastic collisions. For the alpha decay of ^{239}Pu in a crystalline matrix, the ejected alpha particle may dislocate up to 200 matrix atoms by the end of its track. The recoil ^{235}U nucleus may displace over 1000 local atoms, depending on the atomic density and displacement energy of the material. Over the expected lifetime of a geologic repository, waste forms containing actinides could accumulate significant structural damage that may adversely influence the materials performance with respect to radionuclide retention. Alpha-decay studies of crystalline materials or glass materials containing actinide host phases reveal that the crystalline material may become amorphous due to accumulation of dislocated matrix atoms. Amorphization of crystalline phases leads to volume increases that may, in turn, lead to microcracking. Additionally, after prolonged exposure, helium or other gas bubbles may develop also resulting in swelling and cracking of the waste form. This swelling and cracking of the material usually has a detrimental affect on the durability of the waste form. However, some crystalline materials, such as PuO_2, UO_2, and ZrO_2 for example, show little damage to the crystalline structure after prolonged radiation exposure.

Many tests have been conducted to identify the effects of alpha damage on radionuclide release from HLW glass.[9] Some tests show an increased release of plutonium and silicon under high alpha dose rates, while others showed no differences between glasses doped with Cm-244 (4×10^{18} alpha/cm^3) and those doped with Pu-239 (2×10^{14} alpha/cm^3). By comparison, the maximum alpha activity of the CWF is expected to be less than 1.4×10^{7} alpha/cm^3/s (see Table 2). Tests on natural and artificial obsidians showed higher release rates at 60°C but no change at 90°C. This was attributed to rapid annealing at the higher temperatures. Gamma irradiation of glass prior to leach testing did not cause any measurable increase in elemental release.[9]

Iodosodalite has been considered as an immobilizing matrix for ^{129}I. It is identical to naturally occurring sodalite but with occluded iodide salts rather than chloride salts. Both natural sodalite and iodosodalite exhibited no structural changes[25] after gamma irradiation to 10^9 R and fast neutron bombardment to 2×10^{17} n/cm^2.

It is uncertain whether alpha damage will increase overall release rates from the CWF based on the above observations. However, the relatively low activity of the CWF may mitigate this effect while allowing more time for annealing. In the CWF, many of the actinides form small, discrete oxide phases within the glass. This will localize the ballistic damage caused by the recoil nucleus during alpha decay and could minimize radiation damage effects. Any conclusions about radiation damage to the CWF or modifications to the CWF model must be based on experimental evidence.

To investigate the potential long-term effects of alpha-decay damage on CWF durability in a reasonable time period, tests were initiated using a CWF containing surrogate fission products and ^{238}Pu as opposed to ^{239}Pu. The use of ^{238}Pu, with its high specific activity of 3.8×10^{13} decays/min/g and short half-life of 88 years, allows significant alpha-decay dose in a much shorter time as compared to ^{239}Pu. Results from these tests are summarized from approximately the first year and a half of a four-year study with a cumulated alpha-decay dose of approximately 6×10^{17} alpha-decays/gram of material. The total accumulated dose at the end of the four-year study will be approximately 2×10^{18} alpha-decays/gram of material. To acquire an equivalent dose using ^{239}Pu would require approximately 1100 years.

(2) Experimental

Production of the ^{238}Pu-loaded CWF started by occluding the LiCl/KCl eutectic salt containing surrogate fission products and Pu in dry (<0.5 wt% moisture) zeolite 4A. The zeolite was then mixed with a glass binder and consolidated at a temperature of 750°C and a pressure of 5100 psi. During the consolidation process, the zeolite converts to sodalite. The fission-product-surrogate salt contains KBr, KI and chlorides of Na, Rb, Sr, Y, Cs, Ba, La, Ce, Pr, Nd, Sm and Pu. The CWF was loaded to approximately 2.5 wt% ^{238}Pu. This plutonium loading is roughly 3 to 20 times the actual plutonium loading of the CWF that will be produced during the fuel treatment process. After contacting with the zeolite, the plutonium converts to an oxide. This conversion is presumably due to the reaction of plutonium with oxygen from residual water in the zeolite.

Evaluation of the effects of alpha-decay damage on the ^{238}Pu-loaded CWF involves microstructure and bulk phase characterization, bulk density measurement, and waste form durability. The ^{238}Pu-loaded CWF is being analyzed on a periodic basis to evaluate alpha-decay damage to the waste form. The testing schedule is planned for a minimum of four years. The specific methods used to study the extent of alpha-decay damage on the CWF are:

1. Waste form microstructure and elemental distribution investigated by scanning electron microscopy (SEM) in conjunction with energy and wavelength dispersive spectroscopy (EDS/WDS). Transmission electron microscopy (TEM), in conjunction with electron diffraction (ED) and EDS, is also performed.

2. Powder X-ray diffraction (XRD) is used to monitor bulk phase composition and changes to major phase lattice parameters.

3. Density measurements on the CWF are performed using an immersion method. Density measurements provide information on macroscopic swelling as a function of cumulative dose.

4. Durability of the ^{238}Pu-loaded CWF, with cumulated alpha-decay dose, is compared to the nonradioactive CWF reference material using the PCT-A leach method.[26] The leach test uses a crushed material with a −100 to +200 mesh size fraction, demineralized water for the leachant, and a surface area to volume ratio of 2000 m^{-1}. Elemental determination of the leachate is performed by inductively coupled plasma—mass spectrometry.

(3) Results

The results presented here include observations and measurements made prior to the halfway point of the four-year test period. The cumulated alpha-decay dose for these results is approximately 6×10^{17} decays/gram of material. At this time, only one chemical durability test (PCT) has been performed on the ^{238}Pu-loaded CWF and that was made right after production of the material. The PCT results of the ^{238}Pu-loaded CWF indicate that the high Pu-loaded waste form has an elemental release rate similar to the reference CWF. The second chemical durability test of the CWF will be performed in December 2000, with an expected cumulated dose of approximately 7×10^{17} decays/gram of material.

No significant microscopic or macroscopic alteration to the waste form, as a whole, has been observed by microscopy or X-ray diffraction measurements at this time. The microstructure and phase composition of the ^{238}Pu-loaded CWF is very similar to the reference waste form except for a very minor Pu containing aluminosilicate phase that is not observed in the reference CWF. This new phase probably results from the high Pu loading of the material used for these experiments. The unit cell volume of the PuO_2 phase has expanded by approximately 0.6 vol%, which was expected, and results from lattice defects induced by alpha decay. The sodalite unit cell may also be expanding, but to much less extent than the PuO_2 phase.

Because Pu is overwhelmingly found as the PuO_2 phase concentrated in the intergranular glass regions, the majority of decay damage is expected to occur locally in these regions. Due to the concentration of Pu in the radiation damage resistant PuO_2 fluorite structure, very little alpha-decay damage to the total waste form is expected. The one exception to this may

be the formation and accumulation of helium bubbles resulting from alpha decay. Interim results from bulk density measurements of the CWF have remained constant indicating no significant swelling of the waste form during the test period to date.

With the exception of the very minor Pu aluminosilicate phase and the expected unit cell volume increase of the PuO_2 phase, the ^{238}Pu-loaded CWF is very similar in composition and behavior to the reference CWF and has shown no significant alteration due to alpha-decay damage at an accumulated dose of approximately 6×10^{17} decays/gram of material.

IV. REPOSITORY PERFORMANCE ASSESSMENT MODELING

The anticipated impact of the CWF on the performance of the Yucca Mountain repository is evaluated in this section. The waste forms are subjected to repository environmental conditions as represented by the Total System Performance Assessment—Viability Assessment (TSPA-VA) model obtained from the Yucca Mountain Project.[2,3] The following paragraphs briefly describe changes that were made to the TSPA-VA model to facilitate evaluation of the CWF. They also describe how variability in climate and flow conditions introduce increased variability in the release of radionuclides from the engineered barrier system (EBS). Finally, the implementation of the CWF degradation model described in Sect. III and calculations of the release of radionuclides from the EBS are discussed. Radionuclide release from the CWF is compared to release from commercial spent nuclear fuel (SNF), HLW glass, and DOE spent nuclear fuel.

A. Performance Assessment Model

A preliminary assessment of the performance of the ceramic and metal waste forms was reported in Ref. 27. In order to assess waste form performance in the Yucca Mountain Repository, the waste forms were included as separate sources in the TSPA-VA model obtained from the Yucca Mountain Project. The TSPA-VA model was based on the Repository Integration Program (RIP) developed by Golder Associates, Incorporated.[28] The analyses carried out in Ref. 27 made use of a simplified version of the TSPA-VA model developed by Golder Associates, Incorporated.[29] It contained the same EBS model as in the original TSPA-VA model. Simplifications were

introduced to represent the transport of radionuclides through the unsaturated and saturated zones below the repository horizon in Yucca Mountain. Currently, only about 26 MT of sodium-bonded spent nuclear fuel will undergo electrometallurgical treatment. Thus, one can expect that the resulting waste will have a negligible impact on the repository. This would be particularly true for the dose rate to individuals who might use water from a well 20 km distant from the repository. Not surprisingly, calculations with the simplified model verified this expectation. But this also meant that the dose rate would not be a satisfactory indicator of the performance of the ceramic or metal waste forms in the repository. It was, therefore, decided to use the cumulative release of individual radionuclides from the EBS as an indicator of the waste form performance.

For the performance assessment calculations reported here, the EBS model from the TSPA-VA was replicated in the Windows-based simulation program, GoldSim,[30] making use of its contaminant transport module.[31] Several verification calculations were performed in which the cumulative release of ^{129}I and ^{99}Tc from the EBS was compared between RIP and GoldSim. The comparisons used expected values for all stochastic input parameters, and were made for 10,000-, 100,000-, and 1,000,000-year simulations. They showed good agreement at the end of 100,000- and 1,000,000-year simulations (within a few percent), but the GoldSim results were consistently higher than the RIP results in the 10,000-year simulation (in some cases by a few tens of percent). The reason for the poor agreement in the 10,000-year simulation was traced to the fact that the RIP model was predicting initial package failure as much as 600 years later than in the GoldSim calculations. Both codes were using the same waste package failure distributions. Further examination indicated that the initial package failure time was calculated correctly in GoldSim and incorrectly in RIP. It was concluded that the GoldSim model of the EBS was performing properly and that the model could be used for the performance assessment of the CWF. The transport of radionuclides through the unsaturated and saturated zones is not modeled in GoldSim, so calculations can be performed much more quickly than with the simplified RIP model.

B. Conditions for Waste Package Failure

In the TSPA-VA model, waste packages may be placed in each of four different environmental conditions. In the first, packages are exposed to dripping water at all times. In the second,

packages are exposed to dripping water only during long-term-average and super-pluvial climate conditions. In the third, packages are exposed to dripping water only during super-pluvial climate conditions, and in the fourth, the packages are never exposed to dripping water. For each realization, the TSPA-VA model randomly samples the fraction of the total number of packages for each source that are assigned to each of these environmental conditions. The model is constructed so that the same fraction of packages is assigned to given environmental conditions for each source. Thus, if a given fraction of the packages of commercial SNF is assigned to the no-drip environment, then the same fraction of defense HLW packages, DOE SNF packages, CWF packages, and metal waste form packages are assigned to the no-drip environment. Packages in the dripping environmental conditions have a common failure distribution. Packages in no-drip environmental condition have a package failure distribution that prevents package failures for hundreds of thousands of years.

Within each environment, the flow of water dripping onto a waste package depends on the climate. The durations for the current dry climate and for subsequent periods of dry climate are randomly sampled. In addition, the durations for long-term-average climate conditions and of super-pluvial climate conditions are also randomly sampled. Dripping flows for the dry, long-term-average, and super-pluvial climate conditions are randomly sampled.

The variability in the number of packages assigned to various environmental conditions in combination with variability in the duration of a given climate and variability in the dripping flow during that climate contributes significantly to variability in the release from the EBS. This variability in the release will be evident when probability distributions are estimated for the release.

C. Ceramic Waste Form Model Implementation

The CWF degradation rate is calculated according to Eq. (3). Values for $k_f(T, \mathrm{pH})$ are determined by Eq. (7) using the parameters for binder glass dissolution in Table 5. Temperature and pH values as a function of time are provided by the EBS model for the TSPA-VA.

As described in Sect. III-C, an orthosilicic acid saturation value, K, of 370 mg H_4SiO_4/L at 90°C has been determined for the CWF. Because the temperature dependence is not known, the temperature dependence for K_{HLW} is assumed to apply. If the temperature dependence of K_{HLW} is defined by the function $f(T)$ such that at 90°C $f(90) = 1$, then

$$K_{HLW}(T) = K_{HLW}^{90} f(T), \tag{8}$$

where K_{HLW}^{90} is the orthosilicic acid saturation value for HLW glass at 90°C. If the same temperature dependence is assumed to apply to the orthosilicic acid saturation value for the CWF, then

$$K_{CWF}(T) = K_{CWF}^{90} f(T). \tag{9}$$

Dividing Eq. (9) by Eq. (8) and solving for $K_{CWF}(T)$ leaves

$$K_{CWF}(T) = \frac{K_{CWF}^{90}}{K_{HLW}^{90}} K_{HLW}(T). \tag{10}$$

Because in-package chemistry effects are not represented in the EBS model for the TSPA-VA, the value of Q in the CWF degradation model is fixed by the incoming groundwater which is assumed to be in equilibrium with cristobalite. The HLW glass model in the TSPA-VA defines a regression[3] for the ratio of $Q(T)/K_{HLW}(T)$. By using Eq. (10), the ratio of Q/K_{CWF} in the CWF model can be determined using the same regression by simply multiplying by the factor $K_{HLW}^{90}/K_{CWF}^{90}$.

A value for k_{long} has not been established for the CWF. If the value of k_{long} for HLW glass were assumed to apply, it would contribute only a few percent to the overall dissolution rate of the CWF as calculated by Eq. (3). From this observation, it is expected that k_{long} is relatively unimportant and is, therefore, excluded in the present analysis.

Based on an assumed production-scale CWF monolith,[32] the specific surface area of the CWF was fixed at 5.638×10^{-6} m^2/g. The extent of cracking in full-scale PC-CWF monoliths has

not been determined. For the present calculations, no cracking factors were used in the CWF model. Radionuclide inventories for the CWF were obtained from Ref. 33.

Like the HLW glass model used in the TSPA-VA, the CWF model does not take credit for the retention of radionuclides in alteration phases. As a result, radionuclides are made available for transport once released from the waste form matrix. In addition, the CWF model takes no credit for the durability of any containers inside the waste package.

The CWF model was integrated into the performance assessment model through the use of a dynamic link library (DLL) similar to the one used to represent HLW glass degradation in the TSPA-VA. GoldSim provides the DLL with 11 parameters, two of which represent waste package temperature and groundwater pH. The performance assessment model represents uncertainty in the data through the use of stochastic parameters. In addition to temperature and pH, the CWF DLL accepts nine additional parameters sampled from a normal distribution with zero mean and unit variance. Six of the nine parameters are used to sample uncertainty in the regression parameters C_0, C_1, and C_2 for both the acid and base leg of the binder glass regression fit. For example, the regression parameter C_0 for the binder glass would be calculated in the base region as

$$C_0 = -0.944 + N(0, 1)0.107,$$

where $N(0, 1)$ is one of the stochastic parameters provided by GoldSim. The remaining three parameters are used to represent uncertainty in the data used in the TSPA-VA for Q/K_{HLW} and $k_{\mathrm{long}}^{\mathrm{HLW}}$. The DLL provides a single output parameter that represents the CWF degradation rate. Source code for the CWF DLL is listed in Appendix B.

D. Waste Form Performance in the Repository

The paragraphs that follow focus on the cumulative releases for two radionuclides, namely, ^{129}I and ^{237}Np. These radionuclides are two of the three radionuclides found in the TSPA-VA to be dominant contributors to the dose rate at the 20-km well. ^{99}Tc and ^{129}I dominate and contribute about equally to the dose rate during the first 40,000 years. ^{99}Tc is found in the metal waste form[1] but is not expected to be present in the CWF. During the period from about

40,000 years to 60,000 years a transition occurs from dominance by ^{99}Tc and ^{129}I to dominance by ^{237}Np. Following 60,000 years, ^{237}Np is the dominant contributor to the dose rate. For each radionuclide, the cumulative release is evaluated as the integral of the mass rate of release. Normalized cumulative releases are evaluated by dividing the cumulative release by the initial mass of the radionuclide in a given waste form. The results presented are based on the average of 1000 time histories. Each time history was calculated using an independent random sample of all stochastic input parameters in the EBS model. To avoid differences in the release related to the time of initial waste package failure, each source was arbitrarily assigned 1000 waste packages. The releases reported below are for a single average waste package.

1. Release of I-129

Because of its expected high solubility in Yucca Mountain groundwater, the release of ^{129}I from the EBS is controlled by the degradation of the waste form. The presence of ^{129}I in the CWF makes the release of this radionuclide a good indicator of performance. This isotope is not present in the metal waste form. The normalized cumulative release of ^{129}I from the EBS is shown in Figs. 8, 9, and 10, respectively, for the time periods of 10,000, 100,000, and 1,000,000 years. The results show that the normalized releases for the CWF and defense HLW glass are similar. The releases for both waste forms are about a factor of three higher than for commercial SNF. However, the rate at which defense HLW glass degrades includes a cracking factor of 21. As noted earlier, the cracking factor for the CWF is set to unity because of the absence of information on the cracking of the waste form monoliths. If further information reveals that the CWF cracking factor is greater than unity, then release will be higher.

Figures 11, 12, and 13 show estimated percentile time histories for the release of ^{129}I from the EBS for the CWF. The figures present, respectively, results for each of the 10,000-, 100,000-, and 1,000,000-year simulations. The value at each time-point on P^{th}-percentile curve is the release that is greater than or equal to the release on $10 \times P$ out of 1000 realizations. In addition to the percentile time histories, time histories for the upper bound and the mean release are shown for each simulation time. Similar plots, with similar spreads could be constructed for each of the other waste forms. The percentile plots show that on any given realization, a broad range of

releases is possible. In addition, the plots show that at each time point, the probability density for the release is strongly skewed toward low releases. This is evident from the fact that the mean release is almost always in the range between the 75^{th} and the 95^{th} percentiles. In fact, for the first 10,000 years, the median release is zero.

The broad range indicated by the percentiles in Figs. 11, 12, and 13 should not be interpreted to mean, for instance, that there is a significant probability that the release from the CWF or defense HLW glass will exceed the release from DOE SNF. As mentioned earlier, much of the variation indicated by the percentile plots is caused by variation in climate and flow conditions and in the fraction of packages failing under various environmental conditions. These conditions will be the same for each of the waste forms. This means, for instance, that if a high release from the CWF is predicted for a given realization, a high release will generally be predicted from the other waste forms as well.

2. Release of Np-237

The TSPA-VA model assumes that the solubility for neptunium is stochastic. The probability distribution ranges from 0 up to about 13 g/m^3. The distribution has a mean of about 0.78 g/m^3 and a median of about 0.3 g/m^3. Thus, on any given realization, the solubility for neptunium will be relatively small and the release rate of ^{237}Np from the EBS will usually be given by the product of the solubility and the volumetric dripping flow. Only in cases where the inventory of ^{237}Np is relatively small and/or the degradation rate of the waste form very low will the release be controlled by the waste-form degradation. For waste forms releasing ^{237}Np fast enough to keep the concentration in the water at the solubility limit, the normalized cumulative release will be smallest for that waste form having the largest ^{237}Np inventory. So long as the release is controlled by solubility, the normalized cumulative release will not be a good indicator of the performance of the waste form. Therefore, the assessment of waste form performance with respect to the release of ^{237}Np will focus more on the cumulative mass release and less on the normalized cumulative release.

Figure 14 shows the cumulative mass release of ^{237}Np for each of the waste forms included in the TSPA-VA model as well as for the CWF during the first 10,000 years. The result shown is the total mass released divided by the total number of waste packages. The curves for the CWF and defense HLW glass stay together until about 6500 years and follow the curve for DOE SNF. At 6500 years, the curve for the CWF drops below the other curves. This indicates that after 6500 years, the release from the EBS of ^{237}Np from the CWF is no longer controlled by solubility limits but is controlled by the degradation of the waste form matrix. The difference between the curves for DOE SNF and defense HLW glass and the curve for commercial SNF is caused by the fact that the commercial SNF package is a different size than all the other waste packages. The degradation model for the CWF predicts a degradation rate similar to the degradation rate for defense HLW glass. Since the CWF has a ^{237}Np inventory about 27 times smaller than the inventory for defense HLW glass, the CWF release drops away from the solubility limit first.

The cumulative mass release for the first 100,000 years is shown in Fig. 15. The initial mass of ^{237}Np in a defense HLW package is about five times larger than in a package of DOE SNF. However, the degradation rate for DOE SNF is more than five times the degradation rate for defense HLW glass. Thus, the mass release curve for defense HLW glass drops away from the solubility limited curve earlier than that for DOE SNF. At around 70,000 to 80,000 years, the mass release curve for DOE SNF begins to drift away from the curve for commercial SNF. This indicates that the release from DOE SNF is no longer limited by solubility.

Figure 16 shows the cumulative mass releases for a 1,000,000-year simulation. By the end of the simulation, the mass releases are in the same order as the magnitude of the initial mass of ^{237}Np in the waste forms. Some calculations not described here suggest that the release from commercial SNF ceases to be limited by solubility after about 300,000 years. The normalized cumulative release for ^{237}Np is shown in Fig. 17 for the 1,000,000-year simulation. The normalized cumulative release of ^{237}Np is somewhat lower than the corresponding normalized cumulative release for ^{129}I. This is due in part to the fact that ^{237}Np has a half-life of 2,140,000 years while the half-life for ^{129}I is 15,700,000 years.

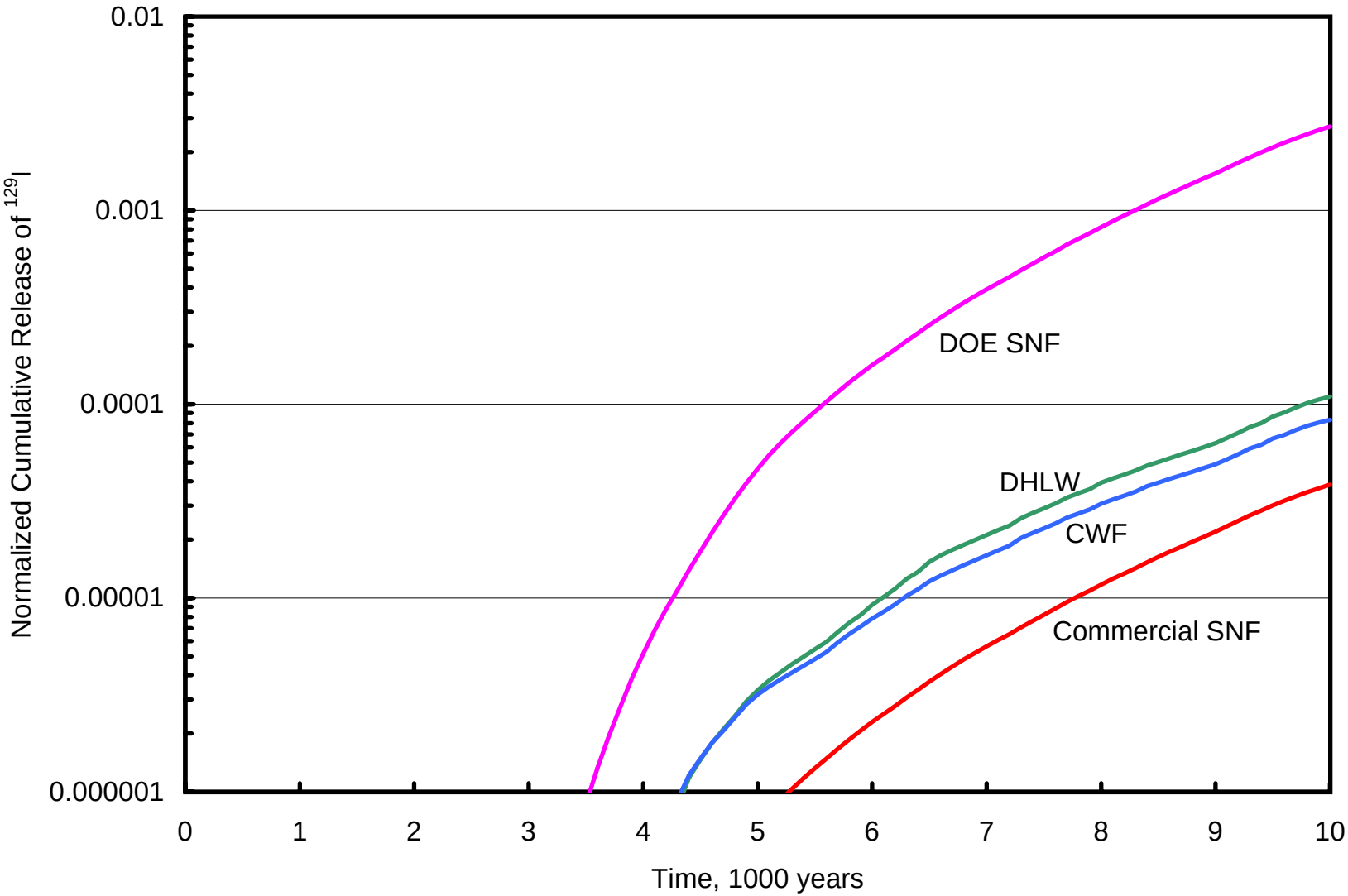

Fig. 8. Normalized Cumulative Release of ^{129}I from the CWF, DOE SNF, HLW Glass, and Commercial SNF Over 10,000 Years. Release from the CWF is based on the model presented here and employs no cracking factors. Release models for the other waste forms are from the TSPA-VA for Yucca Mountain.

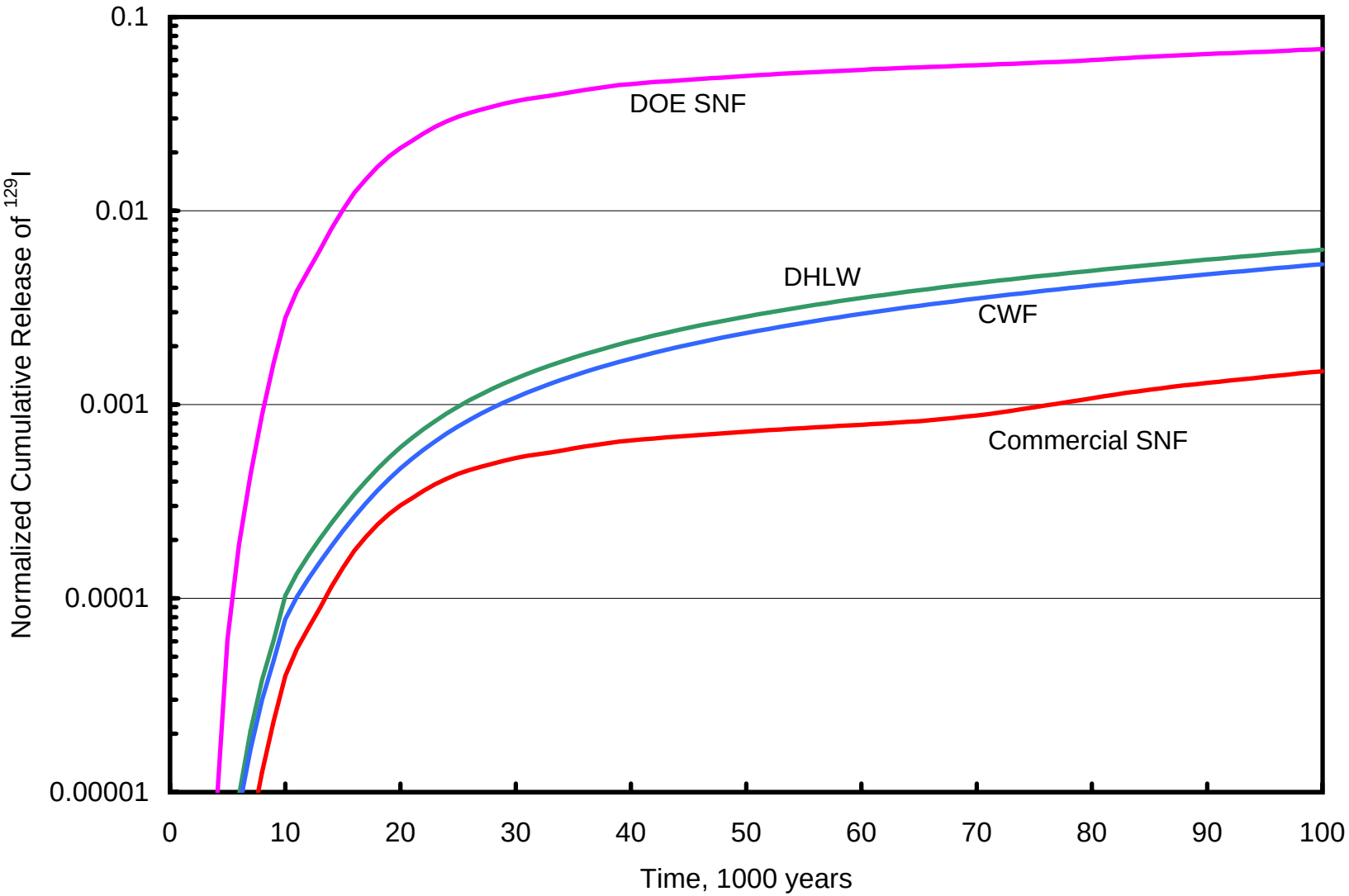

Fig. 9. Normalized Cumulative Release of ^{129}I from the CWF, DOE SNF, HLW Glass, and Commercial SNF Over 100,000 Years. Release from the CWF is based on the model presented here and employs no cracking factors. Release models for the other waste forms are from the TSPA-VA for Yucca Mountain.

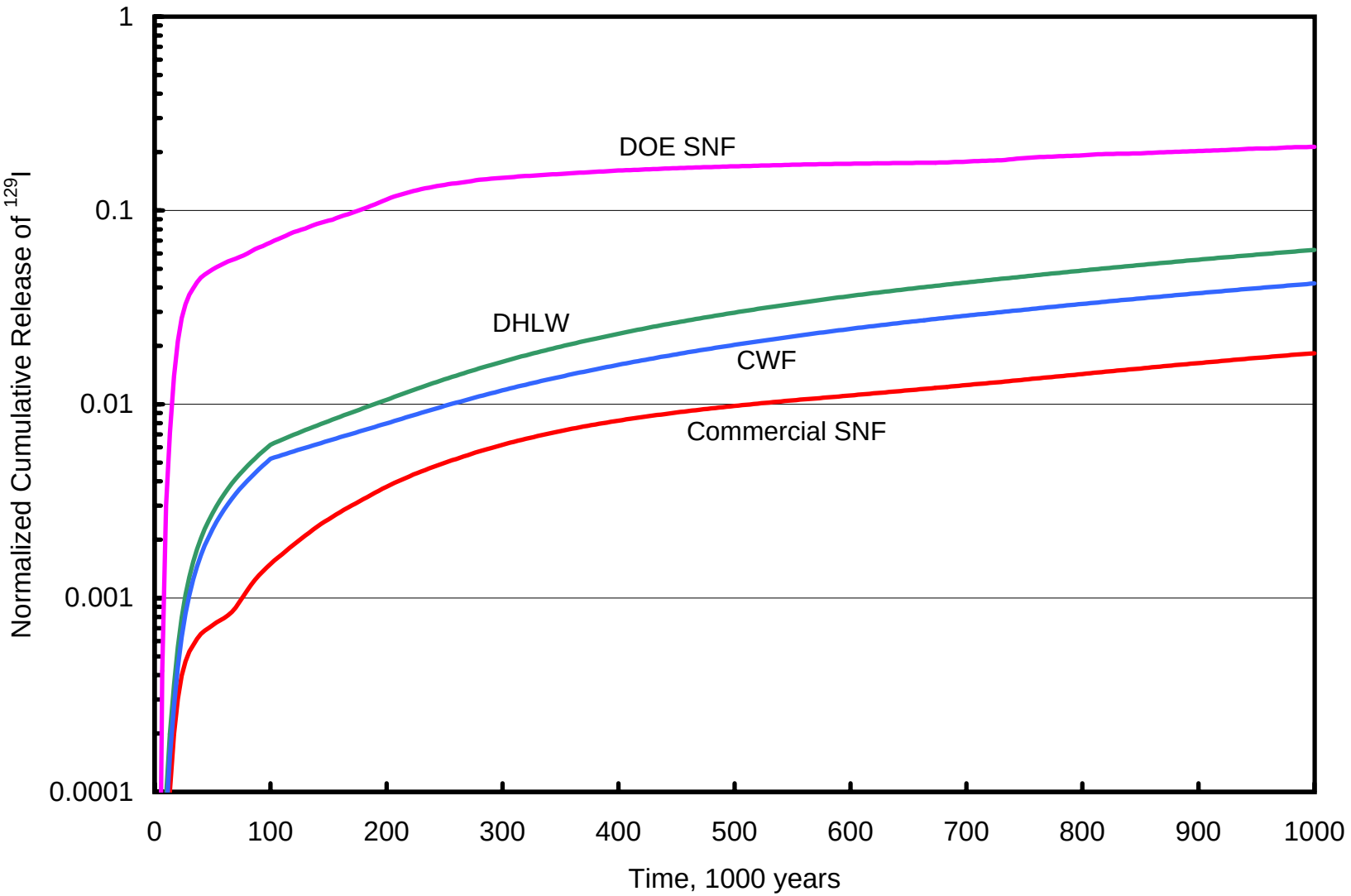

Fig. 10. Normalized Cumulative Release of ^{129}I from the CWF, DOE SNF, HLW Glass, and Commercial SNF Over 1,000,000 Years. Release from the CWF is based on the model presented here and employs no cracking factors. Release models for the other waste forms are from the TSPA-VA for Yucca Mountain.

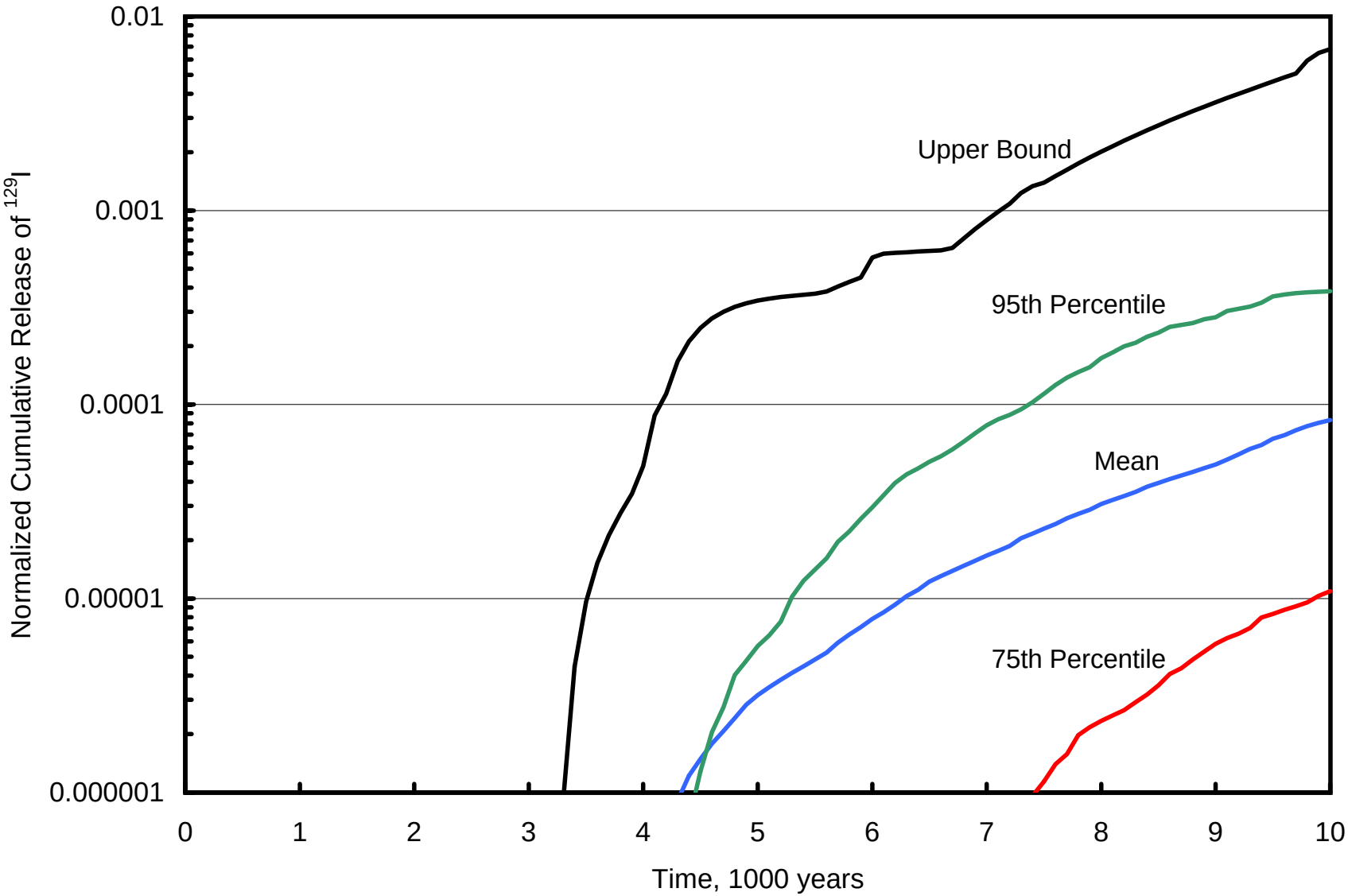

Fig. 11. Probability Distribution for the Normalized Cumulative Release of ^{129}I from the CWF Over 10,000 Years.

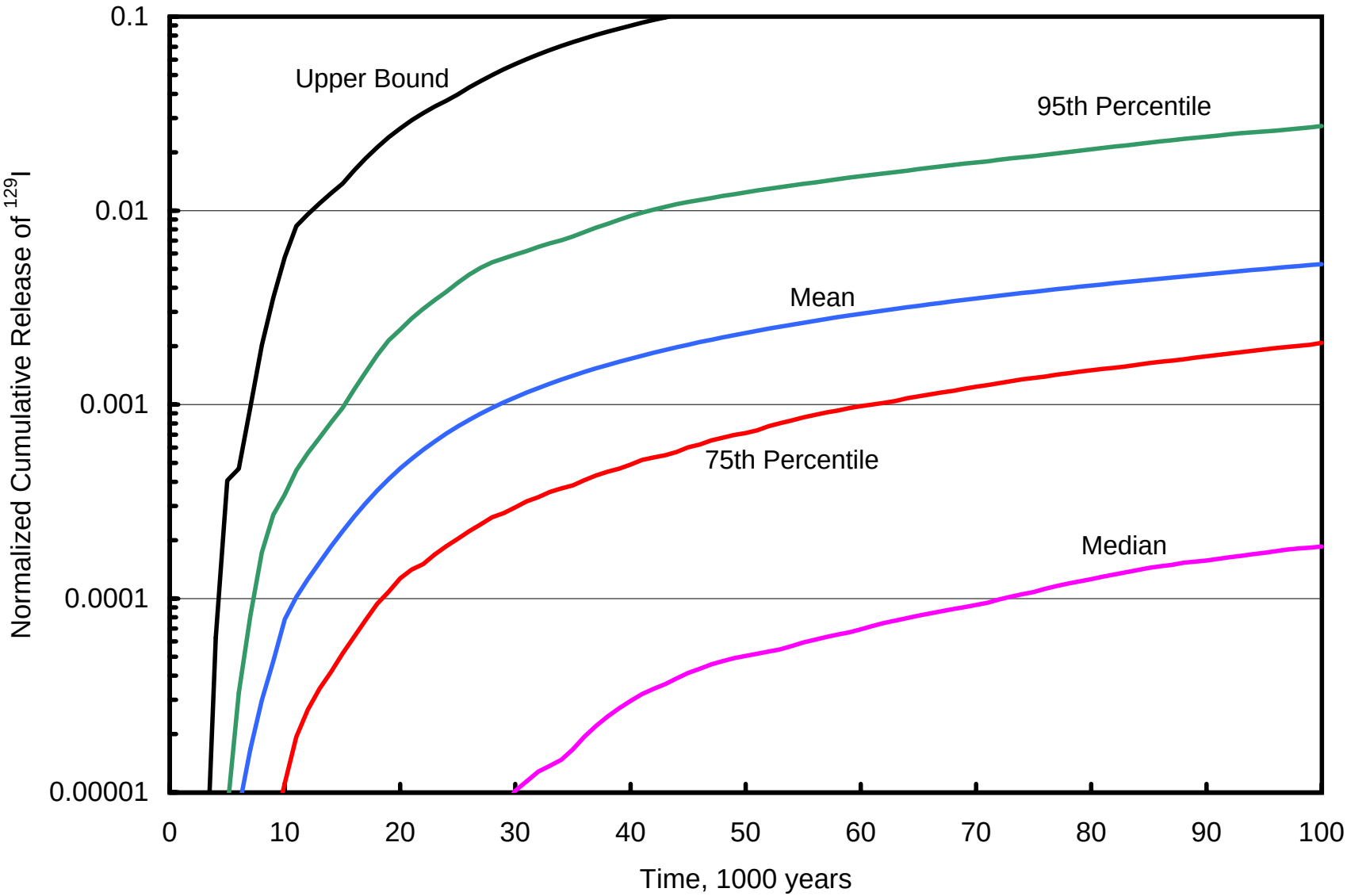

Fig. 12. Probability Distribution for the Normalized Cumulative Release of ^{129}I from the CWF Over 100,000 Years.

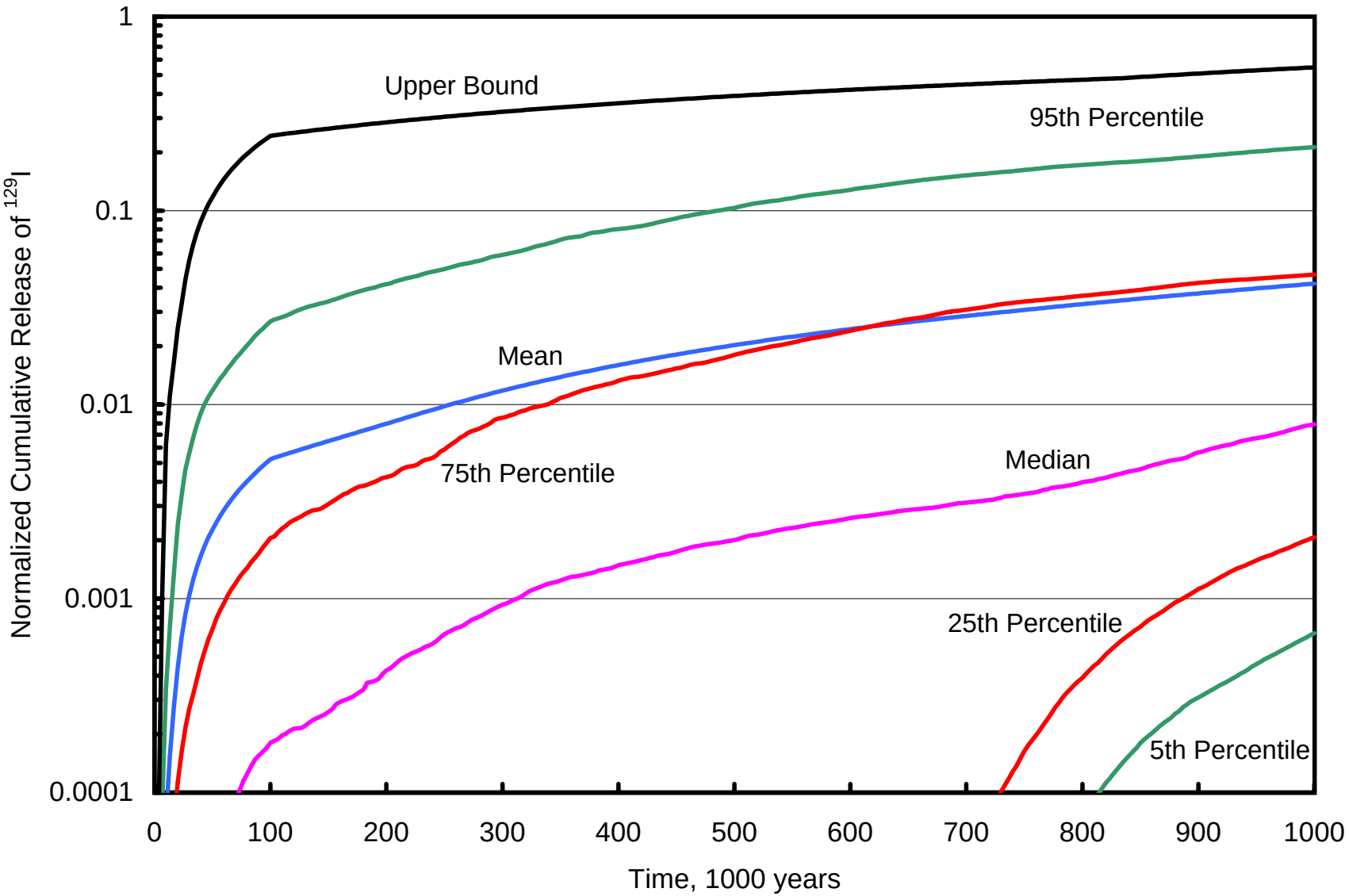

Fig. 13. Probability Distribution for the Normalized Cumulative Release of ^{129}I from the CWF Over 1,000,000 Years.

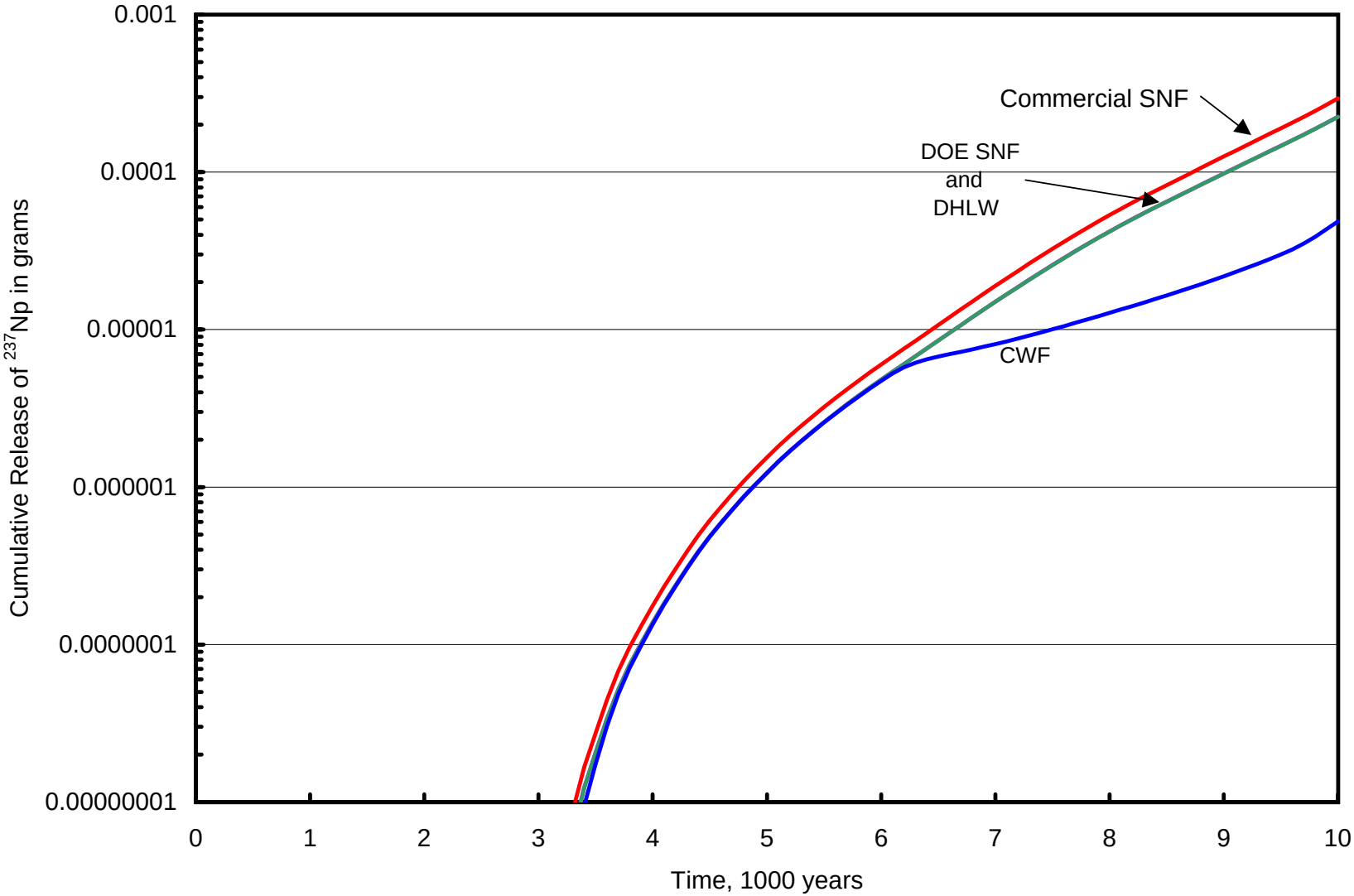

Fig. 14. Cumulative Release of ^{237}Np from the CWF, DOE SNF, HLW Glass, and Commercial SNF Over 10,000 Years. Release from the CWF is based on the model presented here and employs no cracking factors. Release models for the other waste forms are from the TSPA-VA for Yucca Mountain.

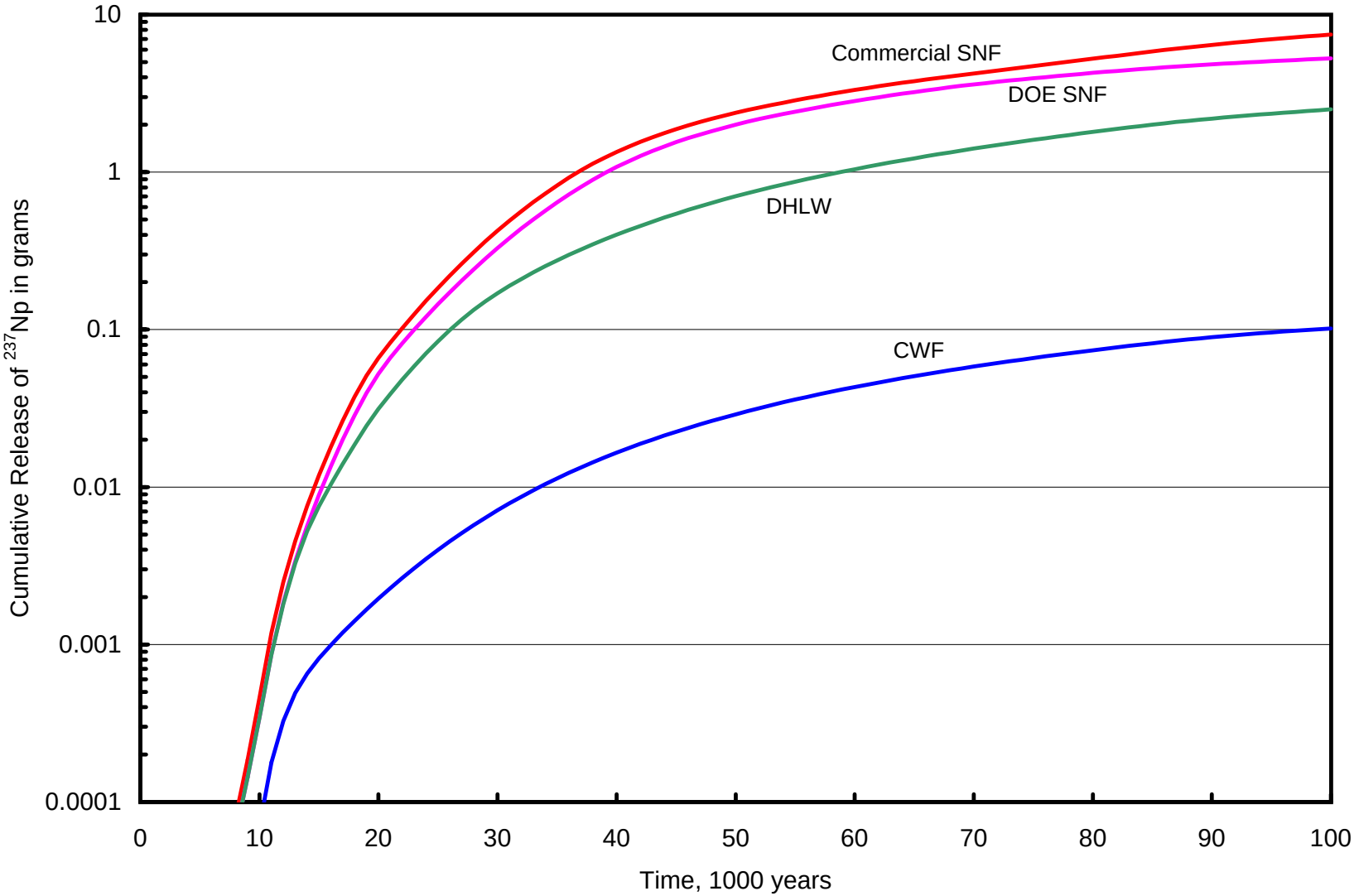

Fig. 15. Cumulative Release of ^{237}Np from the CWF, DOE SNF, HLW Glass, and Commercial SNF Over 100,000 Years. Release from the CWF is based on the model presented here and employs no cracking factors. Release models for the other waste forms are from the TSPA-VA for Yucca Mountain.

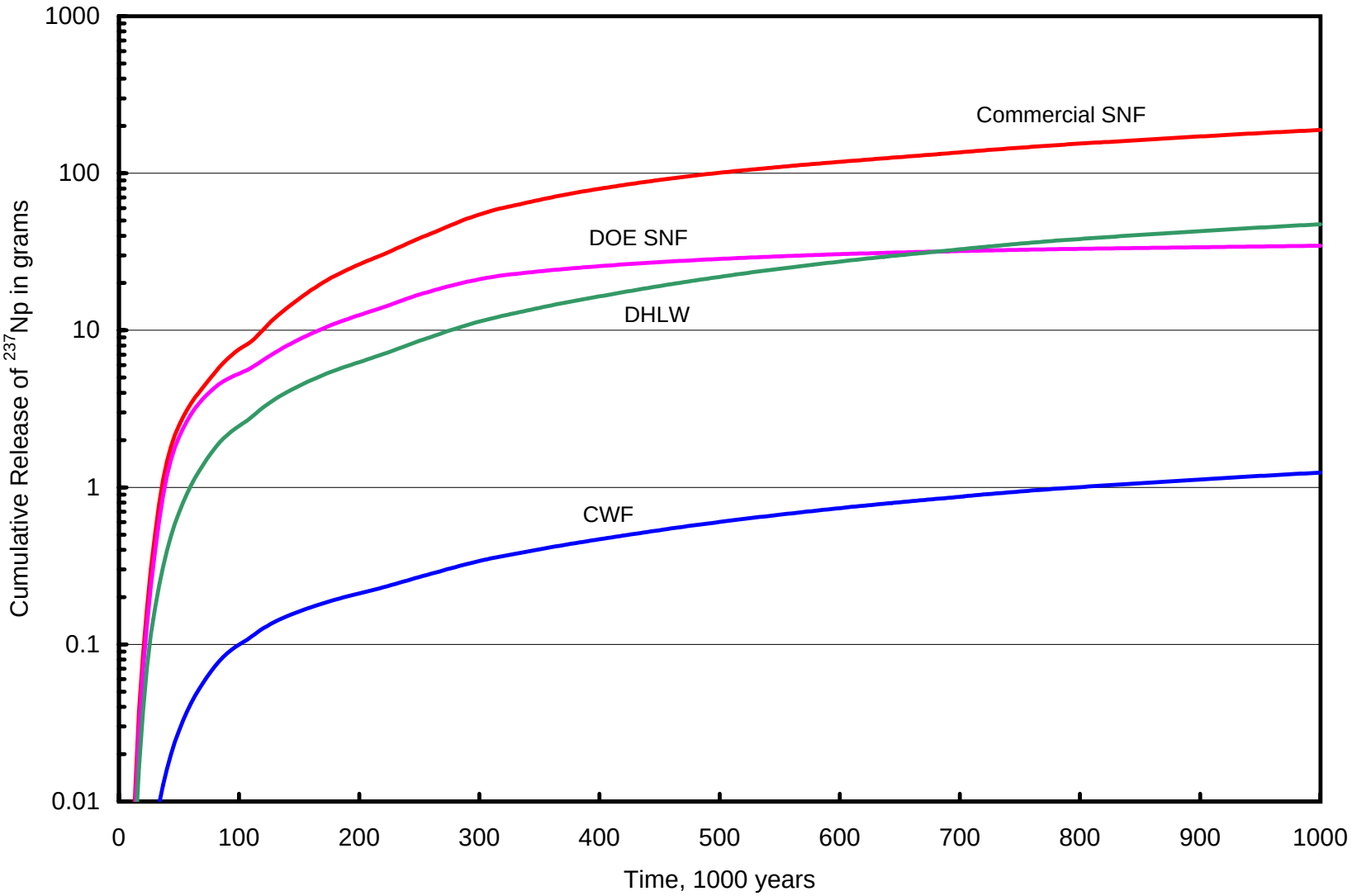

Fig. 16. Cumulative Release of ^{237}Np from the CWF, DOE SNF, HLW Glass, and Commercial SNF Over 1,000,000 Years. Release from the CWF is based on the model presented here and employs no cracking factors. Release models for the other waste forms are from the TSPA-VA for Yucca Mountain.

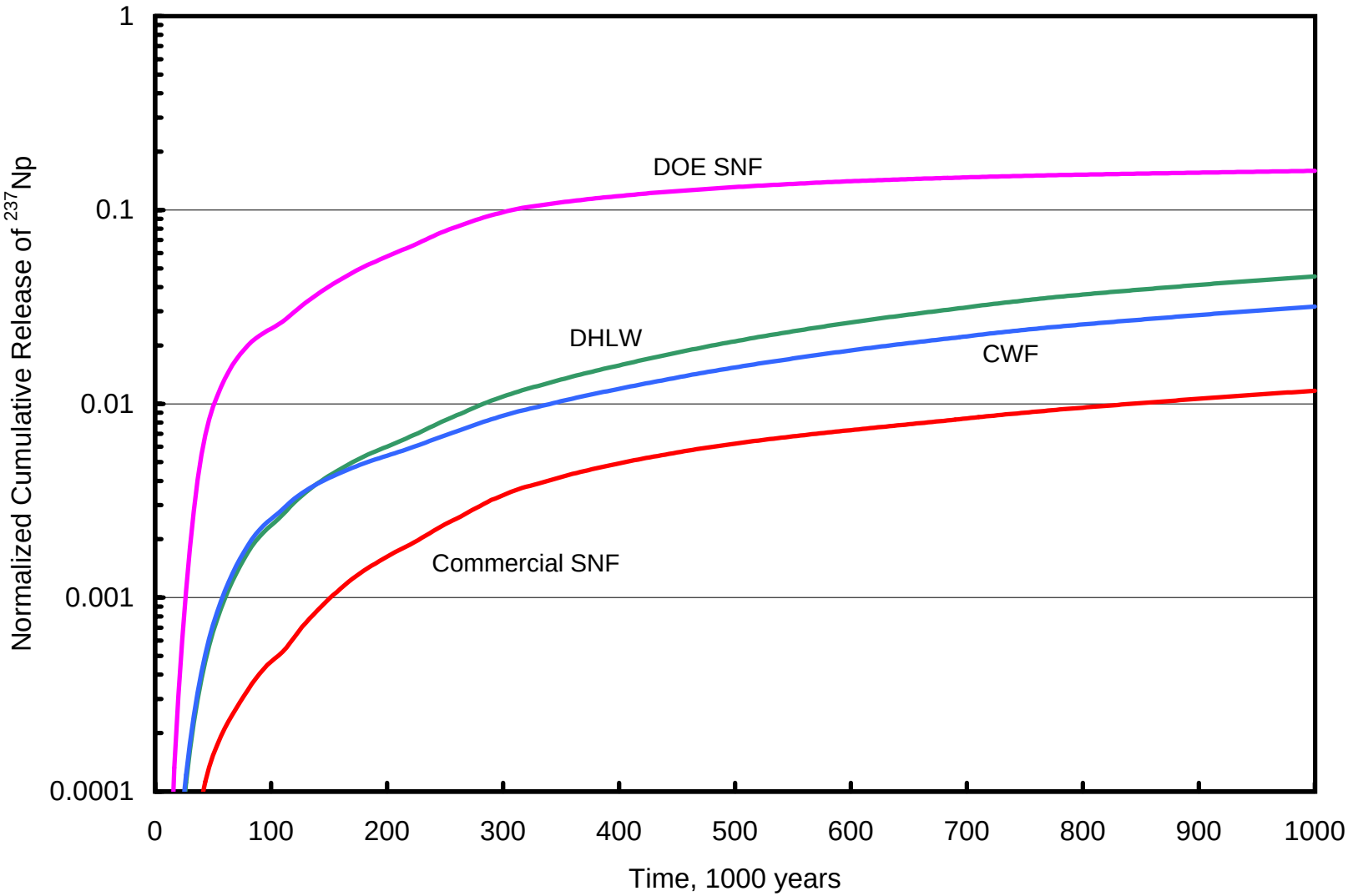

Fig. 17. Normalized Cumulative Release of ^{237}Np from the CWF, DOE SNF, HLW Glass, and Commercial SNF Over 1,000,000 Years. Release from the CWF is based on the model presented here and employs no cracking factors. Release models for the other waste forms are from the TSPA-VA for Yucca Mountain.

V. SUMMARY

As part of the spent fuel treatment program at Argonne National Laboratory, ceramic waste form (CWF) degradation and radionuclide release modeling is being carried out for the purpose of evaluating the impact of the CWF on the performance of the proposed repository at Yucca Mountain. Transition-state theory applied to the dissolution of aluminosilicate minerals provides a mechanistic basis for the CWF dissolution model, while model parameters are obtained by experimental measurements.

Dissolution tests using dilute, pH-buffered solutions have been conducted at 40, 70, and 90°C to measure the temperature and pH dependence on the dissolution rates of sodalite, binder glass, and composite CWF. The forward rate term of the rate equation was fit to the measured dissolution rates using linear regression. Parameter values obtained in the regression have been incorporated into the model. Saturation values for the major phases of the CWF have also been estimated at 90°C, with conservative bounds being employed in the model.

In addition to tests conducted to measure model parameters, additional testing is being conducted to refine and improve the CWF degradation and radionuclide release model. Areas currently being investigated include studying the effects of process changes on CWF durability, estimating the extent of cracking and level of porosity and its effect on increased exposed surface area, comparing the dissolution behavior of the intergranular glass phase of the CWF with the starting glass material, measuring the extent to which waste form generated colloids are produced, evaluating the effects on dissolution due to the presence of different aqueous species, and assessing the impact of radiation damage on CWF durability. Results from these tests can be used to update the CWF model as needed.

Performance assessment modeling calculations were carried out using the EBS model from the TSPA-VA. Because the CWF represents a small fraction of the waste in the proposed repository, it makes a negligible contribution to the calculated dose rates at a well 20 km from the repository. To evaluate the impact of the CWF on repository performance, cumulative fractional release of ^{129}I and cumulative mass release of ^{237}Np from the engineered barrier system was

calculated. Cumulative fractional release for a waste form is defined as the cumulative mass release of a particular radionuclide divided by the initial inventory present in that waste form.

At 10,000 years, the cumulative fractional release of ^{129}I from the CWF is calculated to be 0.0083% of its initial inventory. Comparisons with defense high-level waste (HLW) glass and DOE spent nuclear fuel as modeled in the TSPA-VA show that cumulative fractional release from the CWF is similar to release from HLW glass, but is over an order of magnitude lower than that for DOE spent nuclear fuel.

The current CWF model assumes overall degradation and radionuclide release is controlled by degradation of the least durable phase. This provides a conservative upper bound on the degradation rate of the waste form. Although calculated release rates for the CWF are similar to those calculated for HLW glass, the model does not yet include a cracking multiplier to represent thermal fracturing of the waste form. Lack of conservatism in the cracking multiplier may be offset by the conservative bound used for the degradation rate, however, the level of conservatism provided by this assumption has not been determined. Future tests are being planned to address this issue.

ACKNOWLEDGMENTS

The authors would like to thank M. L. Stanley, C. D. Tatko, and H. J. Retzer for carrying out the pH-buffered waste form corrosion tests, and Y. Tsai for performing chemical analysis.

This work was supported by the U. S. Department of Energy, Nuclear Energy, Science and Technology, under contract W-31-109-ENG-38 at Argonne National Laboratory.

REFERENCES

1. J. K. Fink, E. E. Morris, D. P. Abraham, I. Johnson, and R. A. Wigeland, “Status of Metal Waste Form Corrosion and Release Rate Model,” Argonne National Laboratory, ANL-NT-154 (September 2000).

2. *Viability Assessment of a Repository at Yucca Mountain*, DOE/RW-0508, (December 1998).

3. *Total System Performance Assessment-Viability Assessment (TSPA-VA) Analyses Technical Basis Document*, Chapter 6, “Waste Form Degradation, Radionuclide Mobilization, and Transport Through the Engineered Barrier System,” TRW Environmental Safety Systems Inc., B00000000-01717-4301-00006 REV 01 (November 13, 1998).

4. P. Aagaard and H. C. Helgeson, “Thermodynamic and Kinetic Constraints on Reaction Rates Among Minerals and Aqueous Solutions, I. Theoretical Considerations,” *American Journal of Science*, **282**:237–285 (March 1982).

5. W. L. Bourcier, “Critical Review of Glass Performance Modeling,” Chemical Technology Division, Argonne National Laboratory, ANL-94/17 (July 1994).

6. B. Grambow, “A General Rate Equation for Nuclear Waste Glass Corrosion,” *Mat. Res. Soc. Symp. Proc.*, **44**:16–27 (1985).

7. J. C. Cunnane, J. K. Bates, C. R. Bradley, E. C. Buck, W. L Ebert, X. Feng, J. J. Mazer, D. J. Wronkiewicz, J. Sproull, W. L Bourcier, B. P. McGrail, and M. K. Altenhofen, Eds., *High-Level Waste Borosilicate Glass: A Compendium of Corrosion Characteristics*, DOE-EM-0177, U. S. Department of Energy (1994).

8. W. L. Bourcier, W. L. Ebert, and X. Feng, “Modeling Surface Area to Volume Effects on Borosilicate Glass Dissolution,” *Mat. Res. Soc. Symp. Proc.*, **294**:577–582 (1993).

9. D. J. Wronkiewicz, *Effects of Radionuclide Decay on Waste Glass Behavior — A Critical Review*, Chemical Technology Division, Argonne National Laboratory, ANL-93/45 (December 1993).

10. J. R. Liaw, Argonne National Laboratory, personal communication (December 8, 1998).

11. D. T. Reed and R. A. Van Konynenburg, “Effects of Ionizing Radiation on Moist Air Systems,” *Mat. Res. Soc. Symp. Proc.*, **112**:393–404 (1998).

12. D. J. Wronkiewicz, J. K. Bates, E. C. Buck, J. C. Hoh, J. W. Emery, and L. M. Wang, *Radiation Effects in Moist-Air Systems and the Influence of Radiolytic Product Formation on Nuclear Waste Glass Corrosion*, Argonne National Laboratory, ANL-97/15 (July 1997).

13. D. J. Wronkiewicz, C. R. Bradley, J. K. Bates, and L. M. Wang, “Effects of Radiation Exposure on SRL 131 Composition Glass in a Steam Environment,” Argonne National Laboratory, ANL/CMT/CP-79803 (1993).

14. P. V. Brady, “Summary of In-Package Chemistry for Waste Forms,” ANL-EBS-MD-000050-REV00, Las Vegas, Nevada, DOE Office of Civilian Radioactive Waste Management (CRWMS M&O. ACC: MOL.20000127.0045).

15. P. S. Domski, “In-Package Chemistry Abstraction,” ANL-EBS-MD-000037 REV00, Las Vegas, Nevada, DOE Office of Civilian Radioactive Waste Management (CRWMS M&O. ACC: MOL.20000418.0818).

16. W. L. Ebert, et al., “Ceramic Waste Form Handbook,” Argonne National Laboratory, ANL-NT-119 (August 1999).

17. American Society for Testing and Materials, “Annual Book of ASTM Standards,” 12.01, Standard Test Method for Static Leaching of Monolithic Waste Forms for Disposal of Radioactive Waste, C1220-98, 1-16 (1998).

18. D. M. Strachan, B. O. Barnes, and R. P. Turcotte, “Standard Leach Tests for Nuclear Waste Materials,” *Sci. Basis for Nucl. Waste Mgmt.* **3**:347-354 (1981).

19. Spent Fuel Treatment Project Work Breakdown Structure, Argonne National Laboratory Report, F0000-0035-ES-01 (May 31, 2000).

20. T. H. Fanning and L. R. Morss, “Degradation Modeling of the ANL Ceramic Waste Form,” *Proc. Embedded Topical Meeting on DOE Spent Nuclear Fuel and Fissile Material Management,* 190–197, San Diego, CA, June 4–8, 2000.

21. D. Lexa, L. Leibowitz, J. Kropf, *J. Nucl. Mater.*, **279**:57-64 (2000).

22. Civilian Radioactive Waste Management System Report, “Waste Form Degradation Process Model Report,” TDR-WIS-MD-000001 REV 00C, TRW Environmental Safety Systems Inc. (March 2000).

23. P. K. Abraitis, B. P. McGrail, D. P. Trivedi, F. R. Livens, and D. J. Vaughan, “Single-pass Flow-through Experiments on Q Simulated Waste Glass in Alkaline Media at 40°C. I. Experiments Conducted at Variable Solution Flow Rate to Glass Surface Area Ratio,” *J. Nucl. Mater.*, **280**:196–205 (2000).

24. W. J. Weber, R. C. Ewing, C. R. A. Catlow, T. Diaz de la Rubia, L. W. Hobbs, C. Kinoshita, Hj. Matzke, A. T. Motta, M. Nastasi, E. K. H. Salje, E. R. Vance, S. J. Zinkle, *J. Mater. Res.*, **13**:1432–1484 (1998).

25. E. R. Vance, et al., “Ceramic Phases for Immobilization of I-129,” U. S. Department of Energy, DOE/ET/41900-9 (1981).

26. American Society of Testing Materials, *Annual Book of ASTM Standards*, 12.01, "Standard Test Method for Determining Chemical Durability of Nuclear Waste Glasses: The Product Consistency Test (PCT)," C1285-98 (1998).

27. R. A. Wigeland, L. L. Briggs, T. H. Fanning, E. E. Feldman, E. E. Morris, and M. C. Petri, "Waste Form Degradation and Repository Performance Assessment Modeling," Argonne National Laboratory, ANL-NT-117 (August 1999).

28. I. Miller and R. Kossik, *RIP Integrated Probabilistic Simulator for Environmental Systems: Theory Manual & User's Guide*, Golder Associates (November 1998).

29. R. Kossik, "Description of a Simplified TSPA-VA Model With Comparison of Results to the TRW Base Case Model," Golder Associates, Redmond, Washington (September 1, 1998).

30. "User's Guide, GoldSim Graphical Simulation Environment," Golder Associates (June 23, 2000).

31. "User's Guide, GoldSim Contaminant Transport Module," Golder Associates (June 23, 2000).

32. M. F. Simpson, Argonne National Laboratory–West, personal communication (June 16, 2000).

33. K. M. Goff, et al., "Production Operations for the Electrometallurgical Treatment of Sodium-Bonded Spent Nuclear Fuel," Argonne National Laboratory, ANL-NT-107 (June 1999).

APPENDIX A: pH-BUFFERED MCC-1 TESTS

Tables A1 through A9 show pH-buffered MCC-1 test results for sodalite, binder glass, and CWF at 40, 70, and 90°C in pH buffers ranging in pH from 5 to 10. Solution concentrations of silicon are reported as "corrected concentrations," in which the concentration of silicon in the experimental blank is subtracted from the concentration of silicon in the test solution. Normalized mass loss, NL(Si), is calculated by

$$\mathrm{NL(Si)} = \frac{m_{\mathrm{Si}} - m_b}{f_{\mathrm{Si}} S}$$

where m_{Si} is the mass of silicon in the test solution, m_b is the mass of silicon in the experimental blank, f_{Si} is the mass fraction of silicon in the material, and S is the sample surface area. Testing details are described in Sect. III-B-1.

Test results are shown as a sequence of plots in Figs. A1 through A9, in which linear regression values are shown. The slope of each plot line represents an estimate of the forward dissolution rate for that material at the given temperature and pH. Forward dissolution rates are summarized in Table 4 on page 19.

Table A1. Results of pH-Buffered MCC-1 Tests on Sodalite at 40°C

pH	Duration (d)	Corrected Concentration (μg Si/L)	NL(Si) (g/m^2-d)
4.9	7	16701	9.889
4.9	14	21990	13.051
4.9	28	27750	16.637
4.9	56	8580	5.002
4.9	91	38668	22.994
6.0	7	792	0.438
6.0	14	1126	0.638
6.0	28	4948	2.929
6.0	56	6581	3.902
6.0	91	9490	5.616
7.2	7	893	0.509
7.2	14	1267	0.732
7.2	28	1599	0.915
7.2	56	2209	1.280
7.2	91	2734	1.553
8.3	7	2837	1.232
8.3	14	3256	1.483
8.3	28	4726	2.267
8.3	56	5510	2.736
8.3	91	8423	3.731
9.6	7	1840	1.037
9.6	14	2353	1.343
9.6	28	3340	1.883
9.6	56	5065	2.917
9.6	91	6577	3.538

Table A2. Results of pH-Buffered MCC-1 Tests on Binder Glass at 40°C

pH	Duration (d)	Corrected Concentration (μg Si/L)	NL(Si) (g/m^2-d)
4.9	7	372	0.062
4.9	14	335	0.049
4.9	28	449	0.076
4.9	56	586	0.123
4.9	91	988	0.242
6.0	7	219	0.054
6.0	14	237	0.060
6.0	28	297	0.079
6.0	56	252	0.063
6.0	91	460	0.117
6.8	7	173	0.007
6.8	14	173	0.013
6.8	28	208	0.024
6.8	56	238	0.035
7.2	7	173	0.052
7.2	14	173	0.068
7.2	28	208	0.075
7.2	56	238	0.057
7.2	91	198	0.076
7.8	7	3145	0.023
7.8	14	1449	0.039
7.8	28	2539	0.050
7.8	56	2109	0.129
8.3	7	1275	0.168
8.3	14	1556	0.263
8.3	28	2670	0.586
8.3	56	3145	0.747
8.3	91	7053	1.647
9.6	7	2109	0.678
9.6	14	3225	1.056
9.6	28	5612	1.836
9.6	56	8322	2.754
9.6	91	10137	3.210

Table A3. Results of pH-Buffered MCC-1 Tests on the CWF at 40°C

pH	Duration (d)	Corrected Concentration (μg Si/L)	NL(Si) (g/m^2-d)
4.9	7	19599	9.759
4.9	14	20314	10.114
4.9	28	18400	9.142
4.9	28	20114	9.996
4.9	56	27662	13.794
4.9	91	39916	19.931
6.0	7	1045	0.495
6.0	14	1358	0.652
6.0	28	3727	1.841
6.0	28	3430	1.692
6.0	56	5404	2.683
6.0	91	7874	3.902
7.2	7	796	0.378
7.2	14	1036	0.498
7.2	28	1388	0.662
7.2	56	1503	0.720
7.2	91	2310	1.090
8.3	7	2141	0.684
8.3	14	3075	1.154
8.3	28	3812	1.444
8.3	56	4955	2.020
8.3	91	7511	2.672
9.6	7	1789	0.844
9.6	14	2463	1.183
9.6	28	4203	2.013
9.6	56	5082	2.455
9.6	91	6307	2.832

Table A4. Results of pH-Buffered MCC-1 Tests on Sodalite at 70°C

pH	Duration (d)	Corrected Concentration (μg Si/L)	NL(Si) (g/m^2-d)
4.9	3	13500	8.130
4.9	5	18900	11.383
4.9	9	29000	17.431
4.9	12	26700	16.672
6.4	3	5350	3.219
6.4	5	6730	4.045
6.4	9	11200	6.764
6.4	12	11800	7.208
7.2	3	3530	2.075
7.2	5	4590	2.712
7.2	9	5030	2.983
7.2	12	5360	3.171
8.3	3	5100	2.678
8.3	5	8430	4.680
8.3	9	9420	5.277
8.3	12	9070	5.067
9.4	3	5320	3.129
9.4	5	7300	4.308
9.4	9	8680	5.141
9.4	12	11100	6.597

Table A5. Results of pH-Buffered MCC-1 Tests on Binder Glass at 70°C

pH	Duration (d)	Corrected Concentration (μg Si/L)	NL(Si) (g/m^2-d)
5.1	3	388	0.107
5.1	5	557	0.165
5.1	7	682	0.208
5.1	10	1140	0.344
6.0	3	252	0.061
6.0	5	375	0.092
6.0	7	349	0.095
6.0	10	448	0.127
7.2	3	443	0.075
7.2	5	519	0.101
7.2	7	410	0.064
7.2	10	766	0.185
8.3	3	4140	1.375
8.3	5	5390	1.801
8.3	7	6720	2.253
8.3	10	17900	6.055
9.6	3	8940	2.776
9.6	5	12100	3.851
9.6	7	14800	4.768
9.6	10	7890	2.416

Table A6. Results of pH-Buffered MCC-1 Tests on the CWF at 70°C

pH	Duration (d)	Corrected Concentration (μg Si/L)	NL(Si) (g/m^2-d)
5.1	3	9610	4.766
5.1	5	17800	8.891
5.1	7	22600	11.336
4.9	10	29400	14.712
6.0	3	2760	1.361
6.0	5	4890	2.466
6.0	7	6630	3.327
6.0	10	9320	4.698
7.2	3	3070	1.440
7.2	5	4050	1.934
7.2	7	4580	2.200
7.2	10	4900	2.358
8.3	3	5080	2.514
8.3	5	6720	3.343
8.3	7	8690	4.337
8.3	10	10500	5.242
9.6	3	5390	2.405
9.6	5	7620	3.531
9.6	7	9320	4.412
9.6	10	9620	4.541

Table A7. Results of pH-Buffered MCC-1 Tests on Sodalite at 90°C

pH	Duration (d)	Corrected Concentration (μg Si/L)	NL(Si) (g/m^2-d)
5.1	1	4890	2.941
5.1	2	12600	5.182
5.1	3	18700	11.533
5.1	5	23000	13.813
6.0	1	6680	4.023
6.0	2	8300	4.993
6.0	3	10100	6.079
6.0	5	11000	6.605
7.0	1	4820	2.896
7.0	2	7070	4.252
7.0	3	7600	4.574
7.0	5	7790	4.682
8.1	1	6180	3.719
8.1	2	8810	5.299
8.1	3	12000	7.208
8.1	5	12800	7.690
9.2	1	6710	4.002
9.2	2	9470	5.696
9.2	3	13600	8.184
9.2	5	14700	8.835
10.2	1	16600	9.998
10.2	2	25000	14.649
10.2	3	25100	15.096

Table A8. Results of pH-Buffered MCC-1 Tests on Binder Glass at 90°C

pH	Duration (d)	Corrected Concentration (μg Si/L)	NL(Si) (g/m^2-d)
5.1	1	220	0.075
5.1	2	380	0.129
5.1	3	760	0.252
5.1	5	560	0.190
6.0	1	460	0.157
6.0	2	660	0.225
6.0	3	1000	0.331
6.0	5	1090	0.376
7.0	1	200	0.068
7.0	2	400	0.136
7.0	3	620	0.211
7.0	5	860	0.292
8.1	1	5120	1.739
8.1	2	7400	2.516
8.1	3	13300	4.503
8.1	5	15600	5.301
9.2	1	12700	4.321
9.2	2	21100	7.173
9.2	3	26800	9.120
9.2	5	30800	10.470
10.2	1	38700	13.160
10.2	2	61100	20.775
10.2	3	69900	23.757

Table A9. Results of pH-Buffered MCC-1 Tests on the CWF at 90°C

pH	Duration (d)	Corrected Concentration (μg Si/L)	NL(Si) (g/m^2-d)
5.1	1	2830	1.428
5.1	2	9510	4.801
5.1	3	14400	7.261
5.1	5	17800	8.987
6.0	1	5630	2.846
6.0	2	7440	3.755
6.0	3	10100	5.096
6.0	5	10900	5.497
7.0	1	3660	1.849
7.0	2	5550	2.801
7.0	3	7520	3.807
7.0	5	9130	4.614
8.1	1	5360	2.704
8.1	2	8560	4.319
8.1	3	11800	5.955
8.1	5	15700	7.909
9.2	1	8520	4.221
9.2	2	12000	6.055
9.2	3	16500	8.101
9.2	5	19000	10.334
10.2	1	21700	10.955
10.2	2	30900	15.599
10.2	3	34700	17.497
10.2	5	53900	27.182

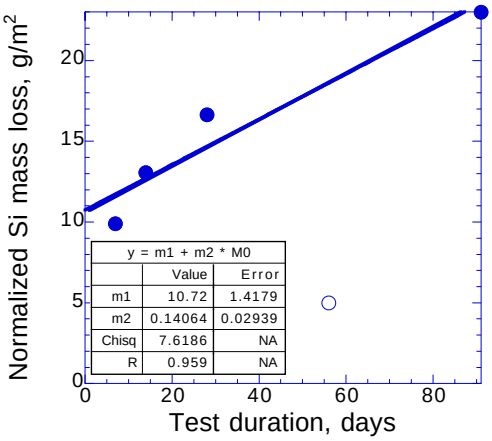

(a) Sodalite, pH 4.9, 40°C

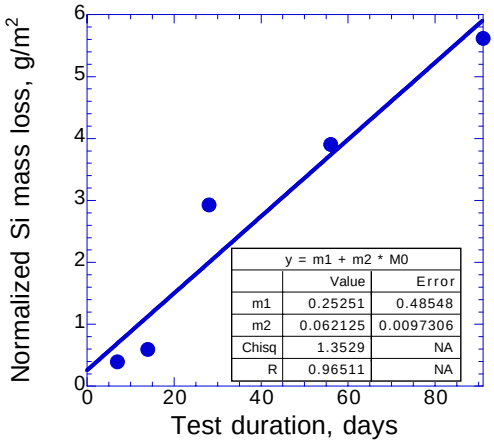

(b) Sodalite, pH 6.0, 40°C

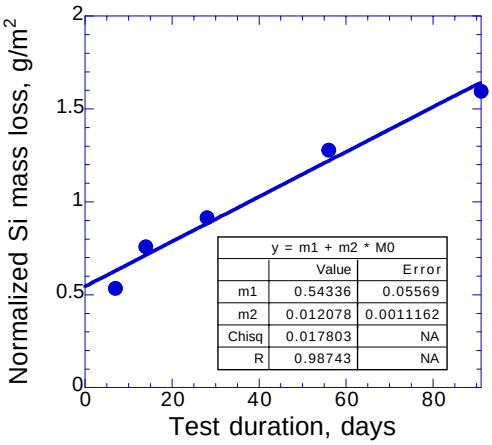

(c) Sodalite, pH 7.2, 40°C

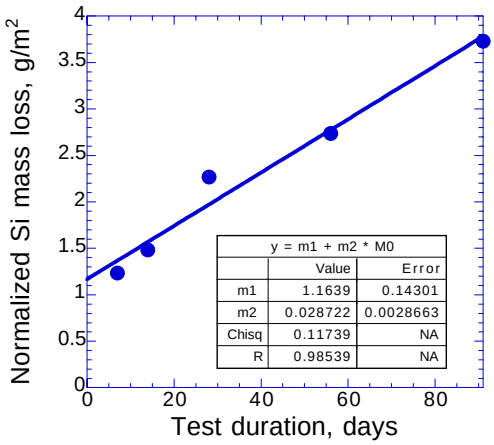

(d) Sodalite, pH 8.3, 40°C

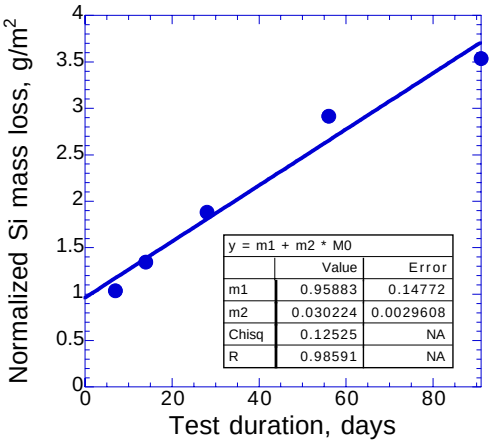

(e) Sodalite, pH 9.6, 40°C

Fig. A1. Normalized Si Mass Losses from Sodalite as a Function of Test Duration in Buffered MCC-1 Tests at 40°C. Regression coefficients are shown. Data represented by open circles were not used in the regression fits.

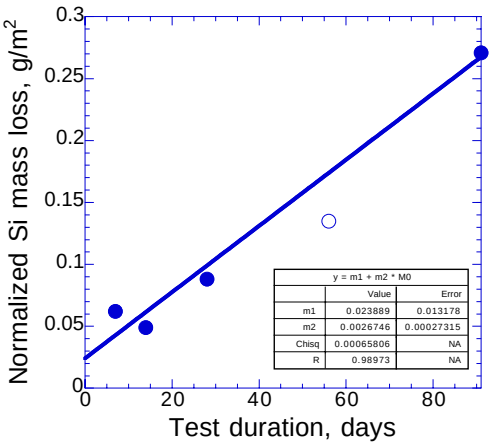

(a) Binder Glass, pH 4.9, 40°C

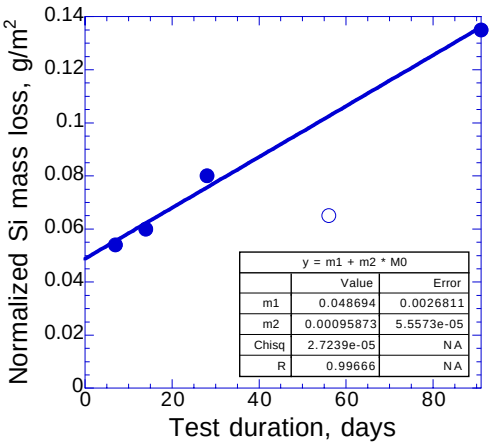

(b) Binder Glass, pH 6.0, 40°C

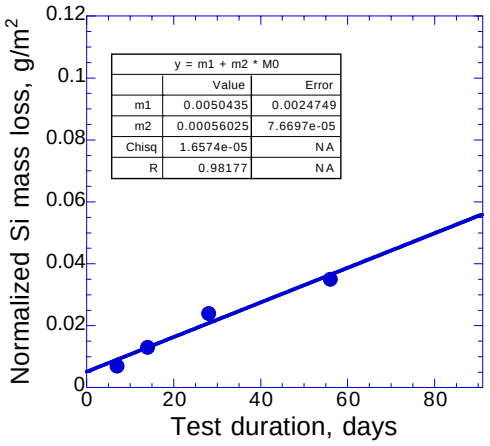

(c) Binder Glass, pH 6.8, 40°C

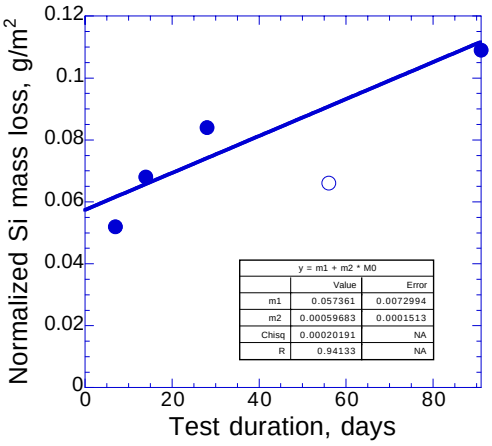

(d) Binder Glass, pH 7.2, 40°C

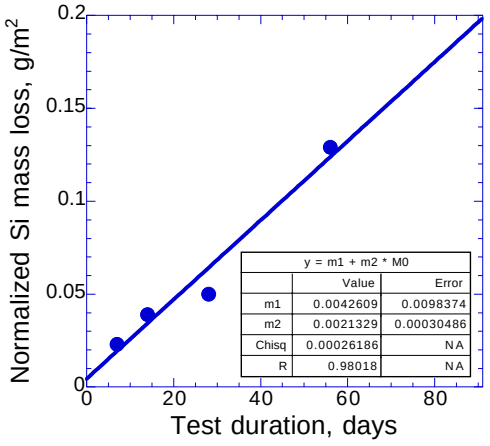

(e) Binder Glass, pH 7.8, 40°C

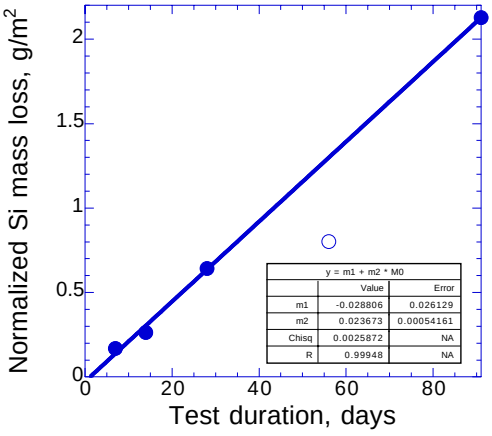

(f) Binder Glass, pH 8.3, 40°C

Fig. A2. Normalized Si Mass Losses from Binder Glass as a Function of Test Duration in Buffered MCC-1 Tests at 40°C. Regression coefficients are shown. Data represented by open circles were not used in the regression fits.

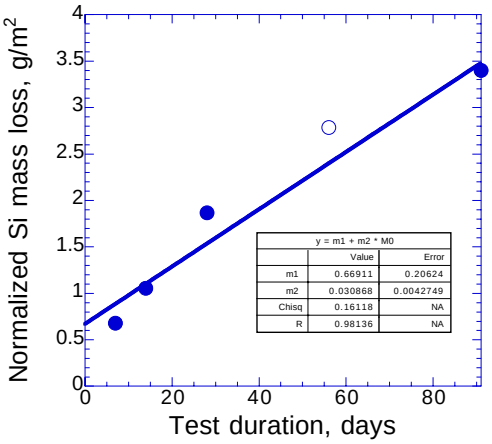

(g) Binder Glass, pH 9.6, 40°C

Fig. A2. Normalized Si Mass Losses from Binder Glass as a Function of Test Duration in Buffered MCC-1 Tests at 40°C. (Continued) Regression coefficients are shown. Data represented by open circles were not used in the regression fits.

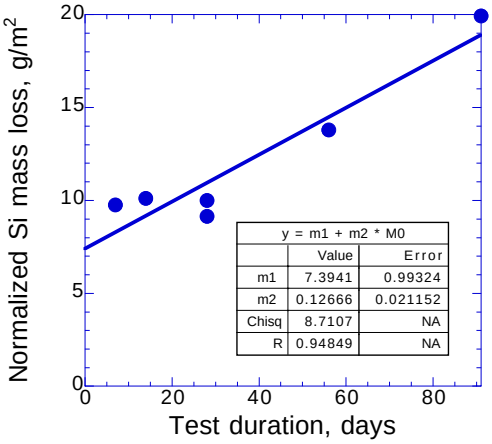

(a) CWF, pH 4.9, 40°C

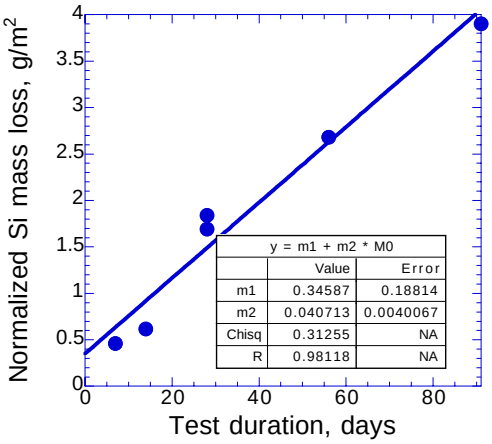

(b) CWF, pH 6.0, 40°C

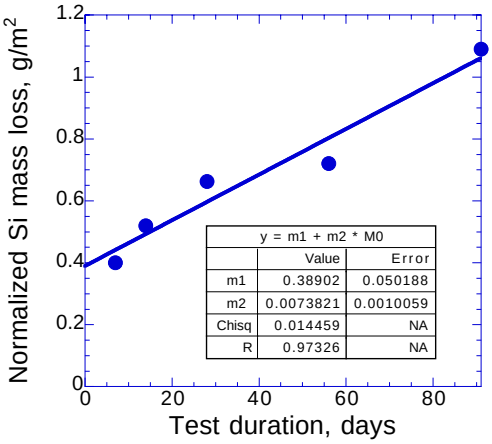

(c) CWF, pH 7.2, 40°C

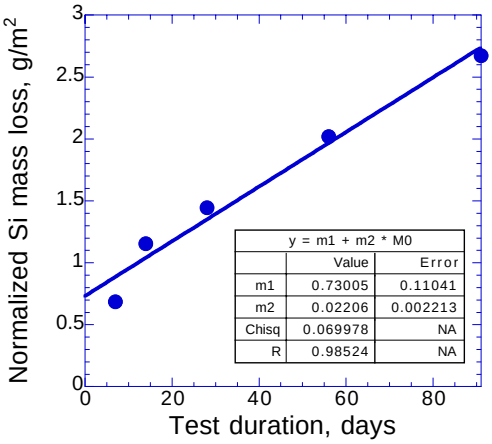

(d) CWF, pH 8.3, 40°C

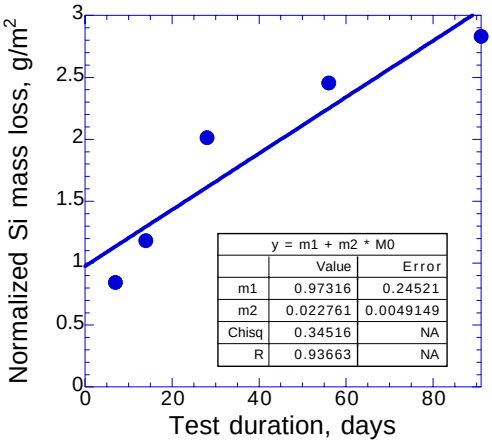

(e) CWF, pH 9.6, 40°C

Fig. A3. Normalized Si Mass Losses from the CWF as a Function of Test Duration in Buffered MCC-1 Tests at 40°C. Regression coefficients are shown. Data represented by open circles were not used in the regression fits.

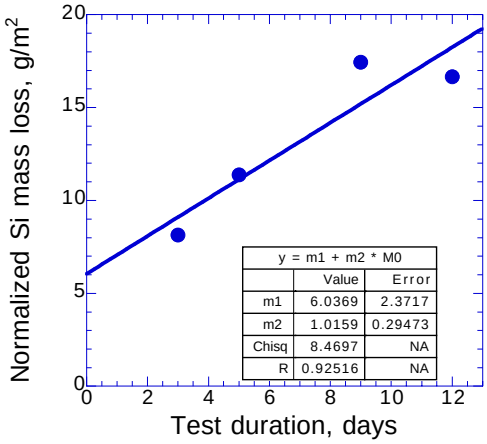

(a) Sodalite, pH 4.9, 70°C

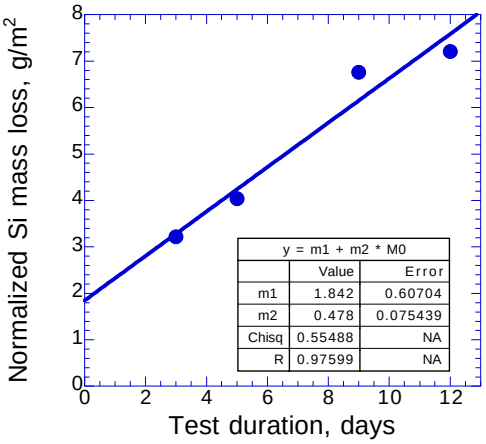

(b) Sodalite, pH 6.4, 70°C

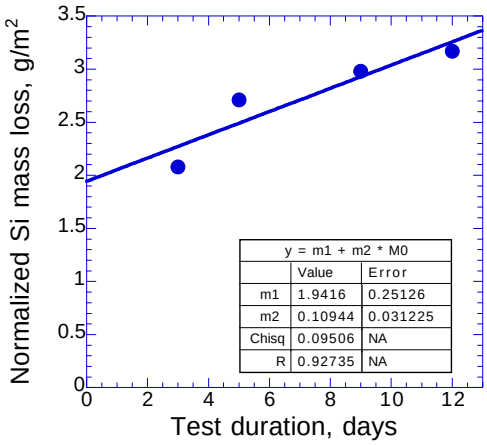

(c) Sodalite, pH 7.2, 70°C

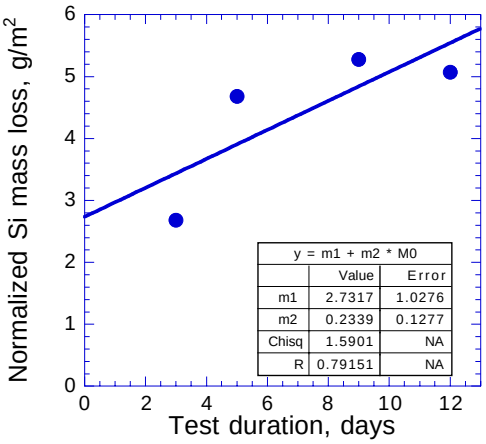

(d) Sodalite, pH 8.3, 70°C

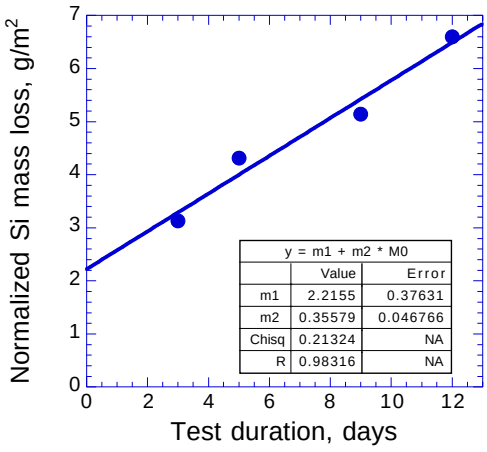

(e) Sodalite, pH 9.4, 70°C

Fig. A4. Normalized Si Mass Losses from Sodalite as a Function of Test Duration in Buffered MCC-1 Tests at 70°C. Regression coefficients are shown. Data represented by open circles were not used in the regression fits.

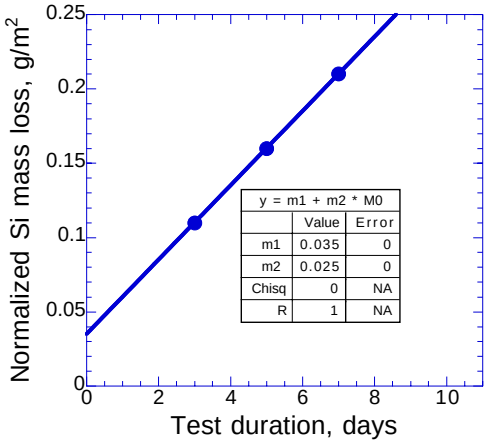

(a) Binder Glass, pH 5.1, 70°C

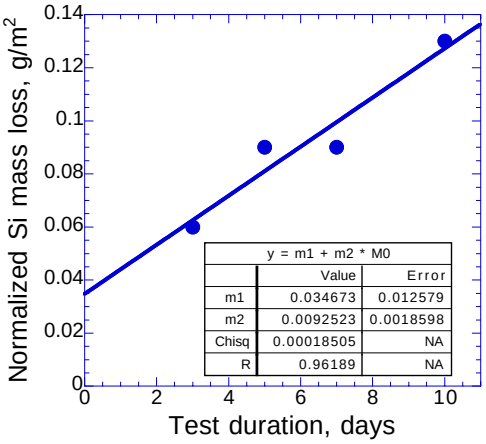

(b) Binder Glass, pH 6.0, 70°C

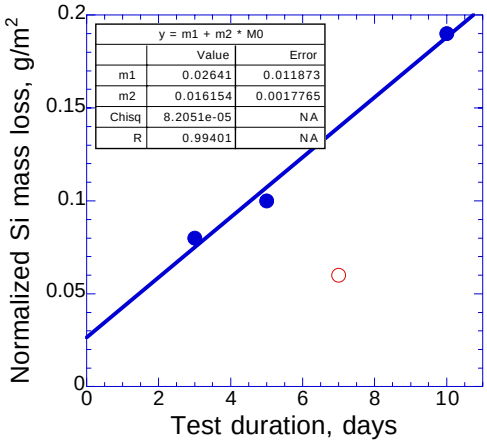

(c) Binder Glass, pH 7.2, 70°C

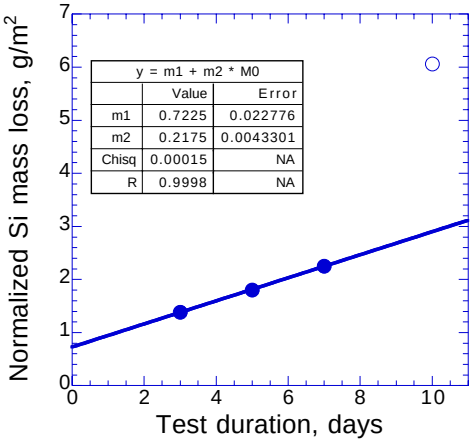

(d) Binder Glass, pH 8.3, 70°C

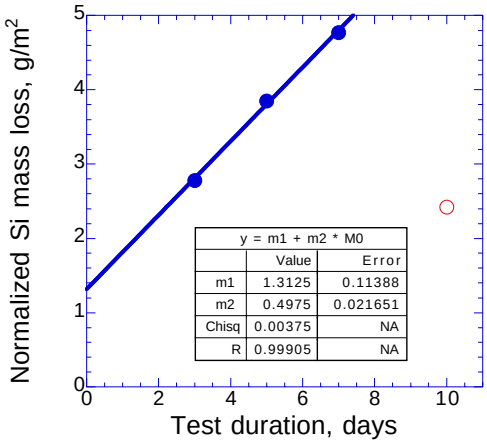

(e) Binder Glass, pH 9.6, 70°C

Fig. A5. Normalized Si Mass Losses from Binder Glass as a Function of Test Duration in Buffered MCC-1 Tests at 70°C. Regression coefficients are shown. Data represented by open circles were not used in the regression fits.

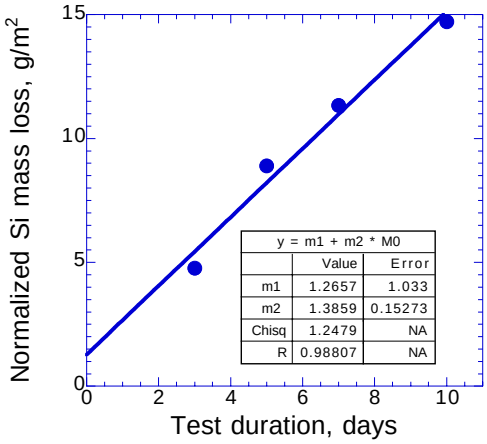

(a) CWF, pH 5.1, 70°C

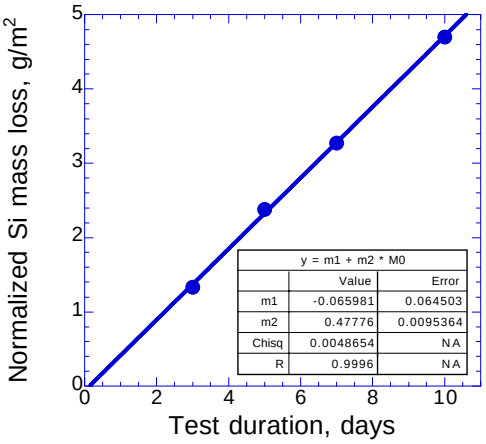

(b) CWF, pH 6.0, 70°C

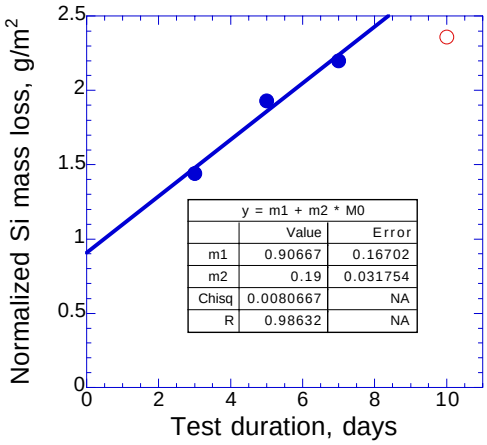

(c) CWF, pH 7.2, 70°C

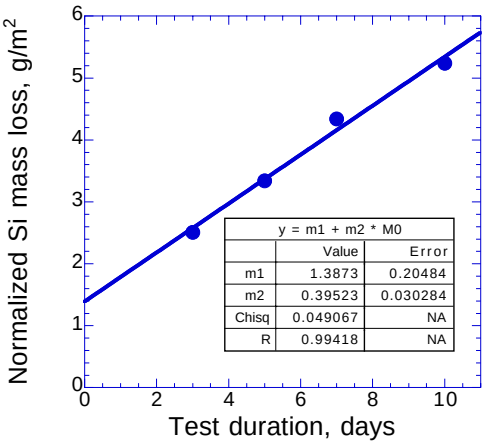

(d) CWF, pH 8.3, 70°C

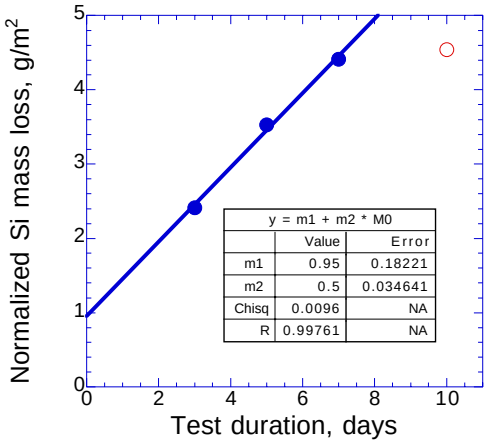

(e) CWF, pH 9.6, 70°C

Fig. A6. Normalized Si Mass Losses from the CWF as a Function of Test Duration in Buffered MCC-1 Tests at 70°C. Regression coefficients are shown. Data represented by open circles were not used in the regression fits.

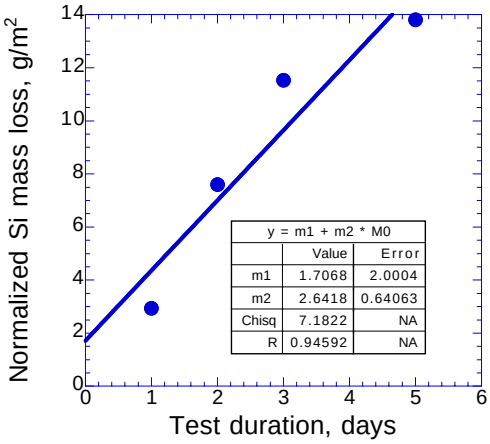

(a) Sodalite, pH 5.1, 90°C

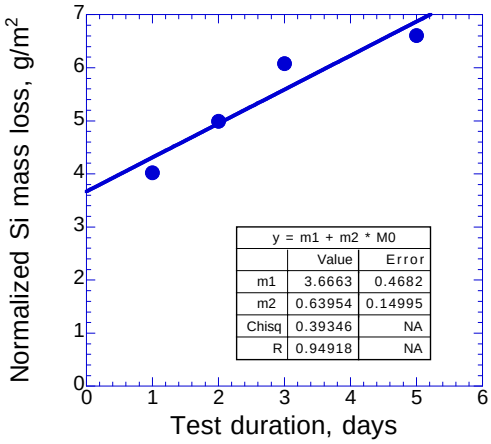

(b) Sodalite, pH 6.0, 90°C

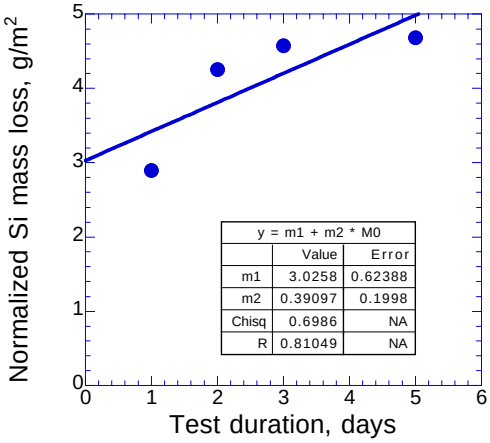

(c) Sodalite, pH 7.0, 90°C

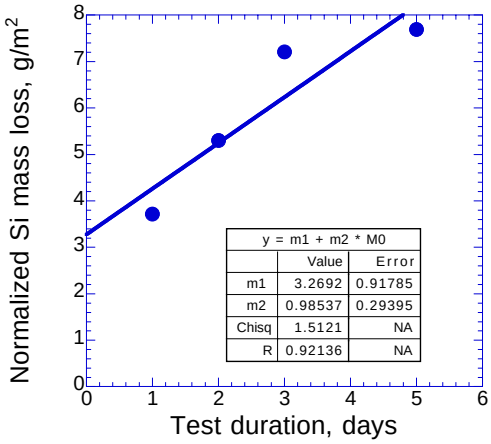

(d) Sodalite, pH 8.1, 90°C

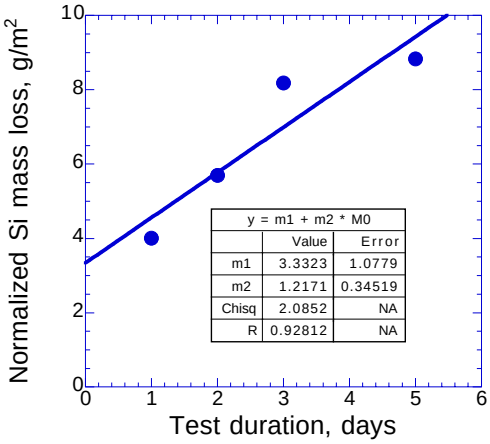

(e) Sodalite, pH 9.2, 90°C

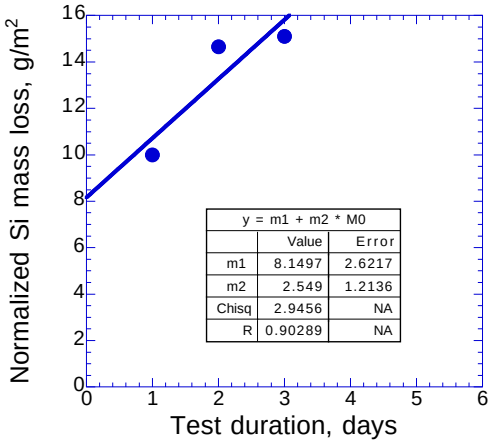

(f) Sodalite, pH 10.2, 90°C

Fig. A7. Normalized Si Mass Losses from Sodalite as a Function of Test Duration in Buffered MCC-1 Tests at 90°C. Regression coefficients are shown. Data represented by open circles were not used in the regression fits.

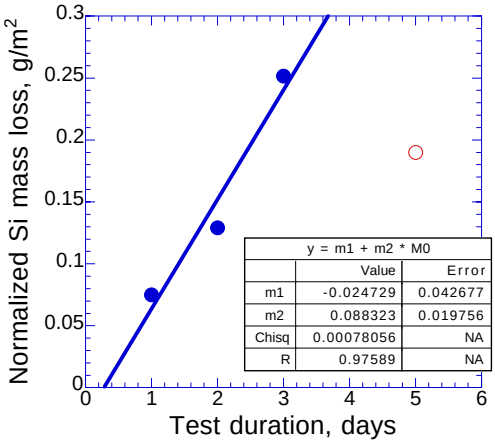

(a) Binder Glass, pH 5.1, 90°C

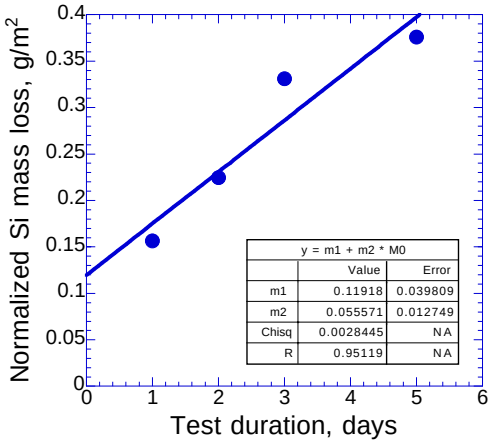

(b) Binder Glass, pH 6.0, 90°C

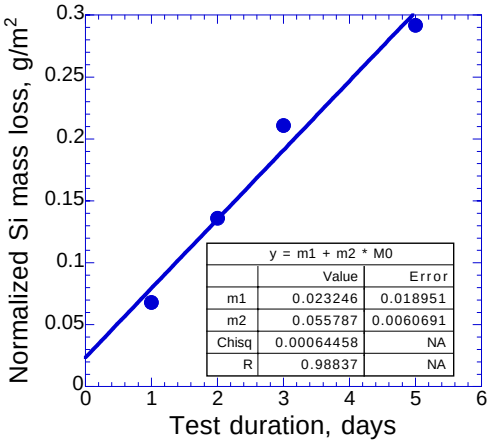

(c) Binder Glass, pH 7.0, 90°C

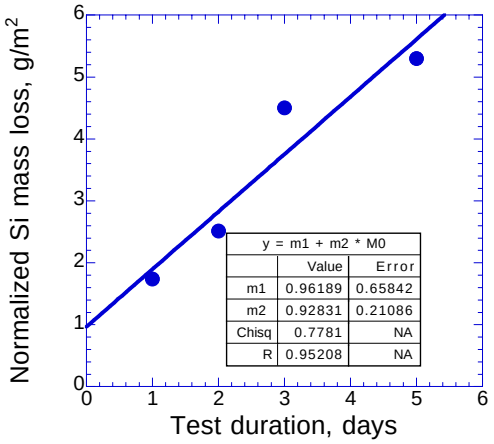

(d) Binder Glass, pH 8.1, 90°C

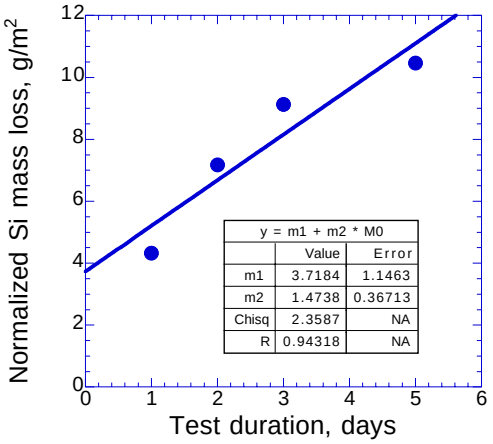

(e) Binder Glass, pH 9.2, 90°C

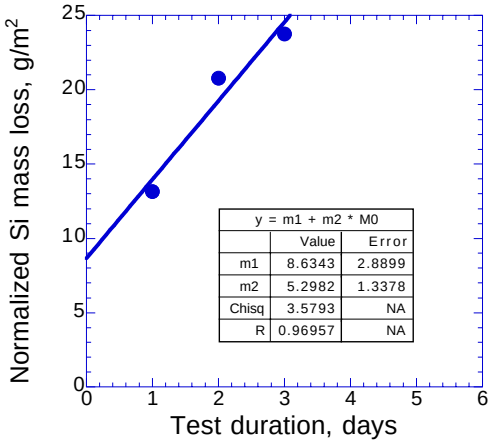

(f) Binder Glass, pH 10.2, 90°C

Fig. A8. Normalized Si Mass Losses from Binder Glass as a Function of Test Duration in Buffered MCC-1 Tests at 90°C. Regression coefficients are shown. Data represented by open circles were not used in the regression fits.

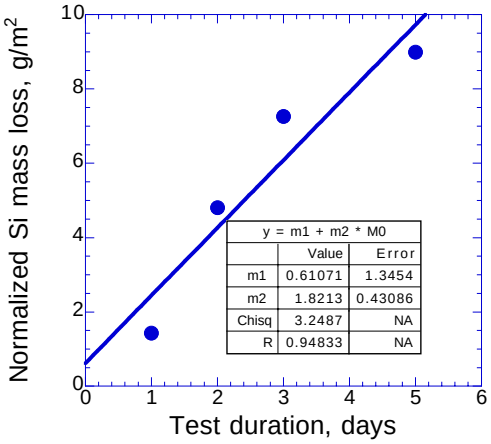

(a) CWF, pH 5.1, 90°C

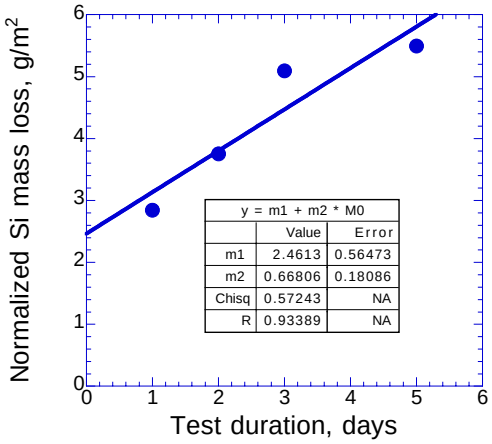

(b) CWF, pH 6.0, 90°C

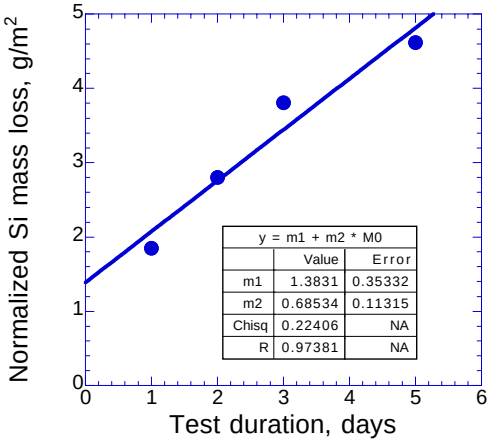

(c) CWF, pH 7.0, 90°C

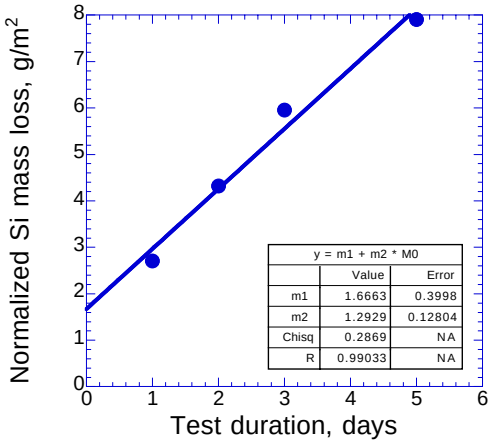

(d) CWF, pH 8.1, 90°C

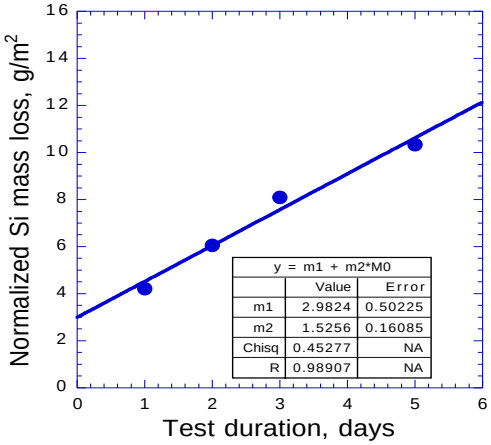

(e) CWF, pH 9.2, 90°C

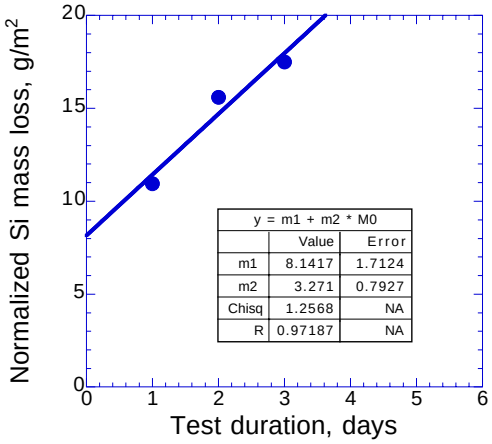

(f) CWF, pH 10.2, 90°C

Fig. A9. Normalized Si Mass Losses from the CWF as a Function of Test Duration in Buffered MCC-1 Tests at 90°C. Regression coefficients are shown. Data represented by open circles were not used in the regression fits.

APPENDIX B: SOURCE CODE FOR THE CERAMIC WASTE FORM MODEL DLL

Dissolution rates for the ceramic waste form were calculated by an external library linked to the model for the engineered barrier system. Source code for the dynamic link library (DLL) is shown in Listing 1. The included header file “ripdll.h” is shown in Listing 2.

Listing 1: Source Code Listing for “CWFdis.c”

```
 1: #include "ripdll.h"
 2:
 3: #include <math.h>
 4: #include <stdio.h>
 5:
 6: #define EXP            __declspec(dllexport)
 7: #define max(a,b)       (((a) > (b)) ? (a) : (b))
 8:
 9: /* VERSION INFORMATION */
10:
11: #define CWFDIS_VERSION  0.41
12:
13: /*  *   *** CWFDIS Version Information ************************************
14:     *
15:     *   Version 0.1:
16:     *      All data used in the initial CWF DLL was obtained from
17:     *      the GLDIS DLL used in the TSPA-VA.
18:     *   Version 0.2:
19:     *      A preliminary regression of rates measured in pH-buffered
20:     *      MCC-1 tests was used to represent the forward dissolution
21:     *      rate of the CWF. Rate data used was from dissolution tests
22:     *      of the glass component only. Solubility products (Ksp) and
23:     *      long-term rates were from the GLDIS DLL used in the TSPA-VA.
24:     *   Version 0.3:
25:     *      Same as 0.2, except regression of forward rate was updated
26:     *      to reflect the exclusion of some measured data. Also,
27:     *      standard errors from the regression fit are included in
28:     *      the calculation of the forward rate. Solubility product (Ksp)
29:     *      and long-term rates are from data used in the GLDIS DLL used
30:     *      in the TSPA-VA.
31:     *   Version 0.31:
32:     *      Corrected a typo that was present in versions 0.2 and 0.3.
33:     *      The incorrect version number was being reported by CWFDIS.
34:     *      Instead, the ACDIS_VERSION number was reported. CWFDIS now
35:     *      correctly reports the CWFDIS_VERSION number.
36:     *   Version 0.311
37:     *      Same as Version 0.31, except uncertainties in the
38:     *      regression for CWF forward dissolution rates have been
39:     *      set to zero to evaluate the sensitivites of the average
40:     *      dissolution rate on regression errors.
41:     *   Version 0.32
42:     *      A new set of basis functions was used for the regression
43:     *      analysis. The new set is centered on the data. This
44:     *      reduces overall uncertainty in the calculated dissolution
```

```
 45:     *      rates and is consistent with what is done in the VA for
 46:     *      HLW glass. Also, the dissolution rate data near pH ~= 7
 47:     *      is included in the regression of the acid leg. Previously,
 48:     *      this data had been excluded from the regression analysis
 49:     *      for the acid leg. Dissolution rate data near pH ~= 7 continue
 50:     *      to be used in the regression of the base leg.
 51:     *   Version 0.4:
 52:     *      Updated parameters are used for the forward rate based
 53:     *      on regressions of additional 40 degree test data. Also,
 54:     *      the ratio of Q/K is determined using the TSPA-VA regression
 55:     *      in conjunction with a scaling factor. The scaling factor
 56:     *      is the ratio of the amorphous silica solubility used in the
 57:     *      TSPA-VA for HLW glass at 90 degrees C and an estimated solubility
 58:     *      of binder glass at 90 degrees C from long-term PCT tests.
 59:     *      By using this scaling factor one assumes that the temperature
 60:     *      dependence is the same for the two materials.
 61:     *   Version 0.41:
 62:     *      The value for K (binder glass at 90 degrees C) was updated
 63:     *      from 340 mg/L H4SiO4 to 370 mg/L H4SiO4.
 64:     *
 65:     *   ****************************************************************** */
 66:
 67:  /* FUNCTION PROTOTYPES */
 68:
 69:  /*  CWFDIS will calculate a dissolution rate based in part on forward
 70:     dissolution rate data from CMT and HLW glass saturation constants
 71:     and long-term rates from the TSPA-VA Technical Basis Document
 72:  */
 73:  EXP void CWFDIS(
 74:         int inMethod,
 75:         int *outState,
 76:         const double inArgs[],
 77:         double *outArgs);
 78:  int CWFDissolution(
 79:         const double inArgs[],
 80:         double *outArgs);
 81:
 82:  /* INPUT AND OUTPUT ARGMENTS */
 83:
 84:  enum {    /* Input Parameter Indices */
 85:     indexStoch1,     /* Stochastic Parameters 1-9               */
 86:     indexStoch2,
 87:     indexStoch3,
 88:     indexStoch4,
 89:     indexStoch5,
 90:     indexStoch6,
 91:     indexStoch7,
 92:     indexStoch8,
 93:     indexStoch9,
 94:     indexTemp,       /* Waste Package Temperature (C)           */
 95:     indexPH,         /* Groundwater PH                          */
 96:     inputCount       /* Total Number of Input Parameters        */
 97:  };
 98:
 99:  /* Output Parameter Indices */
100:  enum {
101:     indexCWFDis,     /* CWF Dissolution Rate (g/m^2/yr)         */
102:     outputCount      /* Total Number of Output Parameters       */
103:  };
```

```
104:
105:  /*
106:     CWFDIS provides an interface between RIP (now GoldSim) and this DLL
107:     for calculating the dissolution rate of the CWF as a function of
108:     temperature and pH. Stochastic parameters are also provided to
109:     represent uncertainty in the model.
110:  */
111:  EXP void CWFDIS(
112:     int inMethod, int *outState,
113:     const double inArgs[], double outArgs[])
114:  {
115:     /* Indicate preliminary success */
116:     *outState = DLL_SUCCESS;
117:
118:     switch (inMethod)
119:     {
120:        case RIP_INITIALIZE:
121:         break;  /* No Initialization is Required */
122:
123:           case RIP_REP_VERSION:   /* Report the version of this function */
124:              outArgs[0] = CWFDIS_VERSION;
125:              break;
126:
127:           case RIP_REP_ARGUMENTS: /* Report the number of arguments */
128:              outArgs[0] = inputCount;
129:              outArgs[1] = outputCount;
130:              break;
131:
132:           case RIP_CALCULATION:   /* Perform the rate calculation */
133:              *outState = CWFDissolution(inArgs, outArgs);
134:              break;
135:     }
136:
137:     return;
138:  }
139:
140:  /*
141:     CWFDissolution calculates a dissolution rate based on forward
142:     dissolution rate data and saturation constants measured for the CWF,
143:     but no long-term rates are used. (i.e. they are set to zero.)
144:     Input parameters are described above. The single output parameter
145:     is the CWF dissolution rate.
146:  */
147:  int CWFDissolution(const double in[], double out[])
148:  {
149:  /*
150:     ************************************************************
151:     *
152:     *   Input paramters are as described above. The first nine
153:     *   parameters are provided by RIP as stochastics drawn from a
154:     *   standard normal distribution, N(0,1). (Zero mean and unit
155:     *   variance)
156:     *
157:     *   The remaining two input paramters are the temperature
158:     *   in degrees C and the groundwater pH.
159:     *
160:     *   The  output parameter is the CWF dissolution
161:     *   rate as determined by
162:     *
```

```
163:     *      R = k(T,pH)[1 - Q(T)/K(T)] + k_long(T),
164:     *
165:     *   where k(T,ph) is the forward rate as determined by regression
166:     *   of pH-buffered MCC-1 tests conducted by CMT. The ratio of
167:     *   Q(T)/K(T) is determined from HLW glass data used in the
168:     *   TSPA-VA. However Q/K is adjusted to reflect estimates of K
169:     *   for binder glass at 90 degrees C. k_long is set to zero.
170:     *
171:     *   The stochastic parameters described above are used to
172:     *   represent uncertainty in the regression fit of the
173:     *   forward rate, k(T,pH), and the ratio of Q(T)/K(T).
174:     *
175:     *   Variance weighting was not used in evaluating the regression
176:     *   fit of the forward rate data from CMT.
177:     *
178:     *   SOME DATA IN THE FUNCTION IS FROM THE TSPA-VA TECHNICAL
179:     *   BASIS DOCUMENT AND IS NOT SPECIFIC TO THE ANL CWF.
180:     *
181:     *   ************************************************************
182:   */
183:
184:     /* CWF forward rate parameters: */
185:
186:     /* Forward Rate Coefficients for low (acidic) pH: */
187:     const double a0 = -2.1088, a1 = -0.3575, a2 = -3750.;
188:     /* Forward Rate Coefficients for high (basic) pH: */
189:     const double b0 = -1.2831, b1 =  0.6437, b2 = -4355.;
190:
191:     /* Uncertainties in forward rate coefficients for low (acidic) pH: */
192:     const double delta_a0 = 0.0257, delta_a1 = 0.0422, delta_a2 = 141.;
193:     /* Uncertainties in forward rate coefficients for high (basic) pH: */
194:     const double delta_b0 = 0.0801, delta_b1 = 0.0756, delta_b2 = 432.;
195:
196:     /* Regression constants for low (acidic) pH: */
197:     const double c_a1 = 5.696, c_a2 = 0.002989;
198:     /* Regression constants for high (basic) pH: */
199:     const double c_b1 = 8.271, c_b2 = 0.002978;
200:
201:     /* Silica saturation values for HLW (amorphous silica)  */
202:     /* and CWF (binder glass, estimated) at 90 degrees C    */
203:     const double KHLW90 = 330.0; /* mg/kg SiO2 */
204:     const double KCWF90 = 231.0; /* mg/kg SiO2 */
205:
206:     /* HLW rate parameters from the TSPA-VA */
207:     /* Coefficient for the long-term rate: */
208:     const double g0 = -4.31, g1 = -4502.9765;
209:     /* Coefficients for Q/K: */
210:     const double t0 = 0.272749, t1 = 0.001958;
211:
212:     /* Uncertainty in coefficient for long-term rate: */
213:     const double delta_g0 = 0.15, delta_g1 = 142.1147;
214:     /* Uncertainties in coefficients for Q/K: */
215:     const double delta_t0 = 0.0107, delta_t1 = 0.000082;
216:
217:     /* Regression constants for the long-term rate */
218:     const double c_g1 = 0.003109;
219:     /* Regression parameter for Q/K: */
220:     const double c_t1 = 70.83;
221:
```

```
222:     /* Dissolution rate terms: */
223:     double inverseKelvin = 1.0/(in[indexTemp]+273.15); /* 1/T in Kelvin^-1 */
224:     double log_ka, log_kb, log_kf, kf, log_kl, kl, QK;
225:
226:     /*
227:        Calculate the regression for the forward rate (kf),
228:        long-term rate (kl), and ratio of Q/K (QK).
229:     */
230:
231:     /* Forward rate is based on measured values for binder glass */
232:     log_ka = (a0 + in[indexStoch1] * delta_a0)
233:           + (a1 + in[indexStoch2] * delta_a1) * (in[indexPH] - c_a1)
234:           + (a2 + in[indexStoch3] * delta_a2) * (inverseKelvin - c_a2);
235:
236:     log_kb = (b0 + in[indexStoch4] * delta_b0)
237:           + (b1 + in[indexStoch5] * delta_b1) * (in[indexPH] - c_b1)
238:           + (b2 + in[indexStoch6] * delta_b2) * (inverseKelvin - c_b2);
239:
240:     log_kf = max(log_ka, log_kb);
241:     kf = 365.25 * pow(10, log_kf);
242:
243:     /* Long-term rate is from the TSPA-VA for high-level waste glass
244:     *   log_kl = (g0 + in[indexStoch7] * delta_g0)
245:     *          + (g1 + in[indexStoch6] * delta_g1) * (inverseKelvin - c_g1);
246:     *   kl = 365.25 * pow(10, log_kl);
247:     */
248:     /* The long-term rate is assumed to be zero: */
249:     kl = 0.0;
250:
251:     /*
252:        Ratio of Q/K is from the TSPA-VA for high-level waste glass.
253:        K is based on solubility of amorphous silica (SiO2) while Q
254:        is based on cristobalite
255:     */
256:     QK = (t0 + in[indexStoch8] * delta_t0)
257:        + (t1 + in[indexStoch9] * delta_t1) * (in[indexTemp] - c_t1);
258:
259:     /*
260:        Assuming K has the same temperature dependence for HLW glass (i.e.
261:        amorphous silica) as it does for the CWF (i.e. binder glass), adjust
262:        the ratio of Q/K based on estimates of K for the binder glass at 90
263:        degrees C
264:     */
265:     QK = QK * KHLW90 / KCWF90;
266:
267:     /* Make sure Q/K does not exceed one */
268:     if (QK > 1.0)
269:        QK = 1.0;
270:
271:     /* Calculate the CWF dissolution rate: */
272:     out[indexCWFDis] = kf * (1.0 - QK) + kl;
273:
274:     /* Successful completion. */
275:     return DLL_SUCCESS;
276: }
```

Listing 2: Source Code Listing for Included Header File “ripdll.h”

```
 1:  #ifndef __RIP_DLL__
 2:  #define __RIP_DLL__
 3:
 4:  #define RIP_INITIALIZE     0
 5:  #define RIP_CALCULATION    1
 6:  #define RIP_REP_VERSION    2
 7:  #define RIP_REP_ARGUMENTS  3
 8:
 9:  #define DLL_SUCCESS        0
10:  #define DLL_FATAL          1
11:
12:  #endif /* __RIP_DLL__ */
```

Distribution for ANL-03/8

Internal (Printed and Electronic Copies):

T. H. Fanning (10)
W. L. Ebert (25)

Internal (Printed Copy Only):

M. J. Steindler

Internal (Electronic Copy Only):

M. R. Hale, TIS
J. P. Ackerman
C. H. Adams
R. K. Ahluwalia
S. E. Aumeier
A. J. Bakel
T. L. Barber
K. J. Bateman
T. J. Battisti
T. H. Bauer
A. R. Brunsvold
D. B. Chamberlain
Y. I. Chang
J. C. Cunnane
S. S. Cunningham
N. L. Dietz
R. N. Elliot
R. A. Evans
R. J. Finch
J. A. Fortner
E. K. Fujita
H. E. Garcia
M. M. Goldberg
K. M. Goff
M. G. Gougar
C. Grandy
D. J. Graziano
D. D. Hagan
J. E. Herceg
R. N. Hill
D. Janney
S. G. Johnson
H. S. Khalil
D. D. Keiser, Jr.
J. R. Kennedy
C. J. Knight
J. R. Krsul
C. E. Lahm
R.M. Lell
G. L. Lentz
D. Lewis
M. A. Lewis
S. X. Li
R. P. Lind
K. C. Marsden
S. D. McBride
S. M. McDeavitt
H. F. McFarlane
E. E. Morris
T. P. OíHolleran
R. L. Parks
D. R. Pedersen
R. D. Phipps
C. L. Pope
M. C. Regalbuto
J. I. Sackett
S. R. Sherman
G. M. Teske
Y. Tsai
K. L. Toews
D. Vaden
G. F. Vandegrift
D. L. Wahlquist
D. P. Weber
B. R. Westphal
R. A. Wigeland
M. A. Williamson
J. L. Willit
T. L. Wright

External (Electronic Copies Only):
M. A. Buckley, ANL Library-E
E. Sackett, ANL Library-W
Chemical Technology Division Review Committee Members:
H. U. Anderson, University of Missouri-Rolla, Rolla, MO
R. A. Greenkorn, Purdue University, West Lafayette, IN
C. L. Hussey, University of Mississippi, Oxford, MS
M. V. Koch, University of Washington, Seattle, WA

V. P. Roan, Jr., University of Florida, Gainesville, FL
J. R. Selman, Illinois Institute of Technology, Chicago, IL
J. S. Tulenko, University of Florida, Gainesville, FL